The Effect of Myostatin-antagonist4 on a Severe Muscle Burn Injury

by

Rachel Marie Laurenson

A thesis submitted in partial fulfilment of the requirements for the degree of

Master of Science

at

2009

Dedicated to Beryl Louisa Laurenson

16.11.1926 – 18.08.2008

My lovely Nana who didn't quite get to see me finish this journey

Abstract

Myostatin is a growth and differentiation factor which belongs to the transforming growth factor-beta superfamily of genes. Mutations or deletions in the myostatin gene leads to the heavy muscling phenotype seen in various cattle breeds, including Belgian Blue and Peidmontese, and also in myostatin knock-out mice. More recently, a human child with the heavy muscling phenotype was also found to carry a mutation in the myostatin gene. Conversely, increased expression of myostatin has been linked to various muscle wasting conditions induced by ageing or disease. Myostatin is therefore regarded as a strong inhibitor of muscle growth. In addition, myostatin has also been shown to control satellite cell activation post-natally, and is therefore considered a potent negative regulator of muscle regeneration and repair.

The ability to block myostatin function has enormous potential in the treatment of muscle injuries and various muscle wasting conditions. The Functional Muscle Genomics group at AgResearch Ltd. have recently developed several myostatin antagonists, produced by truncating the biologically active mature myostatin sequence. The following thesis describes the first *in vivo* study using the myostatin antagonist, Mstn-ant4, where its effect on wound healing was evaluated using a murine muscle burn injury model. Some promising results that Mstn-ant4 could improve muscle wound healing after a severe burn injury were obtained. Specifically, Mstn-ant4-treated mice recovered from the burn-induced loss of body weight earlier than the saline-treated mice. Mighty gene expression, which is a downstream target of myostatin and is involved in muscle hypertrophy, was also significantly higher in the burnt muscles of mice treated

with Mstn-ant4 compared to saline-treated mice. In addition, histochemical analysis indicated that administration of Mstn-ant4 may have been terminated too early during the *in vivo* trial, as reflected by the sudden decrease in centrally formed nuclei in the burnt muscles of Mstn-ant4-treated mice at day 14, with the last subcutaneous injection of Mstn-ant4 occurring at day 15.

Although no other statistically significant results were obtained by histology, immunocytochemistry or gene expression analysis to support these results, it would be difficult to conclude that significant results could not be generated when the antagonist was used under optimised conditions. That is, further studies into the administration schedule of the antagonist need to be undertaken, particularly with regard to the frequency of administration and duration of treatment. Overall, Mstn-ant4 has significant potential to improve wound healing following a severe muscle burn injury.

Acknowledgements

First of all I would like to thank Dr Ravi Kambadur and Dr Mridula Sharma for starting me on this journey. Without your encouragement and support I would never have carried on from my undergraduate degree to a Masters, so for that I will always be grateful.

I would also like to thank my university supervisor Dr Nick Ling, for introducing me to Ravi and Mridula. Also, your assistance with writing this thesis has been greatly appreciated, thank you.

Dr Mônica Senna Salerno, you have been a wonderful workplace supervisor and friend throughout this process. Thank you so much for all your guidance, for always making time to help me no matter how hectic your schedule was, and for having such confidence in me. The time you have spent proof-reading and critiquing this thesis has also been greatly appreciated thank you. I hope everything works out well for you in the future.

Thank you to Neil Cox for all your help with the statistical analysis. I still don't know how you did it all but thank you for patiently trying to explain it to me.

A huge thank you to everyone in the FMG group (both past and present), you were all so willing to help out wherever possible and you created such a friendly working environment which made this experience that much more enjoyable. I will never forget all the wonderful morning tea shouts, the Christmas parties and of course those team-building exercises! In particular I would like to thank

Kelly Dyer for all your help with the PCR's and other general lab stuff. Also to my fellow Masters student Dan Fieten, for helping me with my computer issues, teaching me Real-Time PCR and not minding when I interrupted your writing to ask you questions. It has been great being able to bounce ideas off each other, and all those formula spreadsheets were very handy thank you! To Dr Gina Nicholas, thank you for critiquing this thesis; and a big thank you to Erin Plummer for being such a great office buddy and friend. I really appreciate all the little chats we had when I needed a distraction from work, and for your wonderful proof-reading skills (I still can't believe you actually enjoy doing it!).

And to "the crew", Erin, Nicole Goldthorpe, Murray Ashby, Blair Sowry and Jaime Oswald, I have really enjoyed your company over the past few years. The lunches out, the BBQs, the after-work get togethers and the pub crawls! I look forward to many more in the future.

Thank you to everyone else in the Kirton Wing, you have all been so friendly and welcoming, always stopping to ask how my research and thesis was going.

To my wonderful neighbours, the King family, and my flatmate Erin King, thanks for always having a cold beer waiting for me on a Friday afternoon. I think it is my turn to throw you guys a few BBQs now that I have finally finished this thesis!

And to my family and my future mother and father–in law, I could not have done any of this without your support and encouragement. Hopefully I will be able to spend a bit more time with you all now.

And to the most important person of all, my lovely fiancé Haydn (a.k.a. Digga). Thank you for looking after me during these past 6 years at University, putting up with the late nights and weekends spent studying and all the times when I was incredibly stressed out and grumpy and was just completely horrible to be around! Your love and continual support has been my rock throughout this process and I cannot wait to see where the next phase of our life together takes us. “Like midnight loves the moon…”

Contents

List of Figures

Chapter One: Literature Review

Chapter Two: Materials and Methods

Chapter Three: Results

List of Tables

List of Abbreviations

3’	3 prime
5’	5 prime
α	alpha
β	beta
ºC	degrees Celsius
µg	micrograms
µl	microlitres
µM	micromolar
A-band	anisotropic band
Act RIIA	activin type IIA receptor
Act RIIB	activin type IIB receptor
Alk5	activin receptor-like kinase-5
ANOVA	analysis of variance
ATP	Adenosine triphosphate
bHLH	basic helix-loop-helix
BMP	bone morphogenic protein
bp	base pair(s)
BrdU	bromodeoxyuridine
BSA	bovine serum albumin
CDK	cyclin-dependent kinase
cDNA	complementary DNA
CFN	centrally formed nuclei
CK	creatine kinase
DAPI	4’,6-diamidino-2-phenylingole dihydrochloride

DEPC	diethyl pyrocarbonate
Dex	dexamethasone
DNA	deoxyribonucleic acid
E	embryonic day
E-box	ephrussi box
ERK	extracellular signal-regulated kinase
FGF	fibroblast growth factor
FMG	Functional Muscle Genomics
FOX	forkhead box
g	g-force
g	gram(s)
G0, 1, or 2	gap 0, 1, or 2 phase of the cell cycle
GDF-8	growth and differentiation factor-8
GuHCl	guanidine hydrochloride
h	hour(s)
H and E	haematoxylin and eosin
HGF	hepatocyte growth factor
HS	horse serum
H-zone	hele-sheibe zone
I-band	isotropic band
ICC	immunocytochemistry
IGF	insulin-like growth factor
Il	Interleukin
iNOS	inducible nitric oxide
IPTG	isopropyl thio-β-galactoside
kDa	kilo Daltons

L	litre(s)
LAP	latency associated protein
LB Broth	luria bertani broth
Lbx1	ladybird homeobox-1
LIF	leukaemia inhibitory factor
ln	natural log
M	molar mass
Mac1	macrophage antigen complex-1
MAP	mitogen-activated protein
M-CAM	melanoma cell adhesion molecule
MCK	muscle creatine kinase
MCM1	minichromosome maintenance 1
MEF2	myocyte enhancer factor-2
mg	milligram(s)
MHC	myosin heavy chain
min	minute(s)
ml	millilitre(s)
M-line	middle line
mm	millimetre(s)
mM	millimolar
M-phase	mitosis phase
MRF	myogenic regulatory factor
mRNA	messenger RNA
Mstn-ant	myostatin antagonist
NCAM	neural cell adhesion molecule
NDS	normal donkey serum

nm	nanometre(s)
NO	nitric oxide
NOS	nitric oxide synthase
NOS-I	nitric-oxide synthase I
PBS	phosphate buffered saline
PBS-T	phosphate buffered saline + tween-20
PCR	polymerase chain reaction
PDGF	platelet-derived growth factor
Rb	retinoblastoma
RFU	relative fluorescence units
RNA	ribonucleic acid
RT	room temperature
s	second(s)
SDS	sodium dodecyl sulphate
SED	standard error of the difference
SF	scatter factor
Shh	sonic hedgehog
SP	side population
S-phase	synthesis phase
SRF	serum response factor
TA	*tibialis anterior*
TGF	transforming growth factor
Tn	troponin
TNF-α	tumour necrosis factor alpha
UV	ultra-violet
Z-line	zwishenscheibe-line

Chapter One: Literature Review

The following literature review first describes the various types of muscle tissues present in the mammalian body, and then specifically outlines the structure and function of skeletal muscle and the mechanisms involved in its contraction. The processes involved in myogenesis, from the embryonic origin of muscle through to post-natal development are then summarised, including an overview of the satellite cell and its role in muscle regeneration. The chapter concludes with a review of myostatin, where recent advancements regarding myostatin antagonists and their potential role in wound healing are discussed.

1.1. Muscle Physiology

Three different types of muscle tissues exist in the mammalian body: smooth, cardiac and skeletal muscle. Each is characterised by their location and structure; for example, cardiac muscle is specifically localised to the heart and is striated in appearance. In comparison, smooth muscle is non-striated and is located around blood vessels and the walls of organs associated with the digestive, respiratory, urinary and reproductive systems. Both cardiac and smooth muscles generally consist of mononucleate cells, but cells of cardiac muscle are branched. Approximately 55% of the body mass of mammals is comprised of skeletal muscle, which is involved in all voluntary movements. Skeletal muscle is also striated, but consists of multinucleate cells rather than mononucleate ones (Martini, 2002; Zierath & Hawley, 2004). The following thesis is based around this last type of muscle tissue, and therefore skeletal muscle will be further discussed in the following sections.

1.2. Skeletal Muscle

1.2.1. Skeletal Muscle Structure

In skeletal muscle, individual fibres are arranged into bundles referred to as fascicles. There are two layers of connective tissue specifically associated with these structures, including the perimysium, which surrounds each fascicle; and the endomysium, which surrounds each individual muscle fibre within a fascicle. In addition, a third layer of connective tissue called the epimysium encloses the entire skeletal muscle. Each muscle fibre is divided into smaller subunits called myofibrils, and electron microscopy reveals that it is the structure of these myofibrils which produces the characteristic striated appearance of skeletal muscle. Myofibrils consist of bundles of myofilaments that contain specialised contractile proteins organised into sarcomeres. Sarcomeres contain two types of protein filaments; thin filaments and thick filaments (Figure 1.1A) (Randall et al., 1997; Gordon et al., 2001; Martini, 2002). Actin is the main component of thin filaments, and it exists as two twisted strands of actin molecules with a helical pitch of 36 nm. Nebulin is associated with each actin strand and it has recently been proposed that these large molecules act as a type of 'molecular ruler' involved in length specification of the actin filaments during myogenesis (Martini, 1998; 2002; McElhinny et al., 2005). Tropomyosin and troponin are the regulatory elements of the thin filaments. Chains of tropomyosin molecules join together to form a continuous strand that runs along each of the coiled actin strands. Troponin consists of three subunits, troponin-C, -I and -T (Tn-C, Tn-I, Tn-T), each of which have a specific role during skeletal muscle contraction; Tn-C reversibly binds calcium ions, Tn-I binds actin, and Tn-T binds to both Tn-I and Tn-C, as well as to tropomyosin. There is one troponin complex associated with each

tropomyosin molecule; tropomyosin blocks myosin binding to seven actins. Myosin is the main component of the bipolar thick filament. Each thick filament contains approximately 300 myosin molecules, with myosin heads consisting of two heavy chains and two light chains projecting in a helical configuration from the filament backbone (Squire and Morris, 1998; Gordon et al., 2001).

In the resting sarcomere, distinct regions can be defined based on the arrangement of the thick and thin protein filaments. The H-zone (Hele-Sheibe zone) encompasses the M-line (middle-line), which is the central region of the structure and represents the site where only thick filaments are present. The I-bands (isotropic-bands) represent the region of the sarcomere where only thin filaments are present; these bands are bisected by the Z-line (Zwischenscheibe-line). The Z-line serves as the anchor point for the thin filaments at either end of the sarcomere and therefore the distance between two Z-lines defines the sarcomere unit. Finally, the A-band (anisotropic-band) encompasses the H-zone and the regions either side where the thick and thin filaments overlap (Figure 1.1B) (Randall et al., 1997; Gordon et al., 2001; Martini, 2002).

1.2.2. Skeletal Muscle Contraction

In order to produce force, skeletal muscle contracts via strong binding between myosin and actin filaments. The subsequent conformational changes in the myosin heads, which project out from the myosin filament, pulls the thin filament towards the M-line at the centre of the sarcomere, decreasing the size of the H-zones and I-bands (Squire, 1975; Gestrelius & Borgström, 1986; Martini, 2002).

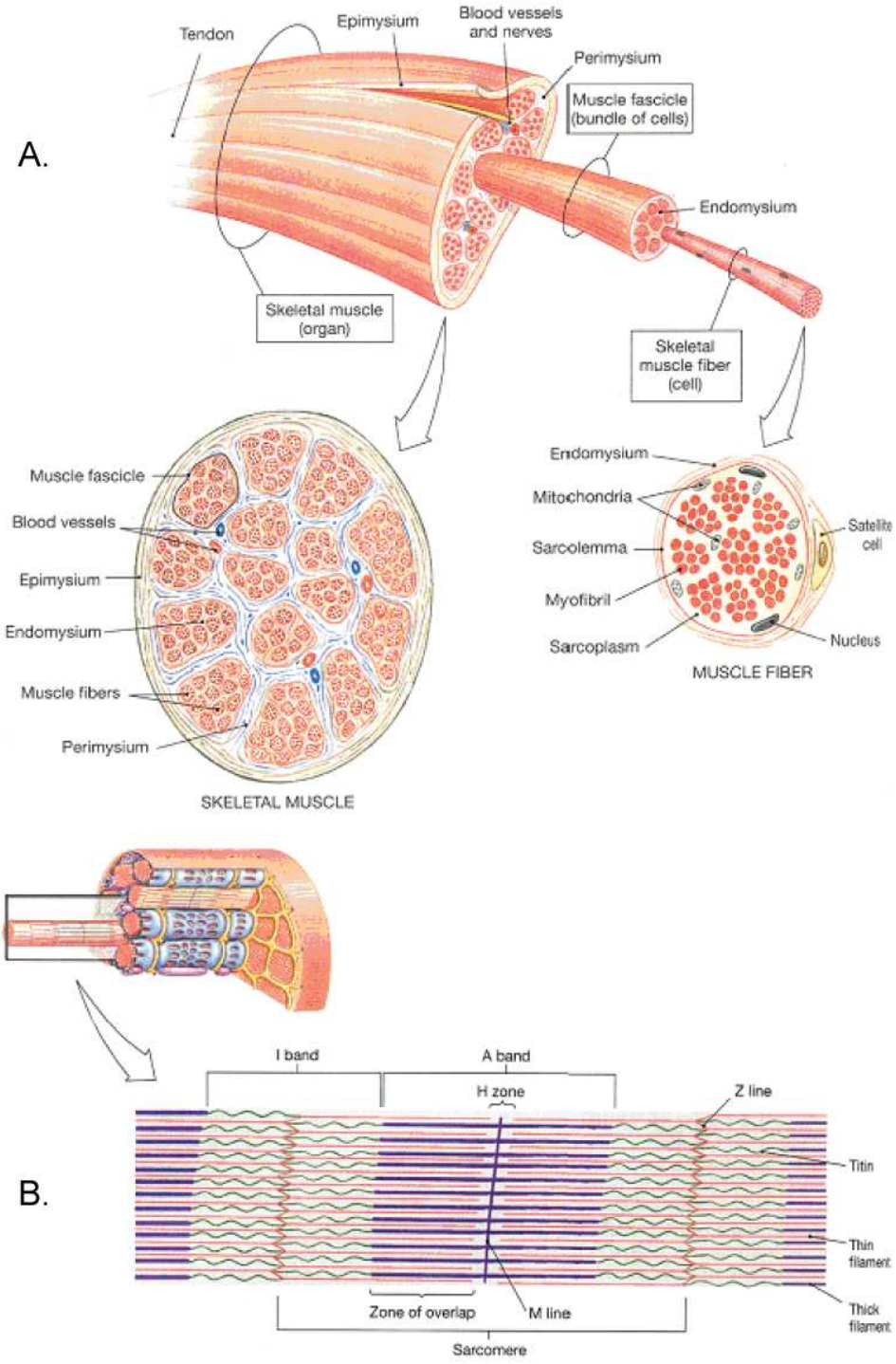

Figure 1.1: The structure of skeletal muscle

A) Skeletal muscle consists of muscle fibres arranged into fascicles. The perimysium surrounds each fascicle, while the endomysium surrounds each individual muscle fibre. The epimysium encloses the entire skeletal muscle structure. Each muscle fibre contains bundles of myofilaments, which consist of repeating sarcomere units. **B)** Sarcomeres are composed of thick and thin filaments which are involved in muscle contraction (Martini, 1998).

More specifically, in a low calcium environment, skeletal muscle exists in a relaxed state where the conformation of the troponin and tropomyosin molecules physically blocks the sites on the actin filament where myosin binds, therefore preventing attachment. When calcium is released in response to action potentials from innervating muscle neurons, it binds to troponin and initiates the change from a relaxed muscle state to an active one. This involves tropomyosin moving out of the way as a direct result of calcium binding, therefore exposing the myosin binding sites on the actin filament (Squire, 1975; Squire & Morris, 1998; Gordon et al., 2001). The myosin heads attach to these binding sites, forming cross-bridges that pull the filaments past each other, allowing the muscle to contract (Tregear & Marston, 1979; Swartz et al., 1990; Martini, 2002).

1.3. Embryonic Myogenesis

1.3.1. Somite/Muscle Precursor Formation

Skeletal muscle development begins with the formation of somites, which are a conglomerate of epithelial cells that originate from presomitic mesoderm tissue in the mammalian embryo. Formation of these somites occurs in an anterior to posterior direction and they lie juxtaposed to either side of the neural tube and notochord. The production of these somites appears to be governed by two different mechanisms; a type of segmentation clock, which regulates the timing of somite formation by initiating oscillating waves of gene expression, and the presence of a determination gradient in the presomitic mesoderm. The overall process of somite formation is strongly synchronised with embryonic axis elongation (Buckingham et al., 2003; Dubrulle & Pourquié, 2004; Brent, 2005; Gridley, 2006; Mallo, 2007).

The concept of a segmentation clock was first proposed by Palmeirim et al. (1997) who observed that expression of c-hairy1, a gene involved in the Notch signalling pathway, occurred as waves in the presomitic mesoderm of the chick. More specifically, c-hairy1 expression moved through the presomitic mesoderm of the chicken embryo every 90 minutes in a posterior to anterior direction; and the frequency of these waves coincided with the formation of a single somite (Palmeirim et al., 1997; Hollway & Currie, 2003; 2005; Mallo, 2007). Further studies have revealed that numerous other genes involved in the Notch signalling pathway also display oscillating expression patterns in the presomitic mesoderm, including c-hairy2, deltaC, her1, her7, Hes2, Hes7 and lunatic fringe (Pourquié, 2001). Mutations in some of these genes can lead to abnormal segmentation, which emphasises the importance of the Notch signalling

pathway in somite formation, particularly during the segmentation phase. Recent studies suggest that the Wnt signalling pathway may also play a key role in the segmentation clock (Aulehla et al., 2003; Mallo, 2007).

Unlike the segmentation clock which regulates the timing of somite formation, the determination gradient establishes the position of somite boundaries as the individual somites bud off from the presomitic mesoderm. This process is achieved by the presence of two opposing morphogen fronts in the presomitic mesoderm, an anterior to posterior directed retinoic acid signalling gradient, and a posterior to anterior directed fibroblast growth factor (FGF)/Wnt signalling gradient (Brent, 2005; Mallo, 2007).

During embryogenesis, the fate of a somite is determined by extrinsic cues provided by the surrounding environment; particularly by the neural tube, notochord and dorsal ectoderm. The signals produced by these structures initiate the division of the somite into the sclerotome, which is ventrally positioned and involved in the development of cartilage and bone in the ventral column and ribs; and the dermomyotome, which is dorsally positioned. Further patterning along the mediolateral axis of the dermomyotome produces distinct medial (referred to as the ‘medial lip’), central and lateral partitions. The medial section delaminates to form the myotome, which goes on to generate the epaxial domain; while the central and lateral sections contain the muscle precursor cells for the dermal and hypaxial domains respectively. It is the muscle precursors of the epaxial domain that give rise to the musculature of the back; while those of the hypaxial domain, consisting of both migrating and non-migrating cell populations, gives rise to limb and other body musculature (Marcelle et al.,

1997; Dietrich et al., 1999; Birchmeier & Brohmann, 2000; Christ & Brand-Saberi, 2002; Buckingham et al., 2003; Gridley, 2006).

Several of the key molecules and signalling pathways involved in the formation of somites and muscle precursors have recently been identified, particularly those important for the correct patterning of the somite compartments during development. Of these, the coordinated actions of bone morphogenetic proteins (BMP), Wnt and sonic hedgehog (Shh) pathways are the most well-documented throughout the literature (Zhao & Hoffman, 2004). BMPs belong to the transforming growth factor-beta (TGF-β) superfamily and approximately 20 BMP family members are currently recognised (Xiao et al., 2007). One of these, BMP-4, is produced by the dorsal neural tube and promotes the upregulation of certain Wnt family members, namely Wnt-1 and Wnt-3a. In turn, these induce the expression of another Wnt family member, Wnt-11, which is present in the medial lip of the dermomyotome. Overall, this pathway indirectly induces formation of the medial lip via Wnt-1 and Wnt-3a, ultimately leading to the muscle precursor cells located within this structure relocating from the medial lip to the myotome. However, Pourquié et al. (1996) and Marcelle et al. (1997) reported that to generate correct patterning in the somite, BMP signalling needs to be restricted to certain areas of the somite; therefore suggesting the existence of a BMP inhibitor. Noggin has been characterised as the BMP inhibitor present in the developing somite (Hirsinger et al., 1997; Krüger et al., 2001). Furthermore, Shh, which is produced by the notochord, has been shown to directly inhibit Wnt-11 (Marcelle et al., 1997).

1.3.2. Migration to the Limb Bud

The migration phase of muscle development begins with the delamination of muscle precursor cells from the hypaxial dermomyotome, at a location opposite to the target limb bud. This is followed by the movement of these cells into a position in the limb bud where the formation of specific muscle masses will be initiated. The presence of the tyrosine kinase receptor, c-Met, and its associated ligand, scatter factor/hepatocyte growth factor (SF/HGF) are essential for both the delamination and migration of the muscle precursor cells. This receptor originates in non-somitic mesodermal cells, and transcription of the c-Met gene is mediated through the transcription factor Pax3 (Dietrich et al., 1999; Buckingham et al., 2003). The importance of both c-Met and Pax3 in precursor cell migration and muscle development is clearly shown in mutant mice, where embryos lacking functional c-Met or SF/HGF fail to develop skeletal muscle. Furthermore, in addition to a lack of limb muscle development, muscle precursor cells of Pax3-mutant mice fail to even delaminate from the hypaxial dermomyotome and thus fail to initiate migration (Tajbakhsh et al., 1997; Dietrich et al., 1999; Birchmeier & Brohmann, 2000; Buckingham et al., 2003; Yusuf & Brand-Saberi, 2006).

Ladybird homeobox 1 (Lbx1) is another transcription factor that plays a key role during the migration of cells from the somite to the limb bud, and its expression is thought to depend on the presence of Pax3. Lbx1 is upregulated before delamination begins, its expression is maintained throughout the migration period, and is then downregulated once muscle-specific gene expression is activated in the limb bud (Christ & Brand-Saberi, 2002). In mutant Lbx1 mouse embryos, the muscle precursor cells are properly formed and delaminate from

the dermomyotome in the same manner as that seen in wild-type embryos. However, the precursor cells display abnormal migration patterns, tending to remain in close proximity to the somites, where alternative cell fates may be adopted. Yet, although there is a significant loss of muscle mass in Lbx1 mutants, it is much less severe when compared to the muscle phenotypes seen in the Pax3-mutant and c-Met-mutant mice (Birchmeier & Brohmann, 2000; Gross et al., 2000; Buckingham et al., 2003; Yusuf & Brand-Saberi, 2006).

The actual regulation of the Pax3 and Lbx1 genes during muscle development is not well understood. Gross et al. (2000) proposed that Pax3 and Lbx1 are co-expressed in all migrating hypaxial muscle precursors, and several studies suggest that Lbx1 is located downstream of Pax3. However, Buckingham et al. (2003) presented the alternative view that Lbx1 can be independently activated. In addition, Wnt-6, which is produced by the surface ectoderm, has been identified as a potential candidate for the activation of Pax3; while members of the FGF family are thought to be involved in Lbx1 regulation (Birchmeier & Brohmann, 2000; Buckingham et al. 2003).

An additional homeobox transcription factor has also been implicated in the migration of muscle progenitor cells to the limb bud, namely Msx1. Msx1 is able to inhibit myogenesis, therefore retaining the muscle precursor cells in an undifferentiated state necessary for migration (Houzelstein et al., 1999). Further conditions required for the migration of muscle precursor cells include the presence of the cell-adhesion molecules, N-cadherin and fibronectin, and the extracellular spaces also need to be large enough to accommodate the migrating cells. In addition, the tyrosine kinase receptor EphA4, and its associated ligand

ephrinA5, are needed to guide the cells into the appropriate locations in the limb buds (Christ & Brand-Saberi, 2002).

1.3.3. Muscle Differentiation and Growth in the Limb Bud

There are two general steps required to complete the myogenic programme once the muscle precursor cells have migrated to the limb buds. These include commitment of the precursor cells to the myogenic lineage, which involves the formation of myoblasts; and then these myoblasts undergo terminal differentiation to form myotubes, providing the basis for muscle growth. During these stages, Pax3 and Lbx1 expression significantly decreases, while the expression of muscle-specific and differentiation markers increase. These markers include the myogenic regulatory factors (MRFs) and the MEF2 family of myocyte enhancer-binding factors, which interact with each other to regulate the transcription of muscle-specific differentiation genes (Yun & Wold, 1996; Wang & Jaenisch, 1997).

1.3.3.1. The MRFs

MyoD, myogenin, Myf-5 and MRF4 comprise the group of basic helix-loop-helix (bHLH) transcription factors, collectively referred to as the MRFs. Each of these MRF family members contains a conserved DNA binding region, which specifically targets the Ephrussi–box (E-box) consensus sequences present in most muscle-specific genes (Tapscott & Weintraub, 1991; Ludolph & Konieczny, 1995). During skeletal muscle formation, the trend of MRF expression is somewhat hierarchical, with Myf-5 appearing first in the mouse somite at embryonic day 8 (E8), followed by myogenin and MyoD emerging in the myotome at E8.5 and E10.5 respectively; concluding with the transient

expression of MRF4 in the myotome between E9 and E11.5 (Zhang et al., 1995). With regard to limb bud development, Myf-5 expression is initiated in the limb buds at E11, myogenin and MyoD appear soon after at E11.5, and MRF4 expression emerges much later, when it is expressed in differentiated muscle fibres (Zhang et al., 1995).

From these timelines it is generally accepted that Myf-5 and MyoD are involved in regulating the determination process resulting in the multipotent somite cells being committed to the myogenic lineage; while myogenin and MRF4 are involved in the initiation of myoblast differentiation, which occurs later in the myogenic programme. Therefore Myf-5 and MyoD are often referred to as the primary MRFs, while myogenin and MRF4 are referred to as the secondary MRFs (Rudnicki et al., 1993; Borycki & Emerson, 1997).

Since these initial observations, phenotypes of knock-out mouse models have been used to further study the MRFs and to clarify their roles in skeletal muscle formation. Rudnicki et al. (1992; 1993), observed that both Myf-5-null mice and MyoD-null mice displayed normal skeletal muscle development; whereas Myf-5/MyoD double knock-out mice failed to produce any skeletal muscle fibres or myoblasts at all, rendering them immobile at birth and resulting in death soon after. This suggests a functionally interchangeable role for Myf-5 and MyoD, as the presence of either one can successfully facilitate the development of skeletal muscle**.** However, additional studies identified a significant rib defect in the Myf-5 mutants and a reduced capacity for muscle regeneration in the MyoD mutants, as well as an overall delay in their skeletal muscle development (Wang & Jaenisch, 1997). Recent evidence has also shown Myf-5 to be genetically

linked to MRF4, and therefore the generation of Myf-5-null mice consequently influences MRF4 expression in these animals. For that reason, it has been proposed that along with MyoD and Myf-5, MRF4 should also be classified as a skeletal muscle determination gene, though this is still widely debated (Kassar-Duchossoy et al., 2004).

In contrast to Myf-5-null or MyoD-null mice, which still display normal skeletal muscle development, mice with a targeted homozygous mutation for myogenin exhibit severe skeletal muscle defects. More specifically, migrating myoblasts are still present in myogenin-null mice, but these fail to terminally differentiate into myotubes, and therefore do not meet the requirements for successful muscle development. However, there are some residual muscle fibres present in the mice at birth, suggesting that a myogenin-independent pathway for muscle differentiation may exist (Hasty et al., 1993; Rawls et al., 1998). Additional complications in these mutant mice include the presence of extensive adipose tissue, particularly in the dorsal neck region, abnormal curvature of the spine and a deformed rib cage. Ultimately these problems lead to the death of myogenin-null mice immediately following their birth (Hasty et al., 1993; Nabeshima et al., 1993; Zhang et al., 1995; Wang & Jaenisch, 1997). The migrating myoblasts of myogenin-null mice express Myf-5 and MyoD, therefore supporting the idea that myogenin functions at a later time point in the myogenic pathway than the primary myogenic factors. In addition, there is a minimal level of MRF4 expression in myogenin-null mice, which is also consistent with the proposed myogenic pathway, where myogenin acts before MRF4 during muscle development (Zhang et al., 1995). This contradicts the earlier idea that MRF4 should be classified as a skeletal muscle determination gene.

Combined myogenin/MyoD-null mutations and myogenin/Myf-5-null mutations have also been investigated. Results indicate that similar phenotypes were produced by these combinations as those seen in mice deficient in the individual factors (Rawls et al., 1998). However, Wang and Jaenisch (1997) brought attention to the varying expression patterns of the MRFs. In particular, expression of Myf-5 and MyoD first appear in the dorsal-medial half and the ventral-lateral half of the myotome respectively, while myogenin and MRF4 expression is detected throughout the whole myotome. Therefore, the authors discovered that when myogenin is expressed in a similar temporal and spatial pattern to Myf-5, it is able to substitute the role of this regulatory factor in myogenic lineage determination, though not as effectively.

Finally, like Myf-5 and MyoD, MRF4-null mice are also viable, displaying normal skeletal muscle development and a normal range of movement immediately after birth. However, they too show severe rib defects which ultimately leads to their death shortly after birth. Interestingly, MRF4-null mice show significant upregulation of myogenin (up to five-fold) suggesting that this myogenic regulatory factor may be compensating for the loss of MRF4 in the mice (Zhang et al., 1995; Arnold & Braun, 1996). However, if MRF4 and myogenin had truly overlapping functions a more severe phenotype in the MRF4/myogenin double mutant mice would be expected compared to the phenotypes of MRF4-null or myogenin-null mice alone. Rawls et al. (1998) reported the MRF4/myogenin double mutant phenotype and the phenotyope of myogenin-null mice alone to be very similar. In contrast, the authors discovered that although MRF4-null or MyoD-null mice were viable at birth and show normal skeletal muscle development, MRF4/MyoD double mutant mice

displayed a severe muscle deficiency similar to myogenin-null mice, indicating a potential compensatory role for MRF4 and MyoD during myogensis (Rawls et al., 1998).

1.3.3.2. The MEF2 Family

As previously mentioned in Section 1.3.3, the MEF2 family also plays a key role during myogenesis, with the majority of muscle-specific genes containing the MEF2 binding site, $CTA(A/T)_4TAG$, in their control regions. This group of proteins was originally identified from the nuclei of skeletal muscle myotubes, after Gossett and colleagues (1989) observed their ability to specifically bind A/T-rich sequences in the muscle creatine kinase (MCK) gene promoter (Brand, 1997). The vertebrate MEF2 family is comprised of four members: MEF2A, MEF2B, MEF2C and MEF2D. Their capacity for high-affinity DNA binding and dimerisation is facilitated through two interacting domains, a distinct 29 amino acid MEF2 domain, and a highly conserved 57 amino acid motif referred to as the MADS-box. The presence of a MADS-box in these genes provides the basis for their inclusion in the MADS-box superfamily of transcriptional regulators, named after the founding members, minichromosome maintenance 1 (MCM1), agamous, deficiens and serum response factor (SRF). The MADS-box transcriptional regulators are involved in a wide range of biological functions, including the pheromone response in yeast, flower development in plants, tracheal development in Drosophila and, as discussed here, in the regulation of muscle-specific genes (Shore & Sharrocks, 1995; Brand, 1997; Black & Olson, 1998; Perry & Rudnicki, 2000).

Unlike the MRFs, MEF2 genes are expressed in a wide range of lineages, including skeletal, cardiac and visceral muscle, as well as in neural cells, T cells and fibroblasts (Molkentin & Olson, 1996a; 1996b; Brand, 1997; Naya & Olson, 1999). During skeletal muscle development there is a significant overlap between MRF and MEF2 expression. MEF2 also shows a hierarchical pattern of expression like that seen in the MRFs. More specifically, MEF2C appears first in the developing myotome at E8.5, closely followed by the expression of MEF2B at E9, and then MEF2A and MEF2D at E9.5 (Molkentin & Olson, 1996a). Interestingly, the MEF2A, MEF2B and MEF2D transcripts are expressed ubiquitously after birth, while MEF2C is restricted to skeletal muscle, brain and spleen tissues (Molkentin et al., 1995).

Consistent with other MADS-box proteins, the MEF2 family members interact with a diverse range of transcription factors to initiate a plethora of different gene expression programmes. Of these, interactions with the MRFs have been the most extensively studied, with many authors concluding that these two transcription factor families act as co-regulators during skeletal muscle development (Black & Olson, 1998). Among the first observations made involved 10T1/2 cells, a multipotential cell line derived from 14- to 17-day whole mouse embryos. It was originally established by Reznikoff et al. (1973) and has been widely used in molecular biology ever since (Pinney & Emerson, 1989). Specifically, the forced expression of MRFs in 10T1/2 cells activated MEF2 DNA binding activity, suggesting that MEF2 factors lie downstream of MRFs in the skeletal muscle regulatory pathway. However, both myogenin and MRF4 contain MEF2 binding sites in their promoters and these are involved in the expression of muscle-specific genes. Therefore, MEF2 and the MRFs appear

to regulate the expression of each other through complex reciprocating circuits (Molkentin et al., 1995; Naidu et al., 1995; Molkentin & Olson, 1996a; Black & Olson, 1998). In addition, Molkentin et al. (1995), and supporting studies by Yu et al. (1992) and Ornatsky et al. (1997), reported that MEF2 factors by themselves, were unable to activate myogenesis in transfected 10T1/2 and 3T3 fibroblasts; with 3T3 being a standard fibroblast cell line derived from Swiss mouse embryo tissue (Todaro et al., 1964). However, muscle-specific gene expression was successful when both MEF2 and MRFs were present, with the authors observing a 3- to 4-fold increase in the number of myosin heavy chain (MHC) positive cells. This suggests MEF2 and MRFs could be acting synergistically to activate myogenesis.

Although a vertebrate loss-of-function model for MEF2 factors is yet to be developed, analysis of loss-of-function mutations in a single MEF2 gene, D-MEF2, in Drosophila supported the idea that MEF2 is necessary for skeletal muscle development. More specifically, this mutation resulted in the complete absence of differentiated skeletal, cardiac and visceral muscle cells. Supplementary studies revealed that nautilus expression, a Drosophila homolog of MyoD, did occur at the correct time and location in the D-MEF2-mutant embryos, but it was unable to initiate the expression of muscle-specific genes; therefore suggesting that D-MEF2 is particularly important for nautilus function (Molkentin et al., 1995; Olson et al., 1995; Molkentin & Olson, 1996b; Black & Olson, 1998).

The actual mechanism of synergy employed by these two transcription factor families to regulate skeletal muscle development is still under investigation. It

is currently accepted that MEF2 factors only associate with the heterodimers formed from myogenic bHLH proteins and non-myogenic E proteins, such as E12, and not with E protein homodimers. E12-MRF heterodimers can convert non-muscle cells to differentiated myotubes, while E12 homodimers cannot. Two key amino acid residues located in the centre of the MRF basic domain, alanine and threonine, have been identified as the determinants of MRF myogenic activity. Substituting these two myogenic residues with the two asparagines located in the corresponding region of E12 abolishes the myogenic activity of the MRFs without affecting DNA binding. On the other hand, generation of a revertant mutant, where the substituted asparagine residues are mutated back to the alanine and threonine residues, restores full myogenic activity in the MRFs. This suggests it is the alanine and threonine residues that are crucial to facilitate the interaction between MRFs and MEF2, by enabling a specific conformational change in the MRFs to allow the recruitment of MEF2 as a co-regulator (Arnold & Winter, 1998; Black et al., 1998; Naya & Olson, 1999).

A two-step model for successful transcriptional activation by the synergistic actions of MRFs and MEF2 has emerged. Specifically, MEF2 first binds to the DNA-bound MRF and relays its activation signal to the transcriptional activation domain of the MRF. This MRF domain then transmits both its own activation signal and that of MEF2 to the basal transcriptional machinery and an active transcriptional complex is generated. In addition to being involved in the association of MRFs and MEF2, the amino acids alanine and threonine also play an important role in facilitating the transmission of activation signals from the MRFs (Black et al., 1998; Black & Olson, 1998).

1.3.4. The Cell Cycle and Myogenesis

As the muscle precursor cells terminally differentiate and fuse together to form mature myotubes, they irreversibly withdraw from the cell cycle (Walsh & Perlman, 1997). This is a complex regulatory circuit which methodically guides the cell through a series of events, ultimately leading to mitosis and the generation of two "daughter cells". The cell cycle has four characteristic phases; the S-phase (synthesis-phase) where duplication of genetic material occurs; the M-phase (mitosis-phase) where the duplicated chromosomes are evenly distributed to the two daughter cells; and G1 and G2, which are the two 'gaps' antecedent to the S-phase and M-phase, respectively. One of the key protein families involved with the transition of a cell through each phase of the cycle is the cyclin-dependent kinases (CDKs), which belong to the serine/threonine family of protein kinases. Various checkpoints have been developed to monitor the progress of a cell through the cell cycle and to specifically ensure that critical events, such as DNA replication and chromosome segregation, are completed successfully before entering into the next phase. These checkpoints have the ability to either permanently arrest defective cycles, or temporarily pause the cycle while adequate repairs and maintenance are carried out (Schafer, 1998; Tessema et al., 2004).

The generation of new muscle fibres, through the fusion of myoblasts and subsequent myotubes, occurs in two distinct waves characterised by specific temporal patterns, structural fibre morphology and gene expression. The first wave of fibres, termed primary fibres, are widely distributed throughout the limb, providing the foundation for further fibre development by defining specific characteristics of the muscle such as type, shape and location. A rapid

increase in diameter (not associated with nucleation) is one of the key identifying features of the primary fibres, along with the ‘doughnut’ shape observed when the fibres are transversely sectioned. In comparison, secondary fibres form on the surface of primary fibres and rapidly increase in number and nucleation (Wigmore & Dunglison, 1998; Christ & Brand-Saberi, 2002; Abmayr et al., 2003).

In vertebrates, the process of myoblast fusion, which ultimately leads to myotube and subsequent skeletal muscle formation, consists of several characteristic stages. Specifically, myoblasts that have been induced to fuse first undergo myoblast recognition, where they become weakly associated with each other. This is followed by the adherence phase, where associations within the cell mass become stronger, therefore making it more difficult to disrupt the aggregate. The membrane union stage concludes the overall process, with myoblasts now being fully fused together. Several molecules are involved with adhesive interactions prior to myoblast fusion, including neural cell adhesion molecule (NCAM) which is upregulated in cells as the formation of myotubes commences. M-cadherin and N-cadherin are also thought to be involved, based on their changing expression levels during myoblast fusion and myotube formation, and the observation that cadherin monoclonal antibodies and polyclonal antisera inhibit myoblast association, therefore reducing myotube formation. However, both M-cadherin-null and N-cadherin-null mice show normal skeletal muscle development, contradicting the idea that these molecules play a key role during myoblast fusion (Abmayr et al., 2003).

Several other molecules implicated in the regulation of myoblast fusion have also been recently discovered. For example, melanoma cell adhesion molecule (M-CAM) is significantly downregulated in human myoblasts during fusion and *in vitro* studies show that inhibition of M-CAM expression using an M-CAM RNA knockdown technique led to enhanced levels of myoblast fusion (Cerletti et al., 2006). Horsley et al. (2003) reported a novel role for Interleukin-4 (IL-4), where signalling by the transcription factor NFATc2 in newly developed myotubes initiates IL-4 expression and secretion, helping to facilitate the fusion of myoblasts with pre-existing myotubes (Chargé & Rudnicki, 2003). Finally, myoferlin is significantly upregulated in myoblasts at the site of their fusion with pre-existing myotubes. Knocking this gene out of the genome produced null mice which still underwent the primary fusion events but displayed defects in their ability to form large myotubes, suggesting a role for myoferlin during the later stages of myogenesis (Doherty et al., 2005).

1.3.5. Skeletal Muscle Fibre Types

Primary and secondary skeletal muscle fibres can be further divided into different fibre types, including fast, slow and intermediate fibres. These can have different nomenculture depending on the species being referred to, but for the purposes of this thesis the murine nomenculture is used. Fast fibres, otherwise known as fast-twitch glycolytic or Type IIB fibres, are defined by their fast contraction speeds and large cross-sectional diameter. Energy production is predominantly by glycolysis, but large quantitities of adenosine triphosphate (ATP) are used during the contraction of fast fibres, and therefore any prolonged activity is maintained by anaerobic metabolism. However, fast fibres ultimately succumb to fatigue quite rapidly. In contrast, slow fibres,

which are also referred to as slow-twitch oxidative or Type I fibres, have significantly slower contraction speeds, taking up to three times as long to contract compared to a fast fibre. Unlike fast fibres, slow fibres contain large oxygen reserves bound to myoglobin, and coupled with the extensive capillary networks and increased numbers of mitochondria present in muscles composed of slow fibres, aerobic metabolism enables them to contract over longer periods of time compared to fast fibres. The intermediate fibres, also known as fast-twitch oxidative or Type IIA fibres, are the other class of skeletal muscle fibres. As their name suggests, they have properties midway between the fast and slow fibres. The original fibre type of the primary fibres during skeletal muscle development is slow, but some later change into fast fibres. Conversely, all secondary fibres start out being fast, and then some change into slow fibres. These conversions are mediated by a range of different factors and are restricted to specific locations in the developing limbs (Pullen, 1977a; 1977b; Martini, 1998; Wigmore & Dunglison, 1998).

1.4. Post-Natal Myogenesis

1.4.1. The Satellite Cell

1.4.1.1. Satellite Cell Morphology, Distribution and Origin

The majority of post-natal skeletal muscle growth, maintenance, repair and regeneration is facilitated through satellite cells which are specialised myogenic precursors located between the sarcolemma and basal lamina of mature skeletal muscle fibres (Hawke & Garry, 2001). Although originally considered unipotent, numerous studies have now shown satellite cells to be multipotent, with the ability to differentiate into myogenic, osteogenic and adipogenic lineages (Asakura et al., 2001). In addition to their characteristic position at the periphery of the fibre, satellite cells contain only a small amount of cytoplasm; they also have a reduced organelle content and a smaller nuclear size with significantly higher levels of heterochromatin than euchromatin, compared to fibre myonuclei**.** This morphology is consistent with the mitotically quiescent state that satellite cells predominantly adopt (Schultz, 1976; Hawke & Garry, 2001; Chargé and Rudnicki, 2004; Holterman & Rudnicki, 2005). These populations of cells have since been identified in all types of vertebrate skeletal muscle (Holterman & Rudnicki, 2005). However, within skeletal muscle, satellite cells show an unequal distribution between the different fibre types, with a higher proportion associated with the slow muscle fibres than the fast muscle fibres based on calculations using total nuclei number in muscle cross sections (Schmalbruch & Hellhammer, 1977; Gibson & Schultz, 1982; Chargé and Rudnicki, 2004).

These unique populations of cells were first discovered in the leg muscle of frogs (Katz, 1961; Mauro, 1961), and Mauro (1961) hypothesised that satellite

cells were simply dormant myoblasts left over from embryonic muscle development. Therefore, instead of fusing with other myoblasts to form myotubes and subsequent myofibres, solitary myoblasts remained in a quiescent state ready to provide additional nuclei if required during muscle growth and repair. Since this original proposal, the origin of satellite cells has been widely debated, with two main arguments emerging. The idea of a somitic origin is supported by traditional chimeric avian transplantation studies, where the development of quail-derived embryonic somites that had been introduced into a host chick embryo were found to produce migrating somitic cells that contributed to both the developing limbs and the post-natal skeletal muscle satellite cell population of the chick. This led to the conclusion that all myogenic cell lineages, including satellite cells, had a universal somitic origin (Armand et al., 1983). However, later studies challenged this idea in favour of an endothelial origin. De Angelis et al. (1999) isolated cells from mouse embryonic dorsal aorta and discovered their morphology and gene expression profiles closely resembled those of satellite cells. Furthermore, when these cells were transplanted into newborn mice, they worked in conjunction with the populations of satellite cells already present in the skeletal muscle, and successfully participated in post-natal muscle growth and regeneration. This therefore suggests there could be an endothelial origin for the satellite cell, or alternatively a derivation from a common satellite and endothelial cell precursor (Hawke & Garry, 2001).

1.4.1.2. Satellite Cell Quiescence

As previously mentioned in Section 1.4.1.1, satellite cells usually reside in a quiescent state, which is represented as G0 in the cell cycle. Quiescence is

typically characterised by minimal amounts of cell division, gene expression and protein synthesis (Dhawan & Rando, 2005; Le Grand & Rudnicki, 2007); however, recent lymphocyte studies by Yusuf and Fruman (2003) have challenged the original view that quiescence simply represents an inactive basal state depleted of any activation signals. Instead these authors suggested this state may actually be under active transcriptional control with several key regulatory molecules promoting the quiescent phenotype, such as lung Krüppel-like factor (LKLF) and the Forkhead Box (FOX) proteins.

Extensive histological studies carried out by Irintchev et al. (1994) led to the discovery that the calcium-dependent cell adhesion molecule, M-cadherin, is widely expressed among quiescent satellite cells. Further studies by Beauchamp et al. (2000) also identified CD34 and Myf-5 as novel markers expressed by the majority of these cells. The small proportion of satellite cells that do not express these markers are thought to be involved in maintaining the rest of the lineage-committed satellite cell population. CD34 is a widely accepted marker of adult hematopoietic stem cells that is commonly used in the isolation of these cells from blood and bone marrow. Two isoforms of CD34 exist. There is the truncated version, which lacks the three phosphorylation sites present in the intracellular domain of the full-length CD34 protein, and this is expressed in quiescent satellite cells. However, upon activation of the satellite cells, alternative splicing leads to a change in expression from the truncated form to the full-length version of CD34.

1.4.1.3. Satellite Cell Activation, Proliferation and Differentiation

Satellite cells are predominantly activated in response to trauma, weight-bearing or exercise-induced muscle injury, or for maintenance during muscle growth. As discussed earlier, this process involves the exit of satellite cells from the quiescent state and their re-entry into the cell cycle, specifically transitioning from the G0 to G1 phase. Following activation, these cells undergo numerous rounds of proliferation before continuing along the myogenic lineage, where they terminally differentiate and amalgamate together to form new myotubes and subsequent myofibres, or alternatively migrate and fuse to the damaged sections of pre-existing muscle fibres (Figure 1.2) (Morgan & Partridge, 2003; Chargé & Rudnicki, 2004; Dhawan & Rando, 2005). Reminiscent of skeletal muscle development from muscle precursor cells, the activation of satellite cells is accompanied by the expression of myogenic regulatory factors. Cooper et al. (1999) demonstrated that during the first 24 hours after activation, satellite cells upregulate MyoD or Myf-5 independently; and then these same factors are co-expressed in the subsequent 24 hour period. Myogenin expression follows later, with a significant proportion of activated satellite cells eventually expressing all four MRFs concurrently (Smith et al., 1994; Cornelison & Wold, 1997; Holterman & Rudnicki, 2005).

In addition to MRFs, numerous growth factors also function as positive and negative regulators of satellite cells and these factors are often produced by the injured fibres themselves, or by cells associated with the immune response. One of the founding experiments carried out in this field was by Bischoff (1986), who demonstrated the successful activation of quiescent satellite cells in cultured crushed muscle extract. Tatsumi et al. (1998) later identified SF/HGF

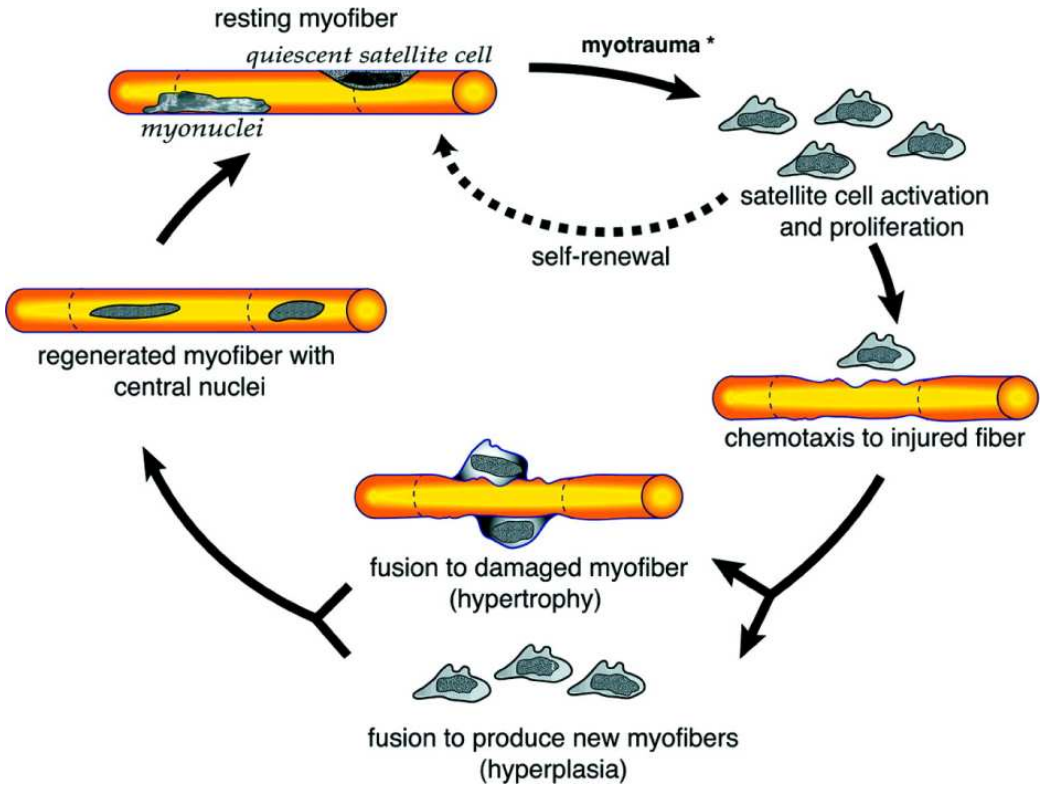

Figure 1.2: Satellite cell function

In response to myotrauma, satellite cells are activated to exit the quiescent state and re-enter the cell cycle where they proliferate and differentiate to repair muscle. Some satellite cells may undergo self-renewal to replenish the quiescent satellite cell pool (Hawke and Garry, 2001).

as the stimulus in the crushed muscle extract that was responsible for the satellite cell activation. Quiescent satellite cells express the tyrosine kinase receptor c-Met, which binds SF/HGF.

Furthermore, in the absence of muscle injury or trauma, the injection of SF/HGF into the *tibialis anterior* (TA) muscle of adult mice efficiently activated quiescent satellite cells. This led to the implication of nitric oxide (NO) in satellite cell activation, as this molecule is suggested to be involved in the release of SF/HGF from the extracellular matrix. Anderson (2000) reported a significant decrease in satellite cell activation post-trauma when nitric-oxide synthase-I (NOS-I), the molecule in the body which produces NO, was inhibited (Holterman & Rudnicki, 2005).

As well as the HGFs, insulin-like growth factors (IGFs), FGFs, and members of the TGF-β family have been extensively studied and shown to have varying effects on the satellite cell population *in vitro* (Allen & Boxhorn, 1989; Zentella & Massagué, 1992; Doumit et al., 1993; Johnson & Allen, 1995; Sheehan & Allen, 1999; Yablonka-Reuveni et al., 1999b; Chakravarthy et al., 2000). Allen and Boxhorn (1989) reported a significant increase in the differentiation of satellite cells in the presence of IGF-1, while FGF increased proliferation and decreased differentiation, and TGF-β decreased proliferation and inhibited differentiation. Furthermore, Sheehan and Allen (1999) studied eight members of the FGF family, FGF1, 2, and 4-9, and discovered that only FGF1, 2, 4, 6 and 9 significantly increased the proliferation of adult rat muscle satellite cells, while FGF5, 7 and 8 did not induce any mitogenic activity in the cells. In addition to their individual effects on the satellite cell population, HGFs, IGFs,

FGFs and TGF-β family members also appear to have a synergistic relationship with each other, and with other growth factors present in skeletal muscle. For example, the interaction of FGFs with IGF-1 or the platelet-derived growth factor-BB (PDGF-BB), results in significantly higher levels of satellite cell proliferation than the sum produced from each individual factor (Doumit et al., 1993). Similar observations were made when both HGF and either FGF2, 4, 6 or 9 were present (Sheehan & Allen, 1999).

Due to the complexity of the multi-step activation process and the numerous molecules involved, the exact signalling pathways and mechanisms which regulate the satellite cell population are yet to be fully defined. However, along with playing a key role in somite and muscle precursor formation, the Notch signalling pathway also appears to be involved in satellite cell activation. Conboy and Rando (2002) demonstrated that Notch-1 becomes activated as satellite cells transition from the G0 to G1 phase of the cell cycle; and that inhibition of Notch-1 by the cytoplasmic protein, Numb, prevents satellite cell activation. In addition, two different pathways are thought to be utilised by IGF-1 during satellite cell regulation, with the calcineurin/NFAT, mitogen-activated protein (MAP) kinase pathway implicated in satellite cell proliferation; and the phosphatidylinositol-3-OH kinase pathway involved with satellite cell differentiation (Coolican et al., 1997; Hawke & Garry, 2001). FGFs have also been shown to use the MAP kinase signalling pathway. Jones et al. (2001) identified the extracellular signal-regulated kinase (ERK) subfamily of the MAP kinase pathway as important for FGF-induced satellite cell proliferation, particularly the ERK1/2 signalling. However, the pathway involved in the depression of satellite cell differentiation by FGFs is not currently known

(Robinson & Cobb, 1997; Hawke & Garry, 2001). Finally, TGF-β family members use the Smad proteins for their signalling pathways, as discussed in Section 1.6.2 of this thesis (Whitman, 1998; Hawke & Garry, 2001).

1.4.1.4. Satellite Cell Self-Renewal

To prevent depletion of the satellite cell pool after repeated rounds of skeletal muscle repair and regeneration, it is suggested that satellite cells have the ability to self-renew. This idea is supported by radiolabel-tracing experiments which have clearly demonstrated the contribution of activated satellite cells to both new myonuclei and the quiescent satellite cell pool after muscle injury (Chargé & Rudnicki, 2004).

Different models have been proposed to explain the process of satellite cell self-renewal. Firstly, the stochastic model where each activated satellite cell divides symmetrically, with one of the subsequent daughter cells being able to relinquish its position in the differentiation programme and adopt a quiescent state, while the remainder continues along the myogenic lineage to terminal differentiation. Alternatively, each activated satellite cell may first divide asymmetrically producing one quiescent daughter cell to replenish the satellite cell pool while the other is committed to the myogenic pathway. The progeny which proceed with normal myogenesis may then undergo asymmetric divisions themselves to produce further satellite cells (Figure 1.3) (Chargé & Rudnicki, 2004; Dhawan and Rhando, 2005; Collins, 2006). Furthermore, Schultz (1996) explored the heterogeneous nature of the satellite cell population. Using bromodeoxyuridine (BrdU) labelling techniques in rat muscles, the author determined that approximately 80% of the population were labelled after five

days of continuous BrdU infusion, while the remaining 20% represented a more slowly dividing subset of cells. The authors therefore suggested that the capacity to self-renew could be restricted to a small proportion of the satellite cell population, as by limiting mitotic divisions the reserve population of satellite cells could conserve their proliferative capacity until required for muscle regeneration and repair.

Although none of these theories have been disproved, there is limited knowledge of the molecular mechanisms involved in regulating satellite cell self-renewal. However, Conboy and Rando (2002) recently investigated the regulation of Notch-1 by its antagonist, Numb; specifically looking at its role in myogenic cell-fate determination and the activation of satellite cells. The authors discovered that injury-induced activation of satellite cells produced a heterogeneous population of daughter cells that differed in their levels of Notch-1 expression. Further studies revealed this coincided with the asymmetric distribution of Numb in dividing satellite cells. A link between the level of Numb expression and satellite cell fate was therefore proposed, specifically that Numb may determine whether a daughter cell becomes committed to the myogenic lineage or adopts the quiescent state. However, the levels of Numb expression associated with each of these states is yet to be determined.

The myogenic regulatory factors Myf-5 and MyoD are also thought to play a role in the regulation of satellite cell self-renewal. As previously mentioned, mice deficient in MyoD show a reduced capacity for muscle regeneration. More specifically, increased levels of proliferation and reduced levels of

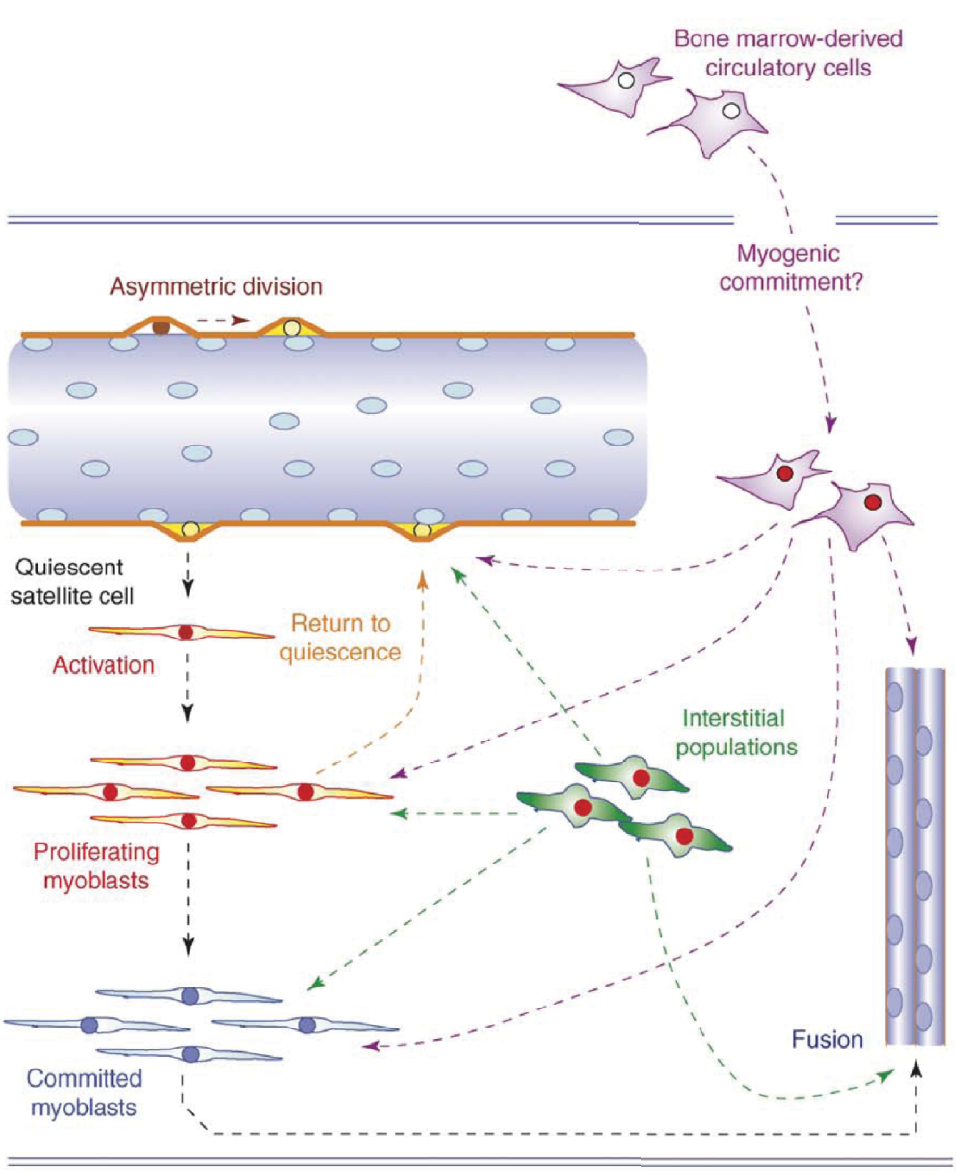

Figure 1.3: Mechanisms of satellite cell self-renewal

Satellite cells may undergo self-renewal via the return of an activated daughter cell to the quiescent state, or by asymmetric division. Other cell types, such as bone marrow-derived cells, may also contribute to the satellite cell population (Collins, 2006).

differentiation are associated with the MyoD-null phenotype. It has been suggested that an intermediate phase between quiescent satellite cells and muscle precursor cells is characterised by this MyoD-deficient phenotype. Furthermore, satellite cells are known to express either Myf-5 or MyoD upon activation and then co-express the two later; therefore leading to the hypothesis that Myf-5+/MyoD- cells represent a population of self-renewing satellite cells (Sabourin et al., 1999; Yablonka-Reuveni et al., 1999a; Cornelison et al., 2000; Chargé & Rudnicki, 2004).

1.4.2. Contributions of Other Cells

It is important to understand that although widely accepted, the satellite cell may not be solely responsible for skeletal muscle regeneration. Other stem cell sources may contribute directly to the quiescent satellite cell pool (Figure 1.3). For example, LaBarge and Blau (2002) recently used transplantation studies to demonstrate the ability of bone marrow-derived cells to give rise to functional muscle satellite cells capable of following a myogenic lineage and participating in skeletal muscle regeneration**.** Side population (SP) cells, which are a muscle-derived source of stem cells, have also been shown to contribute to skeletal muscle regeneration and to the quiescent satellite cell pool. SP cells do not display any key satellite cell markers and therefore represent a completely separate population of cells. However, myogenic colonies have been produced by the co-culturing of SP cells with myoblasts *in vitro* and SP cells have been shown to successfully contribute to the quiescent satellite cell pool following their intramuscular transplantation into skeletal muscle (Asakura et al., 2002; Holterman & Rudnicki, 2005).

1.5. The Inflammatory Response

In addition to the activation of satellite cells, the onset of the inflammatory response is also a key milestone in the highly synchronised sequence of events which occurs following muscle injury or increased muscle load. Although one of the primary functions of the inflammatory response is to provide a defence system against invading pathogens, its role in the tissue repair process, and particularly the regulation of wound healing by molecules secreted by the various types of immune cells, is of interest to this thesis (Park & Barbul, 2004; Tsirogianni et al., 2006).

In the event of muscle injury or increased muscle load, the sarcolemma of individual muscle fibres is usually damaged, resulting in various degrees of fibre necrosis and an overall disruption of the tendon-myofibre-tendon functional unit. The origin of the earliest inflammatory signals is not clear; however current evidence suggests that upon injury, the myogenic cells of the damaged muscle activate the inflammatory cells located within the muscle, and they in turn release substances such as adenosine, ATP and uric acid which act as chemoattractants to facilitate the migration of circulating inflammatory cells to the site of injury. In addition, the injury stimulates platelet-secretion of several growth factors which also aids in this process of inflammatory cell attraction (Tidball, 1995; Kääriäinen et al., 2000; Chargé & Rudnicki, 2004; Martin & Leibovich, 2005). Neutrophils are the first of these immune cells to arrive and their primary roles are to eradicate microbes from the area. They release proteases which aid in the degradation of cellular debris and thereby reduce the possibility of infection (Mutsaers et al., 1997; Park & Barbul, 2004; Martin & Leibovich, 2005; Tidball, 2005; Tsirogianni et al., 2006). However, it has been

suggested that in the process of destroying infectious agents at the injury site, neutrophils may also unwittingly damage healthy surrounding tissues through the release of high concentrations of cytotoxic and cytolytic molecules, such as hydrogen peroxide (Tiidus, 1998; Martin & Leibovich, 2005; Tidball, 2005; Butterfield et al., 2006).

Soon after the infiltration of neutrophils, tissue monocytes migrate to the wound site and differentiate into mature macrophages between 48 and 96 hours after injury (DiPietro, 1995; Park & Barbul, 2004). Macrophages are rapaciously phagocytic, removing any neutrophils from the wound area which have already undergone apoptosis, in addition to extracellular matrix and cellular debris (Martin & Leibovich, 2005). Founding studies carried out by Simpson and Ross (1972) and Leibovich and Ross (1975), which were later supported by Dovi et al. (2003), demonstrated the impaired ability of wounded guinea pigs to clear cellular debris after the administration of antimacrophage serum and steroids; as these compounds removed all circulating monocytes and tissue macrophages from the animals. Interestingly, when this study was repeated in guinea pigs depleted of neutrophils instead of macrophages, no adverse effects on tissue repair were observed. This led the authors to conclude that, unlike neutrophils, macrophages are essential for normal wound healing (Martin & Leibovich, 2005). Furthermore, Dovi et al. (2003) suggested that since neutrophils were not fundamental to the injury repair process, any chemokines released by these cells were thus redundant to wound healing, meaning other cells could produce large quantities of the same substances or some viable alternative.

In addition to their phagocytic abilities, macrophages also secrete various cytokines and growth factors which contribute to the regulation of wound healing. Examples of some of these substances include IGF-1, IL-1 and IL-6, leukemia inhibitory factor (LIF), platelet-derived growth factor (PDGF), TGF-alpha (TGF-α) and TGF-β, and tumor necrosis factor-alpha (TNF-α). These substances recruit other cells involved in wound repair, such as endothelial cells, and regulate fibroblast chemotaxis, proliferation and collagen synthesis. Therefore, macrophages play a key role in the formation of new blood vessels, fibrous tissue and matrix synthesis during wound repair (DiPietro, 1995; Mutsaers et al, 1997; Park & Barbul, 2004). Furthermore, macrophages express inducible nitric oxide synthase (iNOS), which has been shown to mediate wound closure and collagen deposition (DiPietro, 1995; Mutsaers et al, 1997; Park & Barbul, 2004).

Macrophage-released factors are also thought to be directly involved in the regulation of satellite cells. Lescaudron et al. (1993; 1997) discovered that the stimulation of macrophage infiltration in a transplantation model led to earlier activation of satellite cells. Furthermore, an increased proportion of MyoD-positive nuclei (a molecular marker for satellite cell proliferation) was observed in satellite cells co-cultured with macrophages. Of the plethora of substances released by macrophages, it was LIF and TNF-α which appeared to be responsible for stimulating proliferation of the satellite cells (Kurek et al., 1996; Merly et al., 1999).

1.6. Myostatin

The TGF-β superfamily is comprised of a diverse range of growth and differentiation factors that are involved in regulating both pre-natal and post-natal myogenesis. One of the key members of this group is myostatin, also known as growth and differentiation factor-8 (GDF-8), which is expressed in embryonic and adult skeletal muscle. Myostatin has been identified as a potent negative regulator of muscle growth (McPherron et al., 1997; Thomas et al., 2000).

1.6.1. Myostatin Structure and Expression

Myostatin shares a number of common features with the other members of the TGF-β superfamily. These include a secretory signal sequence consisting of a hydrophobic core of amino acids located near the N-terminus, a proteolytic processing site, and a conserved pattern of nine cysteine residues, which forms a distinguishing cystine knot structure at the C-terminus (Thomas et al., 2000; Jeanplong et al., 2001; Langley et al., 2002; Kambadur et al., 2004; Zhu et al., 2004). More specifically, Vitt et al. (2001) described how the presence of cysteine residues in amino acid chains is fundamental for disulfide bonding and loop formation, in order to generate a functional protein motif. Crystal structures have revealed that of the nine cysteine residues characteristic of TGF-β superfamily members, eight of them form four intrachain disulphide bonds which further conform into intertwining loops that create the knot structure, while the ninth cysteine residue forms an interchain disulfide bond which confers stability (Daopin et al., 1992; Sun, 1995). The cystine knot structure directs the three-dimensional arrangement adopted by the protein, which

subsequently exposes hydrophobic residues involved with the formation of homo- or heterodimers required for biological activity.

The myostatin gene itself is organised into three exons and two introns, and is translated as a full-length peptide that is synthesised in skeletal muscle in its precursor form, a 375 amino acid propeptide. The biologically active molecule is generated following two proteolytic processing events; the initial removal of the 24 amino acid signal peptide which is involved with the secretory pathway, and cleavage at the RSRR (Arg-Ser-Arg-Arg) site to produce a 39 kDa N-terminal Latency Associated Protein (LAP), and a 26 kDa carboxyl-terminal (C-terminal) mature myostatin molecule (Figure 1.4) (Thomas et al., 2000; Kambadur et al., 2004; Lee, 2004).

The myostatin sequence is highly conserved, with murine, rat, human, porcine, chicken and turkey species showing 100% homology of the active, proteolytically processed site; while baboon, bovine and ovine mature myostatin proteins differ only in one to three amino acids (McPherron & Lee, 1997; Kocamis & Killefer, 2002).

Expression of myostatin mRNA is first detected at day 9.5 post-coitum in approximately one third of mouse somites, specifically the most mature rostrally located ones. By day 10.5 post-coitum it is expressed in nearly every somite and appears to be limited to the myotome compartment. After further development, myostatin expression can be detected in the majority of developing muscles (McPherron et al., 1997; Kocamis & Killefer, 2002; Bishop et al., 2005). Myostatin expression in muscle appears to be fibre-type specific.

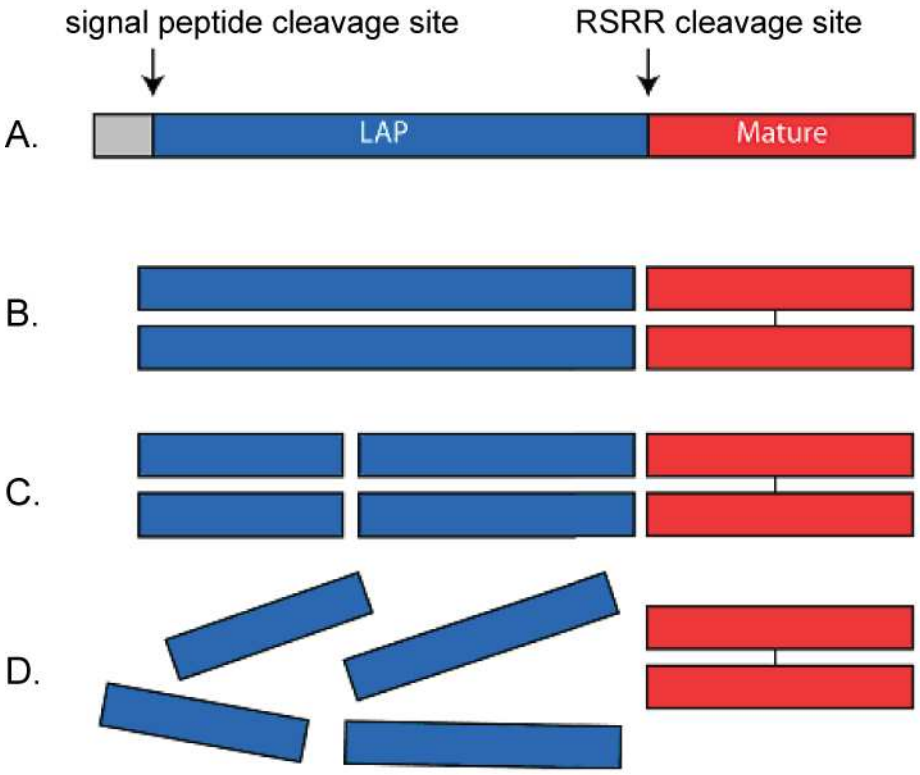

Figure 1.4: The structure of myostatin

A) The biologically active myostatin molecule is generated following two proteolytic processing events; the removal of the amino acid signal peptide, and cleavage at the RSRR site. **B)** After proteolytic processing, the C-terminal dimer remains noncovalently bound to the LAP, forming a latent complex. **C)** Proteolytic cleavage of LAP activates the latent myostatin **D)** The C-terminal dimer is released and thus capable of receptor binding. Adapted from Lee (2004).

The different types of skeletal muscle fibres can be characterised by different myosin heavy chain (MHC) isoforms (Linnane et al., 1999), and a strong correlation exists between myostatin expression and MHC type-IIb expression, which is associated with fast muscle fibres (Carlson et al., 1999; Senna Salerno et al., 2004; Bishop et al., 2005). Although myostatin is predominantly expressed in skeletal muscle tissue, it has also been detected at low levels in adipose tissue (McPherron et al., 1997), lactating mammary gland tissue (Ji et al., 1998), and in the cardiomyocytes and Purkinje fibres of the heart (Sharma et al., 1999).

1.6.2. Myostatin Signalling Pathways

Members of the TGF-β superfamily are secreted growth factors; therefore in order to elicit their biological effect they first need to bind to a receptor which subsequently activates a signal transduction cascade in the target cell (Kambadur et al., 2004; Lee, 2004). Lee and McPherron (2001) suggested that following proteolytic processing, the myostatin C-terminal dimer remains noncovalently bound to the LAP, forming a latent complex. Activation of latent myostatin occurs through the proteolytic cleavage of LAP at the RSRR site (Figure 1.4), after which the C-terminal dimer is capable of binding to its receptor, activin type IIB (Act RIIB). In addition, it can also bind Act RIIA, but to a lesser extent. Based on the signalling mechanisms of other TGF-β related ligands, the type-II receptor kinase is then thought to phosphorylate the recruited type-I receptor kinase, activin receptor-like kinase 5 (Alk5), which in turn phosphorylates the Smad proteins (Kambadur et al., 2004; Lee, 2004). The Smad proteins translocate to the nucleus and function as intracellular signal transducers to regulate the expression of downstream genes (Padgett et al., 1998;

Roberts, 1999; Lee, 2004; Zhu et al., 2004; Bishop et al., 2005). In particular, Zhu et al. (2004) identified Smad2, Smad3 and Smad4 as key molecules in myostatin signal transduction while Smad7 mediates a negative feedback mechanism involved in regulating myostatin signalling (Forbes et al., 2006).

1.6.3. The Function of Myostatin

1.6.3.1. Inactivation of Myostatin

As previously mentioned, myostatin has been identified as a potent negative regulator of muscle mass. McPherron et al. (1997) used gene targeting techniques to disrupt the myostatin gene in mice and reported that myostatin-null animals were significantly larger in size than their wild-type counterparts (Figure 1.5A). This increase in skeletal muscle mass was due to a combination of both hyperplasia (an increase in the number of muscle fibres) and hypertrophy (an increase in individual fibre diameter). The hypermuscularity observed in some cattle breeds, such as the Belgian Blue (Figure 1.5D) and Piedmontese has also been investigated. These breeds are defined by a double muscle phenotype which results in a 15 to 30% increase in muscle mass, but this is accompanied by birthing difficulties and other problems such as low stress tolerance and decreased female fertility (Potts et al., 2003).

The double-muscle phenotype was found to be the result of naturally occurring mutations which inactivate the myostatin gene (Grobet et al., 1997; Kambadur et al., 1997; McPherron & Lee, 1997). More specifically, an 11 base-pair (bp) deletion was found in the myostatin gene of Belgian Blue animals and this led to a frame-shift mutation resulting in premature translational termination of mysotatin. In contrast, a guanine to adenine transition in the myostatin gene was

found to be responsible for Piedmontese hypermuscularity. This caused a cysteine residue to be substituted for a tyrosine, ultimately disrupting the important cystine knot structure of the myostatin molecule, inactivating it (Kambadur et al., 1997; Berry et al., 2002). Recently, Shelton and Engvall (2007) also reported a myostatin mutation in a whippet dog displaying gross muscle hypertrophy (Figure 1.5C); and a human child with the heavy muscle phenotype has been found to carry a mutation in the myostatin gene, thought to be generated by the mis-splicing of myostatin precursor mRNA (Figure 1.5B) (Schuelke et al., 2004; Walsh & Celeste, 2005).

1.6.3.2. Mechanism of Myostatin Action

Numerous studies have suggested that myostatin functions by regulating myoblast proliferation and differentiation during early myogenesis (Thomas et al., 2000; Langley et al., 2002), followed by the control of satellite cell activation post-natally (McCroskery et al., 2003). Thomas et al. (2000) demonstrated a dose-dependent relationship between increasing levels of myostatin and decreasing levels of C_2C_{12} mouse myoblast proliferation. More specifically, myostatin was revealed to inhibit the progression of myoblasts from the G1 to S phase of the cell cycle. The authors proposed that myostatin signalling mediated this effect through an increase in the expression of p21, a CDK inhibitor. This was accompanied by decreased levels and activity of CDK2 protein, the principal cyclin-dependent kinase responsible for cell-cycle progression from the G1 to S phase. As a result, retinoblastoma (Rb) proteins accumulated, leading to myoblasts being detained at the G1 phase, and therefore inhibiting proliferation (Figure 1.6) (Langley et al., 2004).

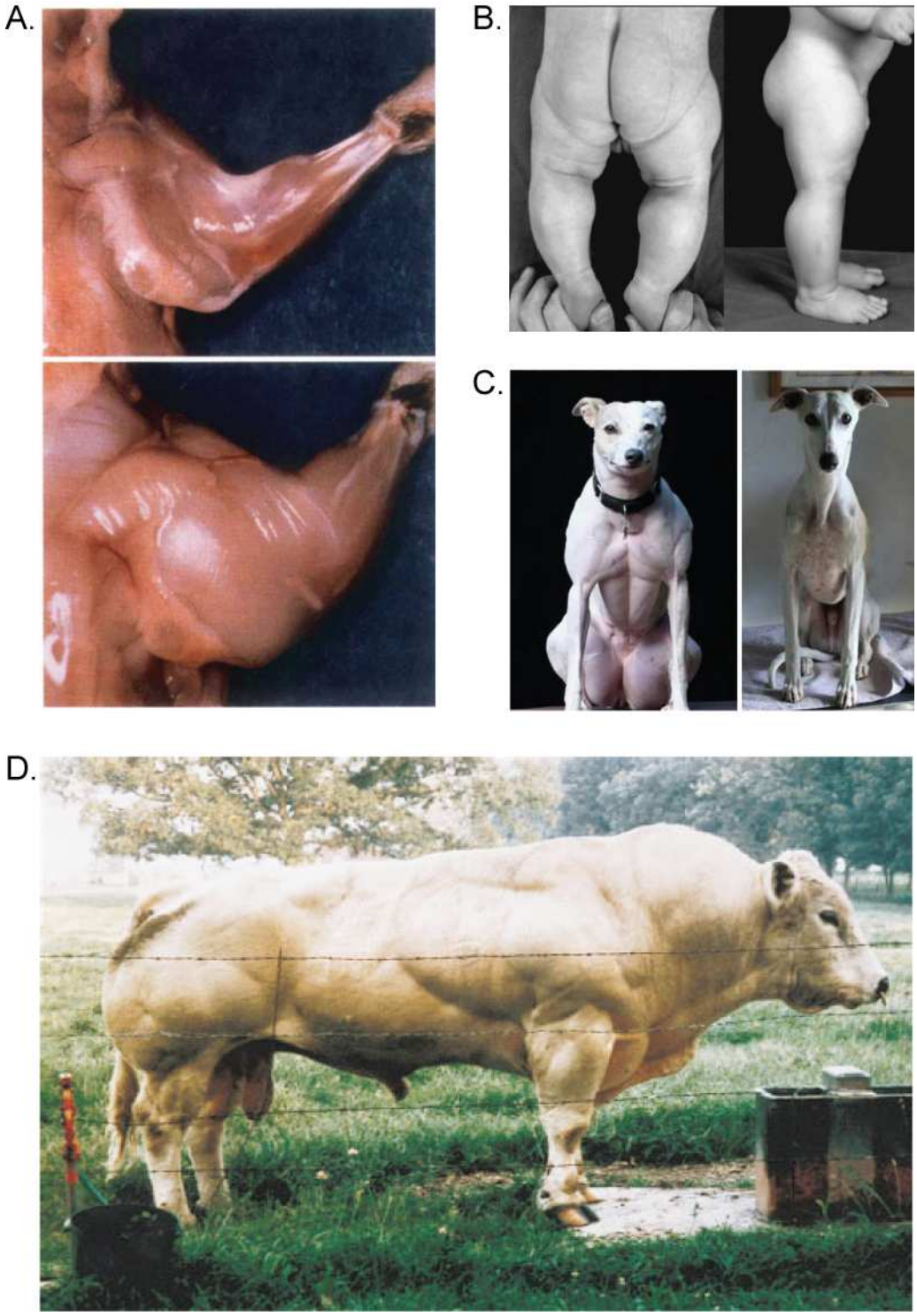

Figure 1.5: Inactivation of myostatin results in double-muscling phenotypes

A) Myostatin-null mice (bottom) show an increase in skeletal muscle mass compared to wild-type mice (top) (McPherron et al., 1997). **B)** Muscle hypertrophy in a human neonate (left) and at 7 months old (right), as a result of a myostatin mutation (Schuelke et al., 2004). **C)** A double muscled whippet dog (left) carries a homozygous mutation in the myostatin gene which is not present in wild-type animals (right) (Shelton and Engvall, 2007). **D)** A Belgian Blue bull showing the double muscle phenotype (McPherron and Lee, 1997).

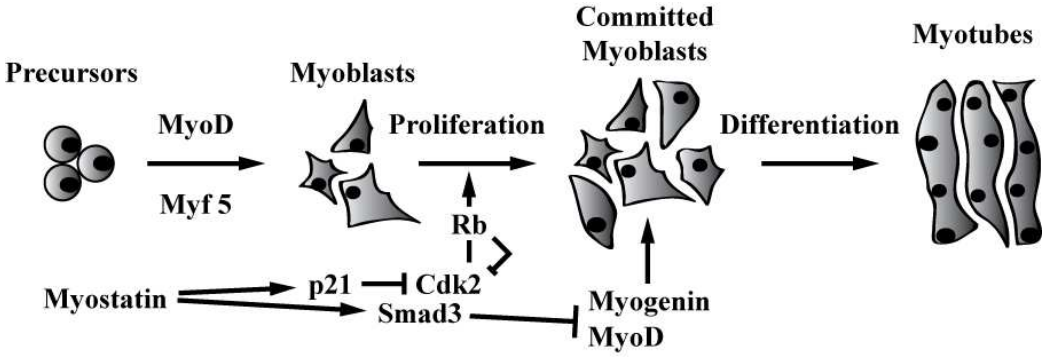

Figure 1.6: Mechanisms of myostatin action

Myostatin regulates myoblast proliferation and differentiation to myotubes through the control of cell-cycle progression. Increased levels of p21 and decreased levels of Cdk2 expression result in accumulated Rb protein which prevents entry into the G1 phase of the cell cycle. Likewise, myostatin signalling through Smad3 results in the decreased expression of myogenin and MyoD, therefore inhibiting myoblast differentiation (Langley et al., 2002).

In regard to the regulation of myoblast differentiation, Langley et al. (2004) recently demonstrated that when myoblasts were cultured in low serum media with increasing concentrations of myostatin, myogenic differentiation of the myoblasts was reversibly blocked. The authors determined that expression of the myogenic regulatory factors MyoD, Myf-5 and myogenin, along with p21, were significantly decreased in the presence of myostatin, thereby inhibiting myoblast differentiation (Figure 1.6). These results support the findings of Rios et al. (2002) and Joulia et al. (2003), who studied the effects of myostatin overexpression on stably transfected C_2C_{12} myoblasts, drawing similar conclusions.

In addition to the expression of myostatin in skeletal muscle fibres, myostatin has also been detected specifically in satellite cells, indicating a role in muscle regeneration and repair (McCroskery et al., 2003; Bishop et al., 2005). McCroskery et al. (2003) reported a significantly higher number of satellite cells per skeletal muscle fibre in myostatin-null mice compared to their wild-type counterparts; and a greater proportion of these cells were in an activated state. The authors suggested that, similar to the regulation of myoblast proliferation and differentiation, myostatin inhibits cell cycle progression, thereby maintaining satellite cells in a quiescent state. Furthermore, myoblasts isolated from myostatin-null mice were found to proliferate faster than wild-type myoblasts, implying that myostatin may also negatively regulate satellite cell self-renewal.

The intrinsic mechanisms involved in satellite cell regulation by myostatin are yet to be fully elucidated however, McFarlane et al. (2008) recently proposed a

model whereby myostatin negatively regulates the expression of the transcription factor Pax7, which in turn regulates satellite cell self-renewal. Pax7 is widely expressed in quiescent satellite cells, is co-expressed with MyoD during satellite cell proliferation, and is then down-regulated prior to differentiation. Pax7-null mice show a reduced capacity for regeneration, with a gradual decrease in satellite cell numbers as a result of cell cycle defects and increased levels of apoptosis (Kuang et al., 2006; Relaix et al., 2006; McFarlane et al., 2008).

1.6.4. Therapeutic Potential of Myostatin Antagonists

The establishment of myostatin as a potent negative regulator of muscle mass, muscle regeneration and muscle repair, has enabled the concept of myostatin antagonists to emerge in the realm of pharmacological therapies. More specifically, the ability to block myostatin function has enormous potential in the treatment of muscle injuries and the many muscle wasting conditions associated with age or disease. The Functional Muscle Genomics (FMG) group at AgResearch Ltd. have recently developed several myostatin antagonists by truncating the biologically active mature myostatin sequence, as shown in Figure 1.7.

Siriett et al. (2007) recently tested the myostatin antagonist, Mstn-ant1. Using a notexin injury model, the authors reported enhanced regeneration levels in Mstn-ant1 treated mice, facilitated through the earlier and increased response of macrophages, and the increased activation and migration of satellite cells, when compared to placebo-treated mice. These results support the findings of

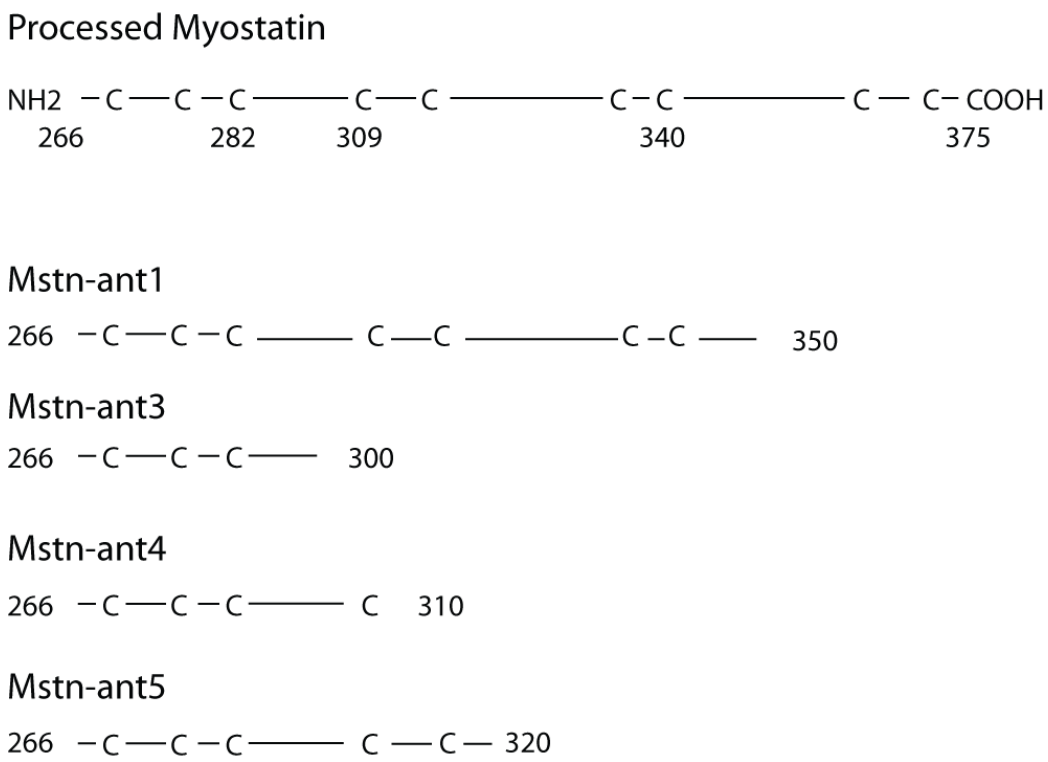

Figure 1.7: Myostatin antagonist truncations

The FMG group at AgResearch Ltd. have developed several myostatin antagonists by truncating the active mature myostatin sequence (processed myostatin) at different amino acid sites. Specifically, Mstn-ant1 was truncated at amino acid 350, Mstn-ant3 at amino acid 300, Mstn-ant4 at amino acid 310 and Mstn-ant5 at amino acid 320. Each antagonist varies in the number of cysteine (C) residues it contains.

McCroskery et al. (2005), who observed a similar response in notexin injured myostatin-null mice. Furthermore, both McCroskery et al. (2005) and Siriett et al. (2007) reported reduced levels of scarring after injury in the myostatin-null animals and wild-type mice treated with Mstn-ant1 respectively. Scarring is a by-product of the inflammatory response and subsequent stages of wound healing. Fibroblasts are attracted to the wound area via chemotactic signals released from the invading macrophages. They secrete growth factors and various extracellular matrix proteins, such as collagen, which aid in the repair of wounded tissue. Unfortunately, excessive amounts of fibrotic tissue are usually produced, forming a physical barrier which hinders skeletal muscle regeneration, resulting in scarring (Zhu et al., 2007; Li et al., 2008). Recent *in vitro* and *in vivo* studies carried out by Li et al. (2008), have revealed that myostatin directly regulates skeletal muscle fibrosis through the stimulation of both fibroblast proliferation and the production of extracellular matrix proteins.

The use of myostatin antagonists in the treatment of sarcopenia has also been investigated. Sarcopenia is the gradual loss of skeletal muscle mass and strength commonly associated with ageing. It is facilitated through impaired satellite cell function and myogenesis, leading to reduced levels of muscle regeneration. Recently, sarcopenia has been linked to myostatin, with studies showing a significant reduction in sarcopenia in myostatin-null mice (Siriett et al., 2006; 2007). Siriett et al. (2007) further studied the effects of short-term myostatin blockade on sarcopenia, using Mstn-ant1. The authors reported significantly increased levels of myogenesis after notexin injury in aged mice treated with Mstn-ant1, when compared to placebo-treated mice. In addition, grip strength measurements indicated that the administration of Mstn-ant1 significantly

increased the muscle strength of aged mice. Again, an earlier and increased response of macrophages and increased activation and migration of satellite cells was observed in the aged mice treated with Mst-ant1 following notexin injury.

An alternative myostatin antagonist, Mstn-ant3, is truncated at a different location to Mstn-ant1, and has been shown to attenuate muscle wasting in *mdx* mice (Kambadur et al., 2006c). This mouse model is representative of Duchenne and Becker muscular dystrophies, a chronic myopathy resulting in repeated rounds of muscle degeneration followed by incomplete regeneration, and ultimately leads to widespread fibrosis (Wagner et al., 2002). *Mdx* mice treated with Mstn-ant3 showed an overall improvement in dystrophic muscle morphology, with reduced areas of necrosis and increased regeneration. In addition, treatment of *mdx* mice with Mstn-ant3 led to decreased levels of creatine kinase (CK), a serum marker of muscle damage and breakdown, usually found at high levels in *mdx* mice. Grip strength measurements also indicated a significant improvement in the strength of dystrophic muscles over the treatment period (Kambadur et al., 2006c). These results reflect those of Bogdanovich et al. (2002) and Wagner et al. (2002) who studied the effect of myostatin-blocking antibodies on dystrophic muscles, and dystrophic muscle in myostatin-null *mdx* mice, respectively.

Studies have also been carried out on the role of myostatin in cachexia, a severe muscle wasting condition seen in many cancer and AIDS patients. Zimmers et al. (2002) demonstrated that systemic administration of myostatin protein in mice produced a muscle and fat-loss phenotype which paralleled that seen in

human cachexia conditions. It was recently suggested that the mechanism behind this myostatin-induced cachexia was the activation of the ubiquitin-proteasome pathway, via the regulation of the transcription factor FoxO1 by myostatin (McFarlane et al., 2006). The administration of the glucocorticoid Dexamethasone (Dex) in mice is a widely accepted laboratory model for cachexia. Ma et al. (2003) reported a significant upregulation in myostatin expression during glucocorticoid-induced muscle atrophy, while Gilson et al. (2007) demonstrated that absence of myostatin could prevent this atrophy. Studies have shown that the expression of Pax7 and MyoD was significantly decreased in mice treated with Dex; however this was reversed with the administration of Mstn-ant3 (unpublished data). These results suggest a potential role for myostatin antagonists in the alleviation of cachexia symptoms.

The actual mechanism of action for the myostatin antagonists is yet to be fully defined. However, it is thought that the antagonist may either form a heterodimer with endogenous myostatin, leading to the impaired ability of the heterodimer to signal through the Act RIIB receptor; or that the antagonist may directly bind to the receptor and therefore play a role in competitive binding (personal communication).

1.7. Objectives and Hypotheses

Myostatin has been identified as a potent negative regulator of muscle mass and functions by regulating myoblast proliferation and differentiation during early myogenesis; followed by the post-natal control of satellite cell activation (Thomas et al., 2000; Langley et al., 2002). In addition, myostatin is thought to inhibit muscle regeneration and repair (McCroskery et al., 2003). Therefore, the ability to block myostatin function has significant potential in the treatment of muscle injury and various muscle wasting conditions associated with age and disease. This concept has been supported by numerous studies carried out using myostatin-null mice, murine models of wound healing, such as notexin and incision injury, and murine models of muscle wasting, such as sarcopenia, *mdx* and glucocorticoid-induced cachexia (Bogdanovich et al., 2002; Zimmers et al., 2002; Wagner et al., 2002; Ma et al., 2003; McCroskery et al., 2005; Siriett et al., 2006; Gilson et al., 2007; Siriett et al., 2007; unpublished data). In addition, the recent development of myostatin antagonists has been a significant advancement in this field of study (Kambadur et al., 2006a; 2006b; 2006c; Siriett et al., 2007).

1.7.1. Development of the Muscle Burn Injury Model

Although various murine muscle injury models exist, there is currently no standardised murine muscle burn injury model. Therefore, a significant proportion of time and research for this thesis was dedicated to developing and testing the first murine muscle burn injury that could be utilised for both this thesis and future wound healing studies. When combined with existing injury models, the murine burn injury model enables a more accurate representation of

muscle wound healing, which is important for the development of pharmaceutical therapies that will aid in the wound healing process.

To develop this burn injury model, numerous different thermal injury techniques that have previously been developed and published were first reviewed. The severity of the burn wound produced by each technique ranged from partial-thickness to full-thickness (determined by the degree of damage to the epidermis, dermis and associated nerve endings) and from 3% to 40% total body surface area. Furthermore, a variety of animal species were used in the development of these burn injury models, including mice, rats, sheep and pigs.

Briefly, Stieritz and Holder (1975) originally isolated an area of shaved skin on the back of a mouse using a flame-resistant plastic card with a window in it. Ethanol was applied to the open area, ignited and allowed to burn for 10 s (Neely et al., 1999, Higashimori et al., 2005). These template devices have also been used with other burn agents, such as exposing the skin area in the window to 100ºC temperature water (Pawlik et al., 2003; Ballard-Croft et al., 2004). Gore et al. (2005) also explored the use of a Bunsen burner flame to produce a severe burn injury on the back and flanks of mice. This method was also used to produce a flame burn wound in sheep (Sakurai et al., 2002). Bairy et al. (1997) used an alternative approach, placing a metal cylinder on the back of a rat and pouring hot molten wax at a temperature of 80ºC down it. The cylinder was removed once the wax had solidified (approximately 8 min), leaving a consistent circular wound. Astrakas et al. (2005) and Padfield et al. (2005) described a less severe method, where the left hind limb of an anaesthetised

mouse was immersed in 90ºC water for 3 s, producing a scald injury that was only 3-5% of the total body surface area.

Other instruments have also been constructed to produce burn injuries. Most popular are brass bars, which are heated in 100ºC boiling water before being applied to the skin (Meyer & da Silva, 1999; Willis et al., 2005; Møller-Kristensen, et al., 2006; Møller-Kristensen, et al., 2007). Alternatively, brass plates heated in 100ºC boiling water were used to produce burn injuries on the sides of larger animals such as pigs (Papp et al., 2005). The use of lasers has also been explored, with the aim of producing burns of a consistent depth to reduce variability (Cohen et al., 2003). With regard to a thermal burn injury specifically to skeletal muscle, there appears to be only one entry in the literature. Toader-Radu (1978) passed a red-hot metallic needle through the skin of the hind limb of rats, and applied it to the surface of the TA muscle. However, this produced only a small burn area, lacking consistency in its severity.

For the purpose of developing a murine muscle burn injury model for this thesis, the methods outlined above were discussed with the Ruakura Animal Ethics Committee. Those involving the use of ignited ethanol and a Bunsen burner flame were not approved and some of the other techniques were not physically appropriate to use on skeletal muscle. In addition, some burn injury techniques had a higher risk of infection, which needed to be avoided.

1.7.2. *In vivo* Trial

In addition to developing a murine muscle burn injury model, this thesis describes the first *in vivo* trial using the myostatin antagonist, Mstn-ant4. Specifically, the ability of Mstn-ant4 to improve wound healing was evaluated using the murine muscle burn injury model. Results from this thesis contributed to a larger study being undertaken by the FMG group at AgResearch Ltd., with the aim of determining the efficacy of myostatin antagonists on different muscle regeneration conditions.

Three key techniques were used to analyse the results of the *in vivo* trial: histology, gene expression analysis using RNA, and immunocytochemistry.

The histological analysis focused on two established staining techniques, Haematoxylin and Eosin (H and E) and Van Geison. One of the characteristic features of skeletal muscle regeneration is the presence of centrally formed nuclei (CFN) in the muscle fibres (Brazelton et al., 2003), which can be detected using H and E staining. Following the burn injury, extensive skeletal muscle regeneration would be expected to occur and therefore an associated increase in CFN would be hypothesised. Van Gieson staining detects collagen deposition in a tissue. As discussed in Section 1.6.4 of this thesis, scarring forms as a result of excessive fibrotic tissue being produced during the inflammatory response and subsequent stages of wound healing. A key component of fibrotic tissue is collagen, and therefore Van Gieson staining can be used as an indicator for the level of fibrogenesis occurring in a tissue. Similar to CFN, an increase in the levels of collagen deposition over time would be expected as muscle regeneration progresses following the burn injury.

There are actually five different types of collagen present in adult skeletal muscle: types I, III, IV, V and VI (Listrat et al., 1999). Collagen types I and III are the most abundant of these and they each have specific localisations. Collagen type I is predominantly found in tendons and the epimysium, but can also appear in small quantities in the perimysium, while collagen type III is predominantly found in the perimysium (Duance et al., 1977). Methods including Semi-Quantitative PCR and Real-Time PCR use RNA to analyse the expression level of targeted genes in a specified tissue, and therefore these techniques were used to evaluate the gene expression levels of collagen types I and III for this thesis. An increase in both collagen types I and III gene expression would be expected to reflect the results of the Van Gieson staining. Furthermore, Garcia-Filipe et al. (2006) recently described a 'fibrotic index' used to evaluate the levels of fibrogenesis during wound healing following a skin burn injury. Specifically, the authors evaluated the ratio of collagen type III to collagen type I production and suggested that a relative increase in collagen type III could be indicative of extensive fibrosis.

In addition to collagen, the expression levels of four myogenic genes were also evaluated for this thesis; namely mighty, MyoD, myogenin and Pax7. Mighty, a downstream target of myostatin, is a novel gene that was discovered by the FMG group at AgResearch Ltd. during studies investigating the mechanisms by which myostatin negatively regulates muscle mass. Mighty was found to play a key role in the enhanced differentiation and hypertrophy of myoblasts, characteristic of reduced levels of myostatin expression (Marshall et al., 2008). Therefore, analysing mighty expression is a useful tool for evaluating the levels of myogenesis occurring in skeletal muscle. Previous analyses of mighty

expression in notexin and incision injury models (Senna Salerno et al., submitted) show mighty expression is first detectable at day 2 post-injury, followed by a peak in expression levels between days 5 and 7 post-injury, before a gradual decline in expression. For this thesis, a similar pattern of mighty gene expression would be expected following the burn injury.

As discussed in Section 1.3.3.1, MyoD and myogenin are MRFs that are essential for the growth of muscle during skeletal muscle development. More specifically, MyoD is involved with regulating the determination process, leading to the multipotent somite cells being committed to the myogenic lineage, while myogenin is involved with the initiation of myoblast differentiation which occurs later in the myogenic programme. Therefore the analysis of MyoD and myogenin expression are useful for evaluating the levels of myogenesis occurring in skeletal muscle, and we would expect MyoD expression to be upregulated earlier than myogenin expression, following the burn injury.

Section 1.4.1 of this thesis discussed the capacity of satellite cells to facilitate the majority of post-natal skeletal muscle growth, maintenance, repair and regeneration. Upon activation from the quiescent state, satellite cells co-express Pax7 and MyoD while they proliferate, and then down-regulate Pax7 prior to differentiation. In addition, to prevent depletion of the satellite cell pool, evidence suggests that satellite cells have the ability to self-renew, and Pax7 has been implicated in the regulation of this process (Kuang et al., 2006; Relaix et al., 2006; McFarlane et al., 2008). Recent studies have shown that myostatin negatively regulates the expression of Pax7 (McFarlane et al., 2008). Therefore,

analysing Pax7 expression can be a useful tool for monitoring regeneration via satellite cells in skeletal muscle. An increase in Pax7 gene expression would be expected following the burn injury; due to more satellite cells being activated to participate in muscle regeneration and also to undergo self-renewal in order to replenish the satellite cell pool that would have subsequently been depleted.

Finally, a key event of the inflammatory response is the infiltration of macrophages to the wound site and this was evaluated for this thesis using Macrophage antigen complex-1 (Mac1) immunocytochemistry (ICC). As discussed in Section 1.5, macrophages are rapaciously phagocytic, removing all cellular debris in preparation for fibre repair and new fibre formation. As a member of the leukocyte-specific beta (2) integrin family, Mac1 is involved with all aspects of the inflammatory response, including phagocytosis, chemotaxis, migration and adhesion (Mayadas & Cullere, 2005; Hu et al., 2008). In addition, evidence suggests that Mac1 plays a key role in inducing the NF-κB transcription factor signalling pathway, which leads to the production of inflammatory factors (Ingalls et al., 1998; Medvedev et al., 1998; Hu et al., 2008). Therefore one would expect the infiltration of macrophages to the site of burn injury to be quite substantial soon after the burn injury is inflicted to clear the area, and then gradually decline as skeletal muscle regeneration progresses.

1.7.3. Hypotheses

Overall, based on the results of previous studies using myostatin-null mice, murine models of muscle wound healing such as notexin and incision injury, and murine models of muscle wasting, such as sarcopenia, *mdx* and cachexia (Bogdanovich et al., 2002; Zimmers et al., 2002; Wagner et al., 2002; Ma et al.,

2003; McCroskery et al., 2005; Siriett et al., 2006; Gilson et al., 2007; Siriett et al., 2007; unpublished data), as well as those using other myostatin antagonists (Kambadur et al., 2006a; 2006b; 2006c; Siriett et al., 2007); it can be hypothesised that following a burn injury in mice, the administration of Mstn-ant4 would significantly improve wound healing compared to placebo-treated mice. Specifically, the levels of CFN and the number of CFN per fibre would be expected to be higher in the Mstn-ant4-treated mice, as well as higher expression levels of the myogenic genes and an increased and earlier migration of macrophages to the site of injury. On the other hand, collagen deposition detected by Van Geison staining, as well as the gene expression levels of collagen types I and III would be expected to be lower in mice treated with Mstn-ant4 compared to placebo-treated mice.

1.7.4. Objectives

The specific objectives for this thesis are as follows:

Objective 1: To develop a murine muscle burn injury model suitable for using in both this thesis and future wound healing studies.

Objective 2: To determine the efficacy of Myostatin-antagonist4 on wound healing following a severe muscle burn injury.

Chapter Two: Materials and Methods

2.1. Materials

2.1.1. Animals

Ten male mice of the wild-type strain C57 bl/6 were used for a pilot trial. These mice were approximately 12 months of age. A further 96 male mice of the wild-type strain C57bl/6 were used in the main *in vivo* trial. These mice were approximately 9 months of age. All animals were bred and housed at the Ruakura Small Animal Colony containment facility, and kept at a constant temperature of 20-22ºC, with a natural day/night cycle, and food and water available *ad libitum*. Approval from both the Ruakura Animal Ethics Committee and The University of Waikato Animal Ethics Committee was granted prior to any animal manipulations were carried out.

2.1.2. Oligonucleotide Primers

Oligonucleotide primers were designed for use in the Semi-Quantitative Polymerase Chain Reaction (PCR) and Real-Time PCR amplifications of cDNA, and were obtained from either Invitrogen or Sigma Aldrich. The oligonucleotides were initially re-suspended in 100 µl of MilliQ sterile water and stored at -20ºC, before being further diluted with MilliQ sterile water to a 10 µM working solution for use in PCR. All diluted primer aliquots were stored at -20ºC. The primer sequences used in this thesis are listed in Table 1.

2.1.3. Antibodies

Antibodies used for ICC in this thesis are listed in Table 2.

Table 1: Oligonucleotide Primers

Gene	Primer Sequence (5' to 3')	Product Size (bp)	Use
Collagen (Type I)	Fwd: ATGTCGCTATCCAGCTGACC Rev: AAGGGTGCTGTAGGTGAAGC	192	RT
Collagen (Type III)	Fwd: ATAAGCCCTGATGGTTCTCG Rev: CTTACGTGGGACAGTCATGG	195	RT
Mighty	Fwd: TGAAGCGGCCCATGGAGTTC Rev: GGTGGGCTGGTCCTTCTTCA	350	SQ
Mighty	Fwd: GATGAAGAAGGACCAGCCCAC Rev: TTGGCCTTGTCCCGTATCGC	217	RT
MyoD	Fwd: CGGCGGCAGAATGGCTACGA Rev: TGCAGTCGATCTCTCAAAGCACC	313	SQ & RT
Myogenin	Fwd: GAAAGTGAATGAGGCCTTCG Rev: AGATTGTGGGCGTCTGTAGG	308	SQ & RT
Pax7	Fwd: GCTGCCGGACTCTACCTACC Rev: CCAGCACAGCGGAGTGTTCC	571	SQ
Pax7	Fwd: ACAGCATCGACGGCATCCTG Rev: GTTACTGAACCAGACCTGCACG	272	RT
18S (HK)	Fwd: AACGTCTGCCCTATCAACT Rev: AACCTCCGACTTTGCTTCT	699	SQ
H3.3A (HK)	Fwd: GGCTCGTACAAAGCAGACTGCC Rev: GCAATTTCTCGCACCAGACG	225	RT

*HK = Housekeeping Gene *RT = Real-Time *SQ = Semi-Quantitative

Table 2: Antibodies

Antibody	Dilution	Source
Rabbit anti-Mighty peptide	1:100	AgResearch
Goat anti-Mac1	1:100	Santa Cruz
Biotinylated Donkey anti-Rabbit Ig	1:300	Amersham
Biotinylated Donkey anti-Sheep/Goat	1:300	Amersham
Alexa Fluor 488	1:400	Molecular Probes
DAPI	1:1000	Molecular Probes

2.1.4. Solutions

Common solutions used in this thesis were made according to Ausubel et al. (1987) and/or Lillie (1965) and are listed in the Appendix.

2.2. Methods

2.2.1. Pilot Trial

A pilot trial was undertaken to determine the conditions for the main *in vivo* trial, including duration and frequency of sample collection. Unfortunately, Orico Ltd., who was funding the Enterprise Scholarship for this research, had not decided which myostatin antagonist to focus on as a lead molecule at this stage, therefore, no antagonist could be tested in conjunction with the burn injury during the pilot trial. Based on animal availability at the time, C57bl/6 mice that were approximately 12 months of age were used.

2.2.1.1. Burn Injury

Mice were anaesthetised using the general anaesthetic ketamine hydrochloride (Class 2) xylazine hydrochloride (Class 2). An incision was made over the left TA muscle of the hind limb, and a red-hot metal rod 1.5 mm wide and 7 mm long was applied directly to the TA muscle for 5 s. The wound was closed with a surgical clip.

2.2.1.2. Sample Collection

Mice were allowed to heal for 5, 7, 14, 21, and 28 days post-injury. On each of these days two mice were sacrificed. The TA muscles were excised and processed for histological analysis by coating with Tissue Tek O.C.T compound (Sakura) and freezing in liquid nitrogen-cooled iso-pentane (BDH) for 10 s. Frozen TA muscles were stored at -80ºC until use.

2.2.2. *In vivo* Trial

Upon the successful completion of the pilot trial, the *in vivo* trial commenced. By this time, Orico Ltd. had decided to focus on the myostatin antagonist truncated at amino acid 310, termed Mstn-ant4, as a lead molecule so this was used for the *in vivo* trial. Ninety-six male mice of the wild-type strain C57bl/6 were used.

2.2.2.1. Production of Mstn-ant4

The myostatin antagonist used in this thesis was generated and purified by members of the FMG group at AgResearch Ltd. as described by Siriett et al. (2007). However, instead of being truncated at the amino acid 350, the biologically active mature myostatin sequence was truncated at amino acid 310. Briefly, a portion of bovine myostatin cDNA truncated at amino acid 310 was PCR-amplified and inserted into the cloning vector pET 16-B (Novagen). The myostatin coding sequence was placed in-frame with 10 histidine residues, which have a high affinity for nickel. The resulting construct was transformed into DH5α cells and then sequenced to verify the absence of mutations. A population of BL21 *E. coli* competent cells (Invitrogen) were then transformed with the recombinant myostatin expression vector, cultured in Luria Bertani (LB) broth for 12 h and 0.5 mM isopropyl thio-β-galactoside (IPTG) added to induce production of the myostatin antagonist protein. After collection via centrifugation, bacteria were re-suspended in lysis buffer and sonicated. The truncated protein was purified from the sonicated cell suspension using Ni-agarose affinity chromatography (Qiagen). To check the purity of the myostatin antagonist, the protein was run on a NuPAGE^{TM} 4-12% Bis-Tris gel (Invitrogen) and stained with Coomassie Blue stain (Figure 2.1).

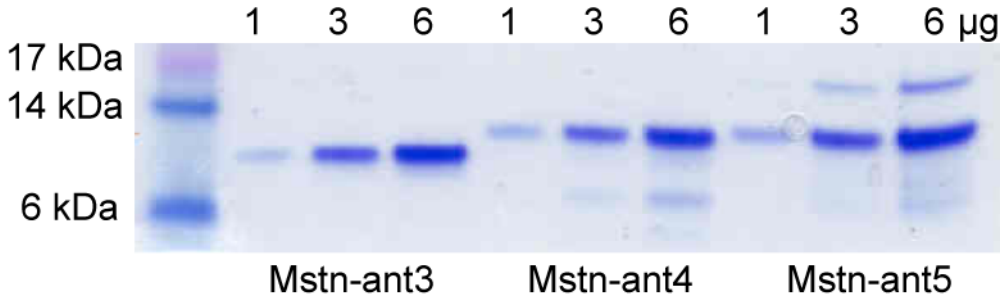

Figure 2.1: Coomassie blue stain of purified myostatin antagonists

Three purified myostatin antagonists developed by the FMG group at AgResearch Ltd. Mstn-ant3 is truncated at the amino acid 300, Mstn-ant4 at amino acid 310 and Mstn-ant5 at amino acid 320. As each of the myostatin antagonists were truncated at a different amino acid, the overall size (kDa) of each molecule is different, as reflected by their mobility on the gel. Furthermore, band intensity increased with increasing concentration (1 µg, 3 µg and 6 µg) of myostatin antagonist.

2.2.2.2. Burn Injury

Mice were subjected to the burn injury described for the pilot trial in Section 2.2.1.1 of this thesis.

2.2.2.3. Administration of Mstn-ant4 or Saline

Mice were injected subcutaneously with 6 µg/g body weight of saline or Mstn-ant4 on days 1, 3, 5, 7, 10 and 15 post-injury (Table 3).

2.2.2.4. Sample Collection

As shown in Table 3, mice were allowed to heal for 2, 4, 7, 14, 21, 28, 35 and 46 days post-injury. On each of these days, 6 saline-injected mice and 6 Mstn-ant4-injected mice were sacrificed. The body weight of the animal was recorded and both the left (burnt) and right (control) TA muscles were dissected out and weighed. For each collection day, the TA muscles from 3 of the saline and 3 of the Mstn-ant4-injected mice were processed for histological and ICC analysis, by coating the muscle in Tissue Tek O.C.T compound (Sakura) and freezing in liquid nitrogen-cooled iso-pentane (BDH) for 10 s. The muscle samples from the other 3 mice were frozen directly in liquid nitrogen for RNA extraction. All samples were stored at -80ºC until use.

Table 3: Injection and Sample Collection Schedule for the *In vivo* Trial

Day	**0**	**1**	**2**	**3**	**4**	**5**	**7**	**10**	**14**	**15**	**21**	**28**	**35**	**46**
Injection	INJURY	■		■		■	■	■		■				
Sample Collection			■		■		■		■		■	■	■	■

2.2.3. Histology

As described in Section 2.2.2.4, a proportion of the muscle samples obtained from the *in vivo* trial were reserved for histological analysis. In preparation, the 96 frozen TA muscles were cut on a Leica Cryocut 1800 and the resulting 10 µm thick sections placed on Esco POLYSINE microscope slides (Biolab Scientific). The slides were stored at -20ºC until use.

2.2.3.1. H and E Staining

The 96 TA muscle sections were defrosted at room temperature (RT) in a humid chamber. They were first submerged in Gill's haematoxylin stain for 4 min, and washed with tap water until the water ran clear. The slides were then submerged in Scott's tap water for 3 min and rinsed in tap water for 2 min. Slides were then stained in eosin for 2 min, washed with tap water until the water ran clear and then rinsed for a further 2 min with tap water. The muscle sections were then dehydrated by submerging the slides in an ascending ethanol series consisting of 50% ethanol for 30 s, 70% ethanol for 1 min, 95% ethanol for 1 min, and then twice in 100% ethanol for 2 min each. Finally the slides were submerged twice in xylene for 5 min each. Cover slips were mounted using xylene-based DPX mounting for microscopy (BHD). Muscle sections were viewed using a Leica AF6000 microscope (Leica Microsystems Ltd.) with an attached Leica DFC300FX digital camera. Images were captured using the Leica Application Suite Version 2.5.0.R1 software (Leica Microsystems Ltd.) and individually analysed using Image Pro-Plus 6.0 software.

2.2.3.2. Van Gieson Staining

The 96 TA muscle sections were defrosted at RT in a humid chamber. The muscle sections were first fixed in 10% formalin for 5 min at RT, and then washed twice with PBS for 4 min each time. Equal volumes of Weigert's iron haematoxylin solution A and solution B were then mixed, and used to stain the muscle sections for 10 min. The slides were then washed with tap water until the water ran clear, and then rinsed for a further 2 min with tap water. The muscle sections were then stained with Van Gieson solution for 10 min and rinsed quickly by dipping the slides into tap water three times. The muscle sections were then dehydrated by submerging the slides in an ascending ethanol series consisting of 50% ethanol with a few drops of picric acid for 30 s, 100% ethanol and picric acid for 1 min, 100% ethanol for 2 min and finally twice in xylene for 5 min each. Cover slips were mounted using xylene-based DPX mounting for microscopy (BHD). Muscle sections were viewed using a Leica AF6000 microscope (Leica Microsystems Ltd.) with an attached Leica DFC300FX digital camera. Images were captured using the Leica Application Suite Version 2.5.0.R1 software (Leica Microsystems Ltd.) and individually analysed using Image Pro-Plus 6.0 software.

2.2.4. Analysis of Gene Expression Using RNA

As described in Section 2.2.2.4, a proportion of the muscle samples obtained from the *in vivo* trial were reserved for RNA extraction, in order to carry out Semi-Quantitative and Real-time PCR reactions to analyse the expression levels of various genes.

2.2.4.1. RNA Extraction

Total RNA was individually extracted from the tissue of 96 TA muscles using TRIzol reagent (Invitrogen), following the manufacturer's protocol.

Each TA muscle was homogenised with 1 ml TRIzol per 50 mg of tissue and centrifuged at 12,000 × g for 10 min at 4ºC to pellet cellular debris. 200 µl of chloroform per 1 ml TRIzol was added and the samples incubated for 2-3 min before centrifugation at 12,000 × g for 15 min at 4ºC. The upper aqueous phase was then transferred to a clean Eppendorf tube and an equal volume of chloroform added. Tubes were then centrifuged at 12,000 × g for 15 min at 4ºC and the upper aqueous layer transferred to a clean tube. 500 µl of isopropanol per 1 ml of TRIzol was added to the aqueous phase and the samples were incubated at RT for 10 min, and then centrifuged at 12,000 × g for 10 min at 4ºC. The resulting RNA pellet was washed with 1 ml 75% ethanol made with diethyl pyrocarbonate (DEPC)-treated water, then centrifuged at 7,500 × g for 5 min at 4ºC. The RNA pellet was then air-dried for 5-10 min before being re-suspended in DEPC-treated water. Incubation at 55-60ºC for 10 min completed the re-suspension. RNA was stored at -80ºC until use.

2.2.4.2. First Strand cDNA Synthesis

cDNA for each of the 96 TA muscles was generated using the SuperScript First-Strand Synthesis System for RT-PCR (Invitrogen), according to the manufacturer's protocol.

1-5 µg of RNA was added to 1 µl of 10 mM dNTPs and 1 µl Oligo$(dT)_{12-18}$, then made up to 10 µl with DEPC-treated water. The sample was incubated at 65ºC

for 5 min and then chilled on ice for at least 1 min. To each reaction, 2 µl of 10x RT buffer, 4 µl 25 mM $MgCl_2$, 2 µl of 0.1 M DTT, and 1 µl RNase OUT Recombinant RNase Inhibitor was added, and then they were incubated at 42ºC for 2 min. 1 µl of Superscript II Reverse Transcriptase was added to each reaction and then incubated at 42ºC for a further 50 min. The reaction was terminated at 70ºC for 15 min and the samples chilled on ice. 1 µl RNaseH was added to each tube then incubated for a final 20 min at 37ºC. All cDNA was stored at -20ºC.

2.2.4.3. Semi-Quantitative PCR

PCR amplifications for 4 myogenic genes plus a housekeeping gene were carried out for each of the 96 TA muscles using Taq DNA Polymerase (Roche), following the manufacturer's protocol.

Each PCR reaction mix contained 1 µl of template cDNA, 5 µl of 10x PCR buffer + Mg^{++} (Roche), 1 µl of 10 mM dNTPs, 1 µl each of 10 µM forward and reverse primer (Table 1) for the specific gene product, 0.5-1 µl of Taq DNA Polymerase, and were made up to a total volume of 50 µl with MilliQ sterile water. In addition, each reaction mix for the PCR amplifications of 18S and mighty also contained 1 µl of 5x Q solution. Thermocycling of the PCR reactions was carried out using a BioRad DNAEngine Peltier Thermal Cycler (BioRad). For visualisation, 10 µl of each PCR reaction product was combined with 1 µl of 10x DNA loading dye and run on a 1% agarose gel with 5 µl of DNA 1kb+ ladder (Invitrogen) as a reference. Gels were exposed to UV light using a BioRad Gel Doc 2000. Images were captured and band density

measured using BioRad Quantity One 4.4.1 software. Analysis was by relative quantitation to the housekeeping gene, 18S.

The PCR amplifications were standardised using cDNA templates derived from control mouse TA muscle obtained during the *in vivo* trial. Various cycle numbers were used during standardisation to determine the linear increase in product during amplification. The PCR primers are listed in Table 1 and the PCR cycle conditions are listed in Table 4.

Table 4: Semi-Quantitative PCR Cycle Conditions

Product	Denaturation	Annealing	Extension	Cycle Number
Mighty	94°C, 20 s	60°C, 45 s	72°C, 1 min	28
MyoD	94°C, 30 s	60°C, 30 s	72°C, 2 min	26
Myogenin	94°C, 30 s	62°C, 30 s	72°C, 2 min	32
Pax7	94°C, 30 s	60°C, 30 s	72°C, 2 min	33
18S	95°C, 20 s	55°C, 45 s	72°C, 1 min	8

2.2.4.4. Real-Time PCR

Real-Time PCR amplifications were carried out for 6 genes plus a housekeeping gene, for each of the 96 TA muscles using LightCycler FastStart DNA Master^{PLUS} SYBR Green 1 (Roche), following the manufacturer's protocol.

Each Real-Time PCR reaction mix contained 3 µl of template cDNA, 0.5 µl each of 10 µM forward and reverse primer (Table 1) for the specific gene product, 2 µl LightCycler Master Mix (Roche), and were made up to a total volume of 10.5 µl with MilliQ sterile water. In addition, each reaction mix for the Real-Time PCR amplifications of Pax7 also contained 1 ul of PCRx. These

reaction mixes were loaded into precooled LightCycler capillaries and amplified using the LightCycler Carousel-Based system (Roche). Absolute quantitation and melting curve analyses were carried out using the LightCycler Software Version 4.0. These were based on standard curves generated using a series of dilutions with known concentrations of cDNA templates derived from control mouse TA muscle from the *in vivo* trial. The Real-Time PCR primers are listed in Table 1 and the Real-Time PCR cycle conditions are listed in Table 5.

Table 5: Real-Time PCR Cycle Conditions

Product	Denaturation	Annealing	Extension	Cycle Number
Mighty	95^{o}C, 5 s	60^{o}C, 10 s	72^{o}C, 10 s	45
MyoD	95^{o}C, 5 s	60^{o}C, 10 s	72^{o}C, 10 s	45
Myogenin	95^{o}C, 5 s	60^{o}C, 10 s	72^{o}C, 10 s	45
Pax7	95^{o}C, 5 s	60^{o}C, 10 s	72^{o}C, 10 s	45
H3.3A	95^{o}C, 5 s	60^{o}C, 10 s	72^{o}C, 10 s	45

2.2.5. Analysis of Gene Expression Using Protein

In order to produce a statistically significant result, all muscle samples obtained from the *in vivo* trial were used for histological analysis and analysis of gene expression using RNA. Due to limitations on the number of mice available for the *in vivo* trial and the Animal Ethics Committee not granting approval to inflict burn injuries on both hind limbs of each animal, there were no samples left to independently extract protein using the normal protocol used in the FMG laboratory. However, an alternative protocol was attempted using the phenol/ethanol phase normally discarded during the RNA extraction described in Section 2.2.4.1 of this thesis.

2.2.5.1. Protein Extraction from Phenol/Ethanol Phase

Protein was extracted from the Phenol/Ethanol phase following the manufacturer's protocol (Invitrogen).

To remove DNA, 0.3 ml of ethanol was added to the phenol/ethanol phase left over from the TRIzol RNA extraction, mixed by inversion and incubated at RT for 2-3 min. Tubes were then centrifuged at 5000 × g for 5 min at 4ºC. The supernatant was transferred to a round-bottom test-tube. To precipitate the protein, 3 ml of acetone was added to each tube and incubated at RT for 10 min, before centrifuging at 10,000 × g for 10 min at 4ºC. To wash the protein, the supernatant was removed and the pellet washed 3 times with 0.3 M guanidine hydrochloride (GuHCl) in 95% ethanol. For each wash, 2 ml of the GuHCl solution was used and the protein pellet was broken up using a pipette tip. The pellet was stored in the GuHCl wash solution for 20 min at RT and then centrifuged at 7,500 × g for 5 min at 4ºC to reacquire the pellet. After the final wash, the protein pellet was vortexed in 2 ml of 100% ethanol, left in the solution for 20 min at RT and then centrifuged at 7,500 × g for 5 min at 4ºC to reacquire the pellet. The protein pellet was then redissolved by removing the ethanol and air-drying the pellet for 30 min at RT. 500 µl of 1% sodium dodecyl sulphate (SDS) was added to each tube, incubated at 50ºC for 10 min then centrifuged at 10,000 × g for 10 min at 4ºC. The supernatant was transferred to a 1.7 ml eppendorf tube and centrifuged at 12,000 × g for 10 min at 4ºC. The supernatant was then transferred to a new tube. Protein was stored at -20ºC until use.

2.2.6. ICC

As described in Section 2.2.2.4, a proportion of the muscle samples obtained from the *in vivo* trial were reserved for ICC. In preparation, the 96 frozen TA muscles were cut on a Leica Cryocut 1800 and the resulting 10 µm thick sections placed on Esco POLYSINE microscope slides (Biolab Scientific). The slides were stored at -20ºC until use.

2.2.6.1. Mighty ICC

The 96 tissue sections were thawed in a humid chamber for 5-10 min and then an outline circle was drawn around each section with a PAP pen (Zymed Laboratories Inc). Sections were blocked with PBS-T + 0.2% bovine serum albumin (BSA) + 10% normal donkey serum (NDS) for 2 hours at RT in a humid chamber. The primary rabbit anti-Mighty antibody was added at 1:100 in PBS-T + 0.2% BSA + 5% NDS and the sections were left overnight at 4ºC in a humid chamber. As a negative control, primary antibody was not added to one section. The following day, the primary antibody was removed and the slides washed three times in PBS for 4 min each wash. Sections were then fixed in 10% buffered formalin for 5 min at RT in a humid chamber and then washed three times in PBS for 4 min each wash. The secondary Amersham biotinylated donkey anti-rabbit antibody was added at 1:300 in PBS-T + 0.2% BSA + 5% NDS and left for 1 hour at RT in a humid chamber. The secondary antibody was then removed and the slide rinsed in PBS, washed three times in PBS-T for 4 min each time and then rinsed in PBS again. The tertiary Molecular Probes Alexa fluor 488 antibody was added at 1:400 in PBS-T + 0.2% BSA and left for 1 hour at RT in a dark humid chamber. The tertiary antibody was then removed and the slides washed two times in PBS for 4 min each wash. To counterstain,

DAPI was added to each section at 1:1000 in PBS for 5 min at RT in a dark humid chamber and then the slides were washed twice in PBS for 4 min each wash. Slides were then dried and coverslips mounted with DakoCytomation fluorescent mounting medium (Med-bio Ltd). Slides were stored wrapped in tinfoil at 4^{o}C. Muscle sections were viewed using a Leica AF6000 microscope (Leica Microsystems Ltd.) with an attached Leica DFC300FX digital camera. Images were captured using the Leica Application Suite Version 2.5.0.R1 software (Leica Microsystems Ltd.) and individually analysed using simple visual estimation.

2.2.6.2. Mac1 ICC

The 96 tissue sections were thawed in a humid chamber for 5-10 min and then an outline circle was drawn around each section with a PAP pen (Zymed Laboratories Inc). Sections were blocked with PBS-T + 0.2% BSA + 10% NDS for 30 min at RT in a humid chamber. The primary goat anti-Mac1 antibody was added at 1:100 in PBS-T + 0.2% BSA + 5% NDS and the sections were left overnight at 4ºC in a humid chamber. As a negative control, primary antibody was not added to one section. The following day, the primary antibody was removed and the slides washed three times in PBS for 4 min each wash. Sections were then fixed in 10% buffered formalin for 5 min at RT in a humid chamber and then washed three times in PBS for 4 min each wash. The secondary Amersham biotinylated donkey anti-sheep/goat antibody was added at 1:300 in PBS-T + 0.2% BSA + 5% NDS and left for 1 hour at RT in a humid chamber. The secondary antibody was then removed and the slide rinsed in PBS, washed three times in PBS-T 0.2% for 4 min each time and then rinsed in PBS again. The tertiary Molecular Probes Alexa fluor 488 antibody was added

at 1:400 in PBS-T + 0.2% BSA and left for 1 hour at RT in a dark humid chamber. The tertiary antibody was then removed and the slides washed two times in PBS for 4 min each wash. To counterstain, DAPI was added to each section at 1:1000 in PBS for 5 min at room temperature in a dark humid chamber and then the slides were washed twice in PBS for 4 min each wash. Slides were then dried and coverslips mounted with DakoCytomation fluorescent mounting medium (Med-bio Ltd). Slides were stored wrapped in tinfoil at 4^{o}C. Muscle sections were viewed using a Leica AF6000 microscope (Leica Microsystems Ltd.) with an attached Leica DFC300FX digital camera. Images were captured using the Leica Application Suite Version 2.5.0.R1 software (Leica Microsystems Ltd.) and macrophages individually counted using Image Pro-Plus 6.0 software.

2.2.7. Statistical Analysis

Due to the skewed nature of the raw data, natural log (ln) transformations were applied to all data prior to statistical analysis. Analysis of variance (ANOVA) was then carried out on the transformed data, with each response variable, treatment (saline versus Mstn-ant4), muscle condition (burn versus control), time (days after injury) and their interactions followed at each individual time point by Student t-tests, using the pooled standard error from the ANOVA.

Chapter Three: Results

3.1. Development of the Muscle Burn Injury Model

For the purpose of developing a murine muscle burn injury model for this thesis, several previously published burn injury methods (see Section 1.7.1) were discussed with the Ruakura Animal Ethics Committee. The use of lasers would have been the preferred method to produce consistent burn injuries; however this type of equipment was not available at the time of the *in vivo* trial. Therefore, a cold burn injury was developed and tested, which involved a pellet of dry ice being applied to the exposed TA muscle of a mouse for 30 s. However, this did not generate a sufficient burn injury to the muscle. A branding method using a metal bar (1.5 mm wide and 7 mm long) was then adopted, where the bar was cooled in liquid nitrogen and then applied to the exposed TA muscle of the mouse for 30 s. Again, this did not produce the expected damage to the muscle because the metal bar was too small to retain the cold temperature, but the size of the bar was limited by the small size of the mouse TA muscle. The use of drops of liquid nitrogen directly onto the TA muscle was then discussed, but it was predicted this would produce a burn injury of inconsist size. Therefore a hot burn injury model was eventually designed and tested. Specifically, the metal bar was heated in a Bunsen burner flame until it was red-hot and then applied to the exposed TA muscle of the mouse for 5 s. A severe burn injury was produced, as shown in Figures 3.1 and 3.2. Approval for this method was granted by both the Ruakura Animal Ethics Committee and the University of Waikato Ethics Committee.

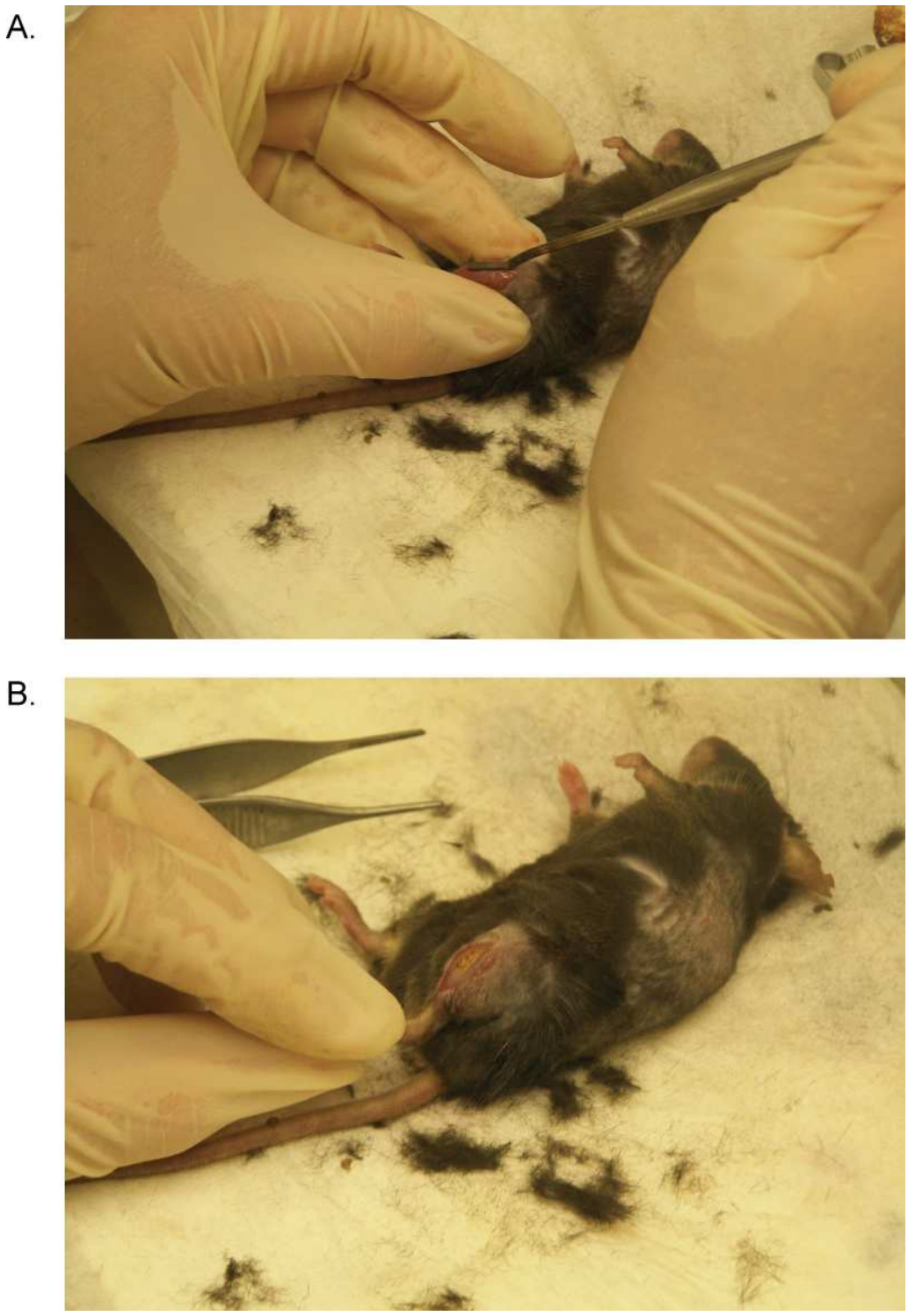

Figure 3.1: The murine muscle burn injury model

A) A red-hot metal rod 1.5 mm wide and 7 mm long was applied directly to the TA muscle of anaesthetised mice for 5 s. **B)** This produced a severe burn injury to the muscle.

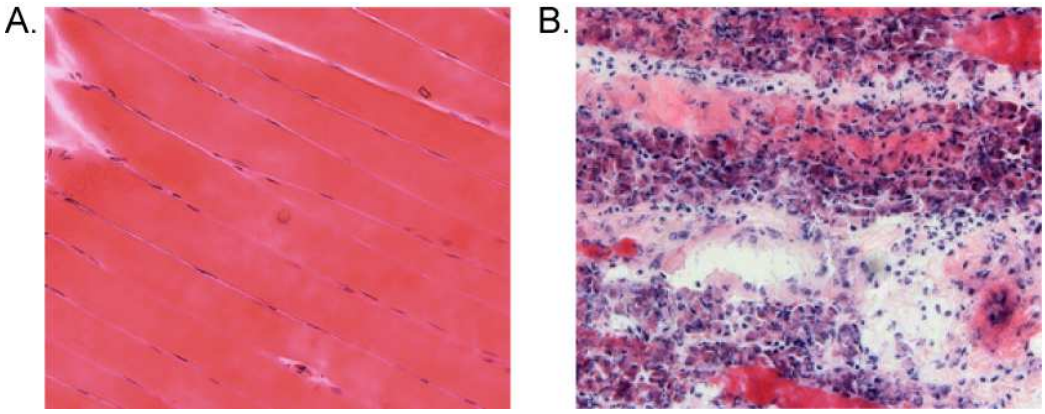

Figure 3.2: Burn injury damage to mouse *tibialis anterior* muscle

A) Haematoxylin and eosin staining of uninjured muscle. Muscle fibres are stained pink and nuclei are stained purple. **B)** Applying a red-hot metal rod to the TA for 5 seconds produced a severe burn injury. Images were taken on day 2 post-injury. Magnification: 200x.

As discussed in Section 2.1.1 of this thesis, mice that were approximately 9 months of age were used for the *in vivo* trial. Studies have shown that the regenerative capacity of skeletal muscle decreases with age, and this is related to a decrease in satellite cell number and activity (Shefer et al., 2006; Le Grand & Rudnicki, 2007). Therefore, younger mice would recover quite quickly from the burn injury and any improvements in wound healing as a result of Mstn-ant4 administration would be difficult to detect. In contrast, at 9 months of age, skeletal muscle regeneration occurs more slowly in mice, allowing the effect of Mstn-ant4 administration on wound healing and muscle regeneration to be more accurately evaluated.

3.2. Pilot Trial

A pilot trial was carried out with the assistance of Mônica Senna Salerno of the FMG group, to determine a suitable duration for the main *in vivo* trial and the frequency of sample collection. A previous notexin injury trial undertaken by the FMG group at AgResearch (Siriett et al., 2007) spanned a time period of 0 to 28 days and so this same duration was used for the pilot trial. However, results suggested that due to the severity of the burn injury, the main *in vivo* trial should be extended to 46 days to allow adequate healing. In addition, the frequency of sample collection needed to be slightly modified, with the earliest time-points changed to days 2 and 4 post-injury instead of day 5, to ensure no early regeneration events were missed.

3.3. *In vivo* Trial

3.3.1. Effect of Muscle Burn Injury on Body and Muscle Weight

The body weight of each of the 96 mice involved in the *in vivo* trial was recorded on the day of injury (day 0) and then again on the day of euthanasia. As shown in Figure 3.3, a decrease in body weight was observed in both the saline-treated and Mstn-ant4-treated mice in the first 2 weeks following the burn injury. The Mstn-ant4-treated mice recovered from this weight loss earlier than the saline-treated mice, with body weight exceeding original levels by day 21 post-injury, while the saline-injected mice still showed a decreased body weight. However, both the saline-treated and Mstn-ant4-treated mice displayed erratic patterns of weight gain or weight loss at the subsequent time points. Overall, there was no significant difference in body weight change between the saline-treated and the Mstn-ant4-treated mice during the course of the *in vivo* trial.

The weight of both the left (burnt) and right (control) TA muscle for each of the 96 mice involved in the trial were also measured at the time of excision. ANOVA analysis revealed no significant differences between the weight of the saline-treated and Mstn-ant4-treated burnt TA muscles. Similarly, no significant treatment differences were found when the control muscles were compared (Figure 3.4). Within each treatment group the burnt TA muscles appeared to decrease in weight over time in relation to the control TA muscles. Figure 3.5 shows the saline-treated burnt TA muscles weighed significantly less ($p<0.01$) than the control TA muscles at days 28 and 46. While the Mstn-ant4-treated burnt TA muscles were significantly lower in weight than the control muscles at days 21 and 28 ($p<0.05$) and days 35 and 46 ($p<0.01$) post-injury. However,

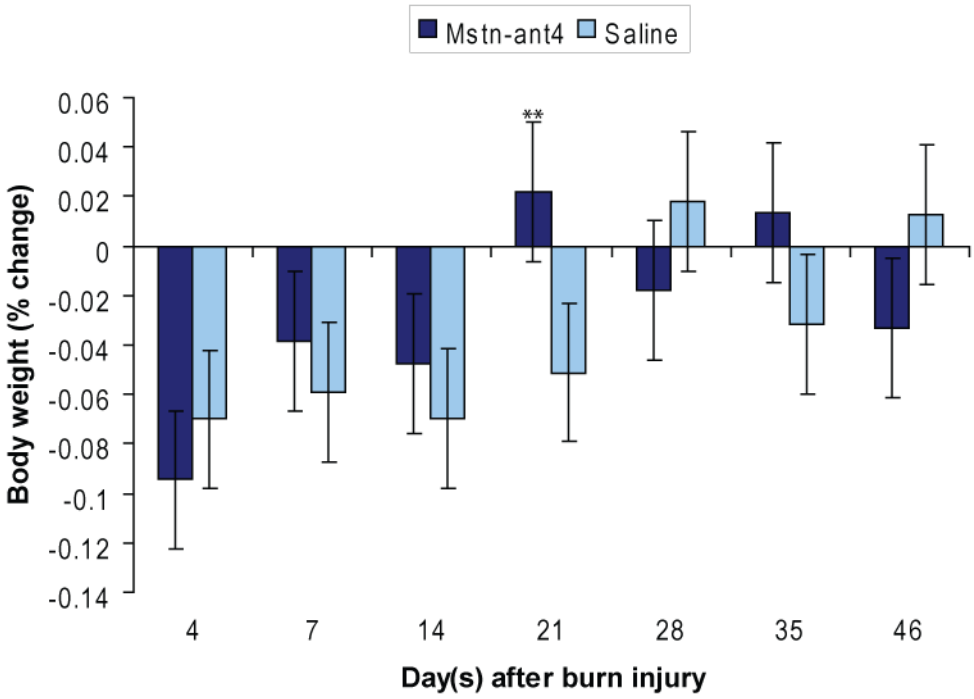

Figure 3.3: Change in body weight during muscle regeneration following burn injury

Over the first 14 days following burn injury, a decrease in body weight was observed in both the saline-treated (light bars) and Mstn-ant4-treated (dark bars) mice. The Mstn-ant4-treated mice recovered from this weight loss earlier than the saline-treated mice (day 21), but the erratic pattern of weight loss and weight gain at the subsequent time points leads to no significant treatment differences in body weight change overall. Values represent the mean of 6 animals ± SED. SED calculated as the pooled standard error of all animals. Weight change is relative to the animal's weight at Day 0. **$p<0.01$ by Student's t-test.

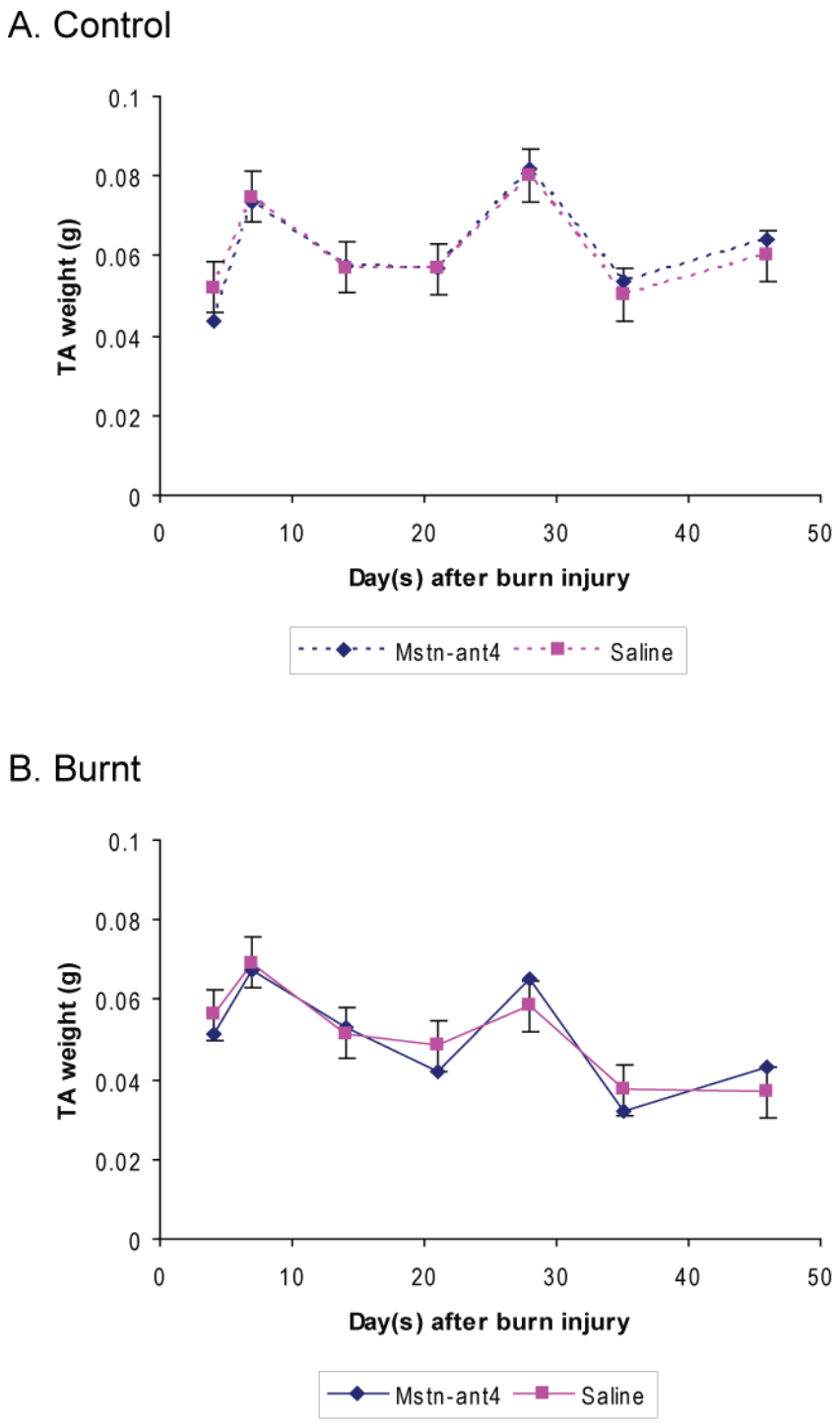

Figure 3.4: Comparison of right and left *tibialis anterior* weights between the two treatment groups

A) There were no significant differences in the weights of the right (control) TA muscles between the saline-treated and Mstn-ant4-treated mice over the trial period. **B)** There were no significant differences in the weights of the left (burnt) TA muscle between the saline-treated and Mstn-ant4-treated mice over the trial period. Values represent the mean of 3 animals ± SED. SED calculated as the pooled standard error of all animals.

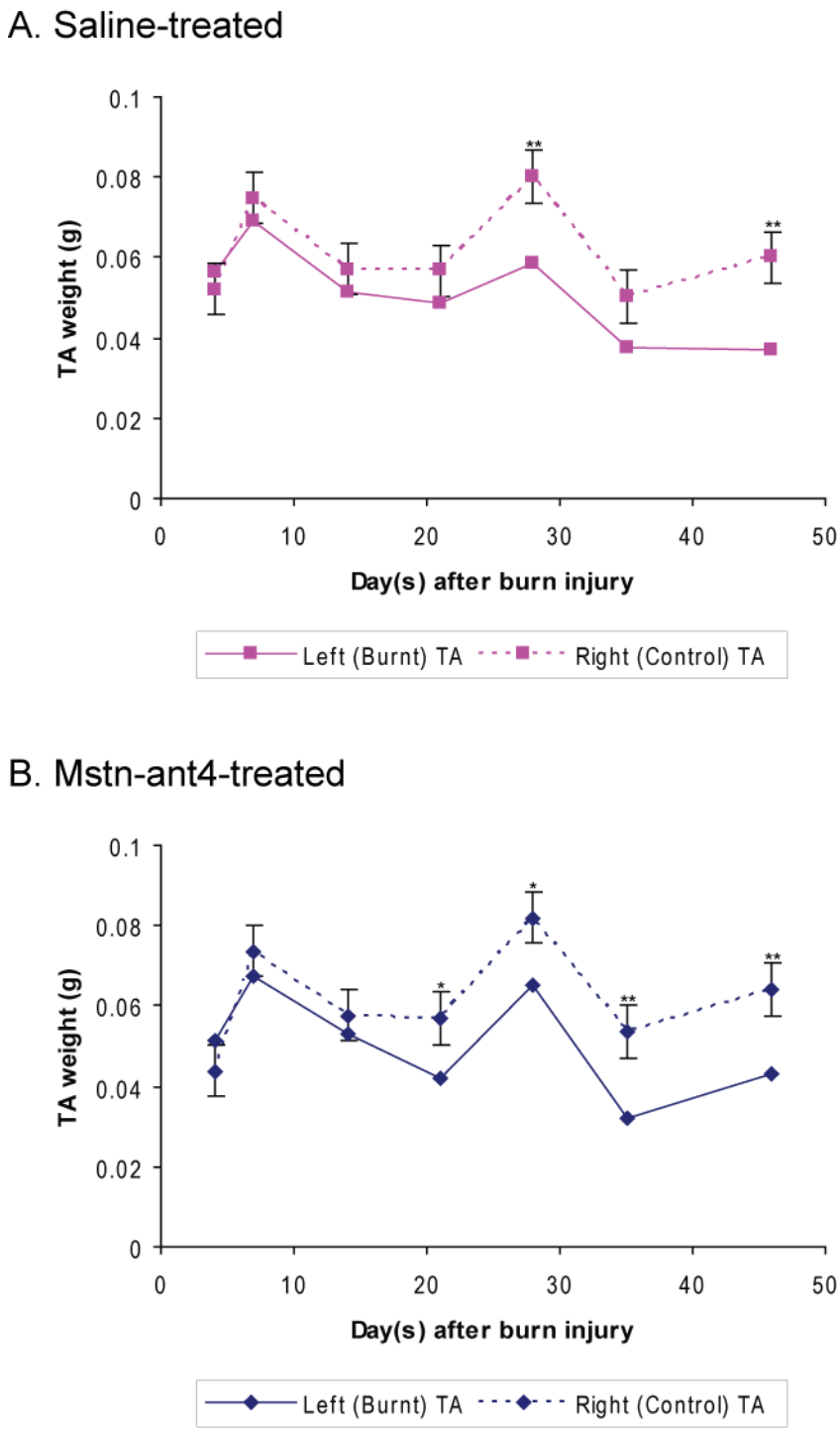

Figure 3.5: Change in weight of *tibialis anterior* during muscle regeneration following burn injury

A) The weight of the saline-treated burnt TA muscles were significantly lower than the control TA muscles at day 28 and 46 post-injury. **B)** The weight of the Mstn-ant4-treated burnt TA muscles were significantly lower than the control TA muscles at day 21, 28, 35 and 46 post-injury. However, no overall significant treatment differences were detected by ANOVA analysis. Values represent the mean of 3 animals ± SED. SED calculated as the pooled standard error of all animals. *p<0.05 and **p<0.01 by Student's t-test.

ANOVA analysis detected no overall differences between the weights of burnt and control muscles over time, for both the saline-treated and Mstn-ant4-treated animals.

3.3.2. Effect of Burn Injury on the Histological Profile of Muscle

3.3.2.1. CFN

The presence of CFN in skeletal muscle fibres is one of the key features which characterise skeletal muscle regeneration (see Section 1.7.2). Figure 3.6 shows the expected steady increase in the number of CFN present in the muscle fibres of both the Mstn-ant4 and saline-treated mice following the burn injury. From day 21 onwards, the number of CFN present in the burnt muscle for each treatment group was significantly higher ($p<0.001$) than that of their respective control muscles. When the burnt and control muscles are analysed independently (Figure 3.7) there is some variation between the Mstn-ant4 and saline-treated control muscles. There were significantly fewer numbers of CFN at days 21 ($p<0.05$), 28 ($p<0.001$) and 35 ($p<0.05$) post-injury in Mstn-ant4-treated mice compared to the saline-treated mice. This lead to a slight treatment effect being detected by ANOVA analysis, which suggested higher levels of CFN were generated from the saline-treatment overall. However, when the number of CFN in the burnt muscles was analysed, no overall treatment differences were detected despite the saline treated mice initially showing a higher level of CFN than the Mstn-ant4 treated mice. Interestingly, by day 46 post-injury it appeared that the burnt muscle from Mstn-ant4-treated mice had slightly more CFN than the saline-treated, but this difference is not statistically significant. The number of muscle fibres containing CFN showed very similar trends to those described for the absolute number of CFN (data not shown).

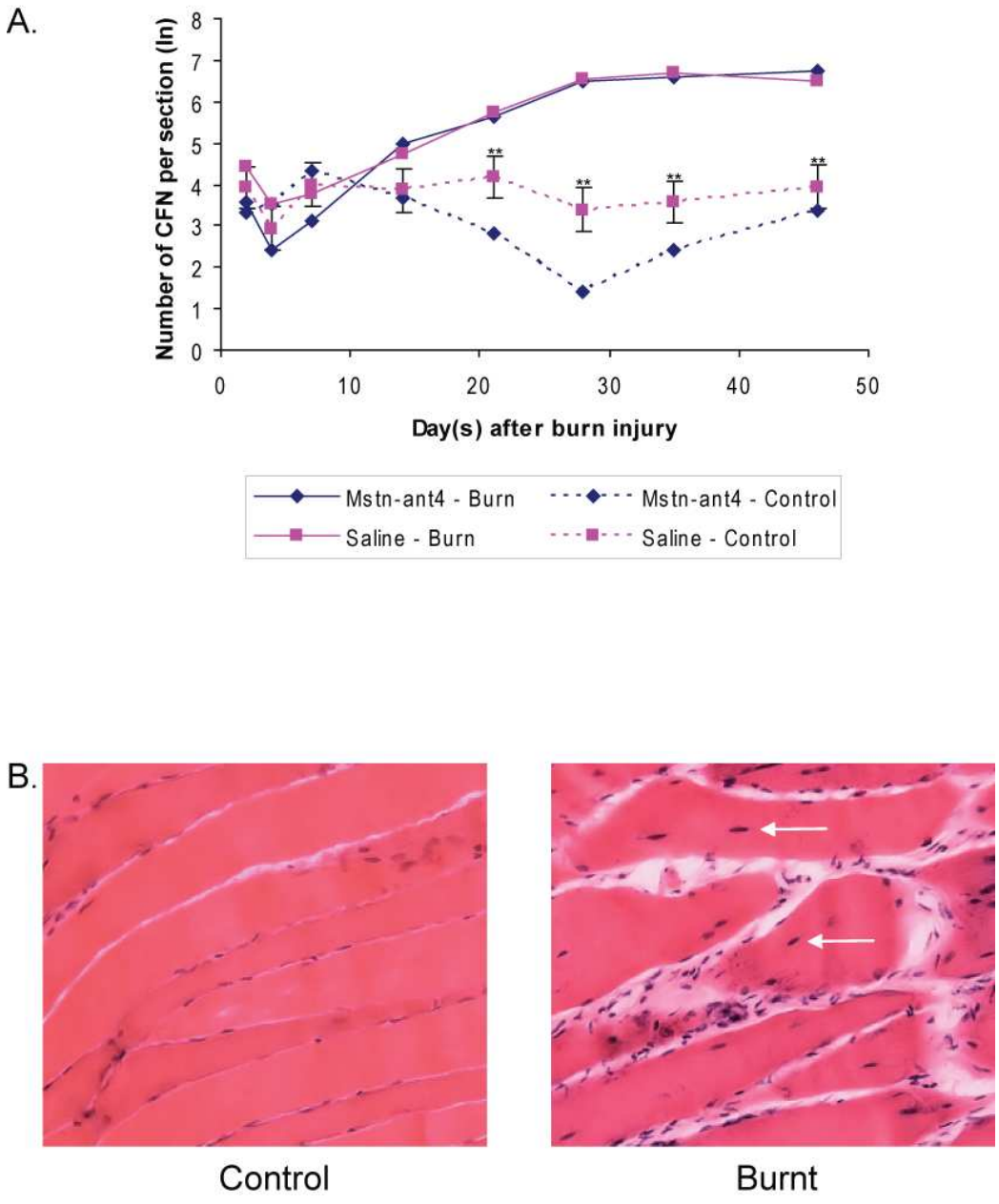

Figure 3.6: Centrally formed nuclei in the control and burnt muscles of Mstn-ant4 and saline-treated mice.

A) The number of CFN in the muscle fibres of both Mstn-ant4 and saline-treated mice increased following the burn injury. From day 21 onwards, the number of CFN in the burnt muscles was significantly higher ($p<0.001$) than the respective control muscles. Values represent the mean of 3 animals ± SED. SED calculated as the pooled standard error of all animals.**$p<0.01$ by Student's t-test. **B)** White arrows highlight some CFN in the burnt muscle of Mstn-ant4-treated mice at day 28 post-injury, which are not present in the corresponding control muscle. Magnification: 200x.

A. Control

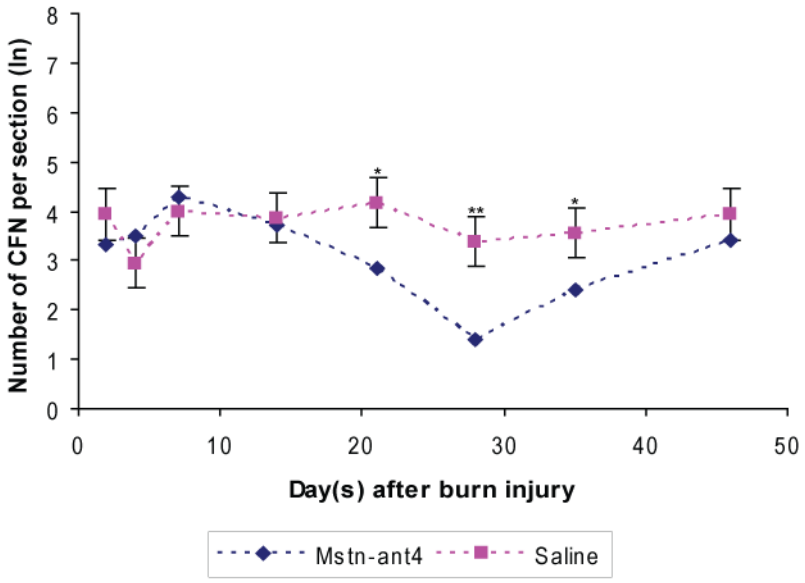

B. Burnt

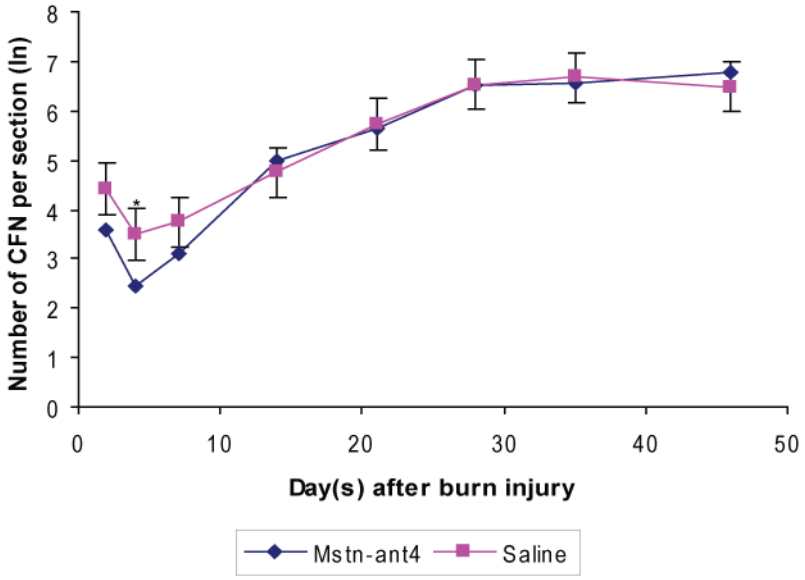

Figure 3.7: Centrally formed nuclei in the control and burnt muscles of Mstn-ant4 and saline treated mice.

A) Variability exists between the number of CFN in the treatment controls. The number of CFN in Mstn-ant4-treated mice were significantly lower than the saline-treated mice at day 21 ($p<0.05$), 28 ($p<0.001$) and 35 ($p<0.05$) post-injury. **B)** In the burnt muscles, saline-treated mice appeared to initially have more CFN than the Mstn-ant4-treated mice. However, no overall significant treatment differences were detected by ANOVA analysis. Values represent the mean of 3 animals ± SED. SED calculated as the pooled standard error of all animals. *$p<0.05$ and **$p<0.01$ by Student's t-test.

In addition to analysing the absolute values of CFN and the number of fibres containing CFN, the ratio of CFN to CFN fibre number was also examined for both treatment groups. No significant differences between the CFN to CFN fibre ratio in Mstn-ant4 and saline-treated mice were found in the control muscles (Figure 3.8). However, Figure 3.8 shows that the CFN to CFN fibre ratio was signficantly lower ($p<0.05$) in the burnt muscle of Mstn-ant4-treated mice at day 4 post-injury compared to the saline-treated mice. At day 14 post-injury this was reversed, with the Mstn-ant4-treated mice having a significantly higher ($p<0.01$) ratio of CFN to CFN fibre number than the saline-treated mice. However, no overall treatment differences were detected by ANOVA analysis.

The ratios of CFN and CFN fibre number to the damaged area of the burnt muscle sections were also evaluated. In both instances, the Mstn-ant4-treated and saline-treated mice showed very similar trends with no significant treatment differences detected, except for a slightly higher ($p<0.05$) CFN fibre number to damaged area ratio at day 46 post-injury in the Mstn-ant4-treated mice (data not shown).

3.3.2.2. Fibrogenesis

As discussed in Section 1.7.2 of this thesis, Van Gieson staining can be used as an indicator for the level of fibrogenesis occurring in a tissue, by specifically detecting levels of collagen deposition. As collagen deposition is not one of the initial stages of the inflammatory response, a gradual increase would be expected over time. Figure 3.9 shows this steady increase in the levels of collagen present in the tissues of both the Mstn-ant4 and saline-treated mice following the burn injury. From day 21 onwards, the amount of collagen

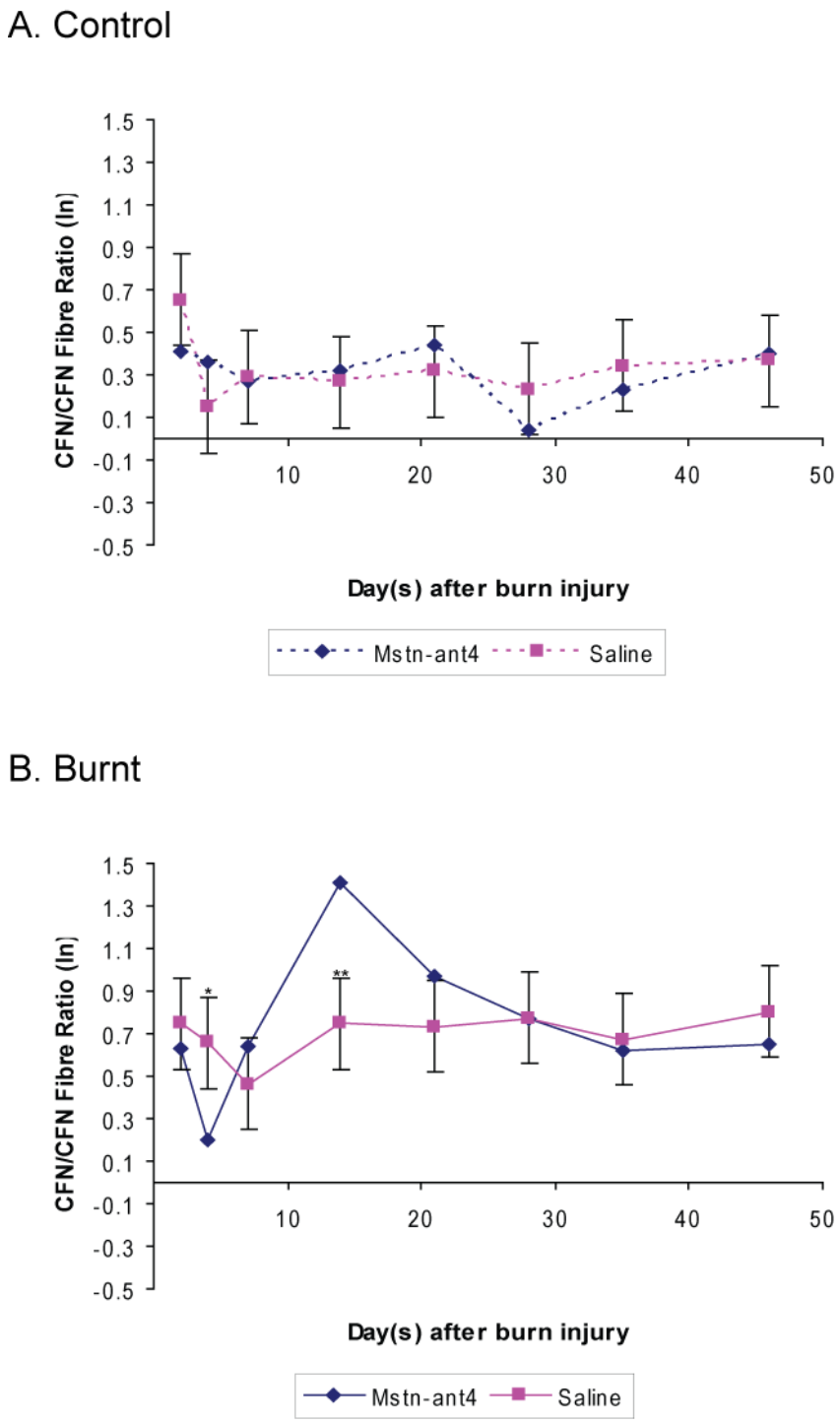

Figure 3.8: The ratio of CFN to CFN fibre number in the control and burnt muscles of Mstn-ant4 and saline-treated mice.

A) There were no significant treatment differences between the CFN/CFN fibre ratio in the control muscles of Mstn-ant4 and saline-treated mice. **B)** At day 4 post-injury, the CFN/CFN fibre ratio was significantly higher ($p<0.05$) in the burnt muscles of saline-treated mice, compared to the Mstn-ant4-treated mice. This was reversed at day 14 post-injury ($p<0.01$). However, no overall significant treatment differences were detected by ANOVA analysis. Values represent the mean of 3 animals ± SED. SED calculated as the pooled standard error of all animals. *$p<0.05$ and **$p<0.01$ by Student's t-test.

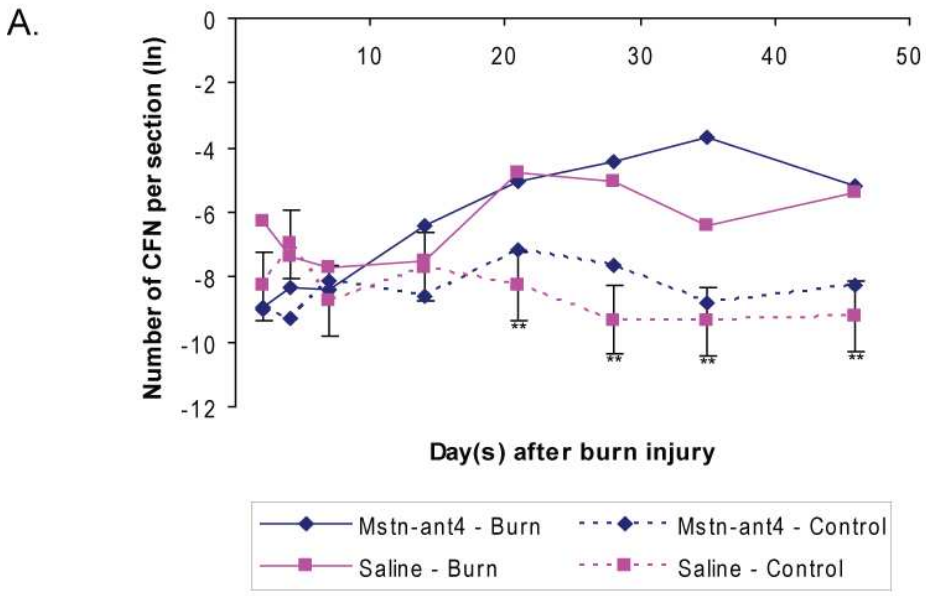

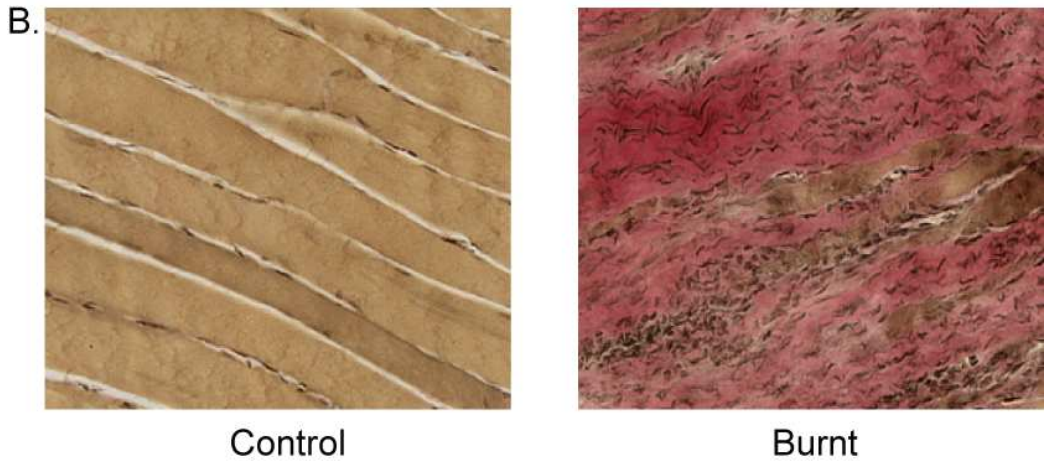

Figure 3.9: Collagen deposition in the control and burnt muscles of Mstn-ant4 and saline-treated mice.

A) Collagen deposition in the burnt muscles of both Mstn-ant4 and saline-treated mice increased over time. From day 21 onwards, the levels of collagen in the burnt muscles of saline-treated mice were significantly higher ($p<0.01$) than the saline control muscles. The same trend was seen between the Mstn-ant4-treated burnt and control muscles from day 28 onwards. Values represent the mean of 3 animals ± SED. SED calculated as the pooled standard error of all animals. **$p<0.01$ by Student's t-test. **B)** Collagen (red) can be detected in the burnt muscles by Van Geison staining. Magnification: 200x.

deposition in the burnt muscle of saline-treated mice was significantly higher ($p<0.01$) than the saline control muscle. The same trend was observed between the Mstn-ant4-treated muscles from day 28 onwards, indicating that administration of Mstn-ant4 may cause a slight delay in collagen deposition following a burn injury. When the burnt and control muscles are analysed independently (Figure 3.10), no significant differences in the amount of collagen in the control muscles of saline and Mstn-ant4-treated mice were detected. In the burnt muscles however, the saline treated mice had a signficantly higher ($p<0.01$) level of collagen deposition at day 2 post-injury, compared to the Mstn-ant4-treated mice, but this was reversed at day 35 when the Mstn-ant4-treated mice showed a significantly higher level ($p<0.01$) of collagen deposition in the muscle. However, ANOVA analysis did not detect any overall significant differences between the two treatment groups.

To supplement the results generated from the Van Gieson staining, gene expression levels of the two most abundant types of collagen, types I and III, were evaluated in the burnt and control muscles of Mstn-ant4 and saline-treated mice using Real-Time PCR, and normalised to the housekeeping gene H3.3A (Figures 3.11 and 3.12). ANOVA analysis detected a significant effect for muscle condition, with an overall tendancy for collagen I and III expression to be significantly higher ($p<0.01$) in the burnt muscles of both Mstn-ant4 and saline-treated mice compared to their relative control muscles (data not shown). When the burnt and control muscles are analysed independently, only one significant difference occurring at day 4 post-injury is detected. Specifically, collagen I ($p<0.05$) and III ($p<0.01$) expression was significantly higher in the

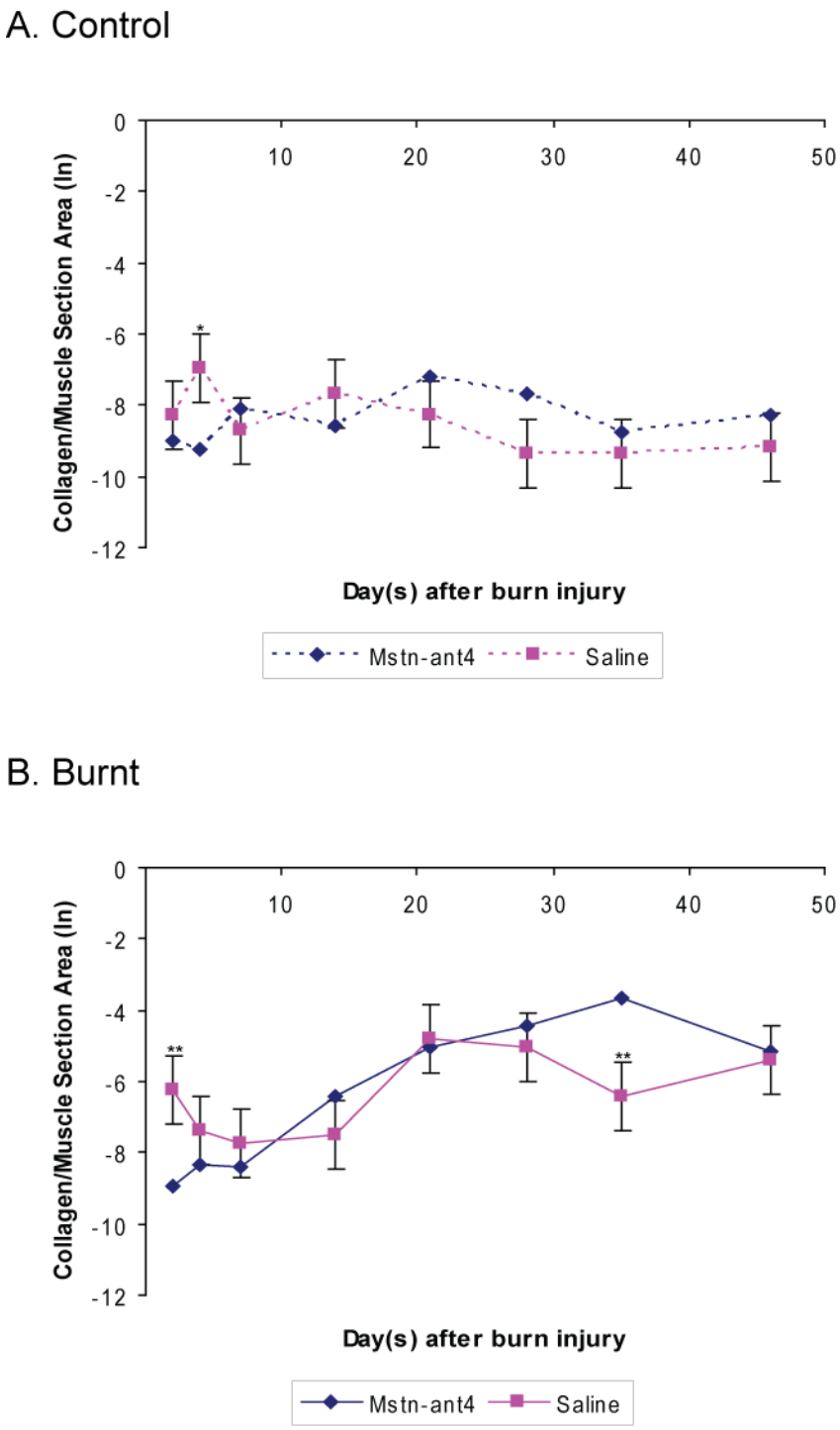

Figure 3.10: Collagen deposition in the control and burnt muscles of Mstn-ant4 and saline-treated mice.

A) There were no significant treatment differences in the level of collagen deposition between the control muscles of Mstn-ant4 and saline-treated mice. **B)** In the burnt muscles, the amount of collagen deposition in the saline-treated mice was significantly higher ($p<0.01$) than the Mstn-ant4 mice at day 2 post-injury. This was reversed at day 35 post-injury ($p<0.01$). However, no overall significant treatment differences were detected by ANOVA analysis. Values represent the mean of 3 animals ± SED. SED calculated as the pooled standard error of all animals.
* $p<0.05$ and ** $p<0.01$ by Student's t-test.

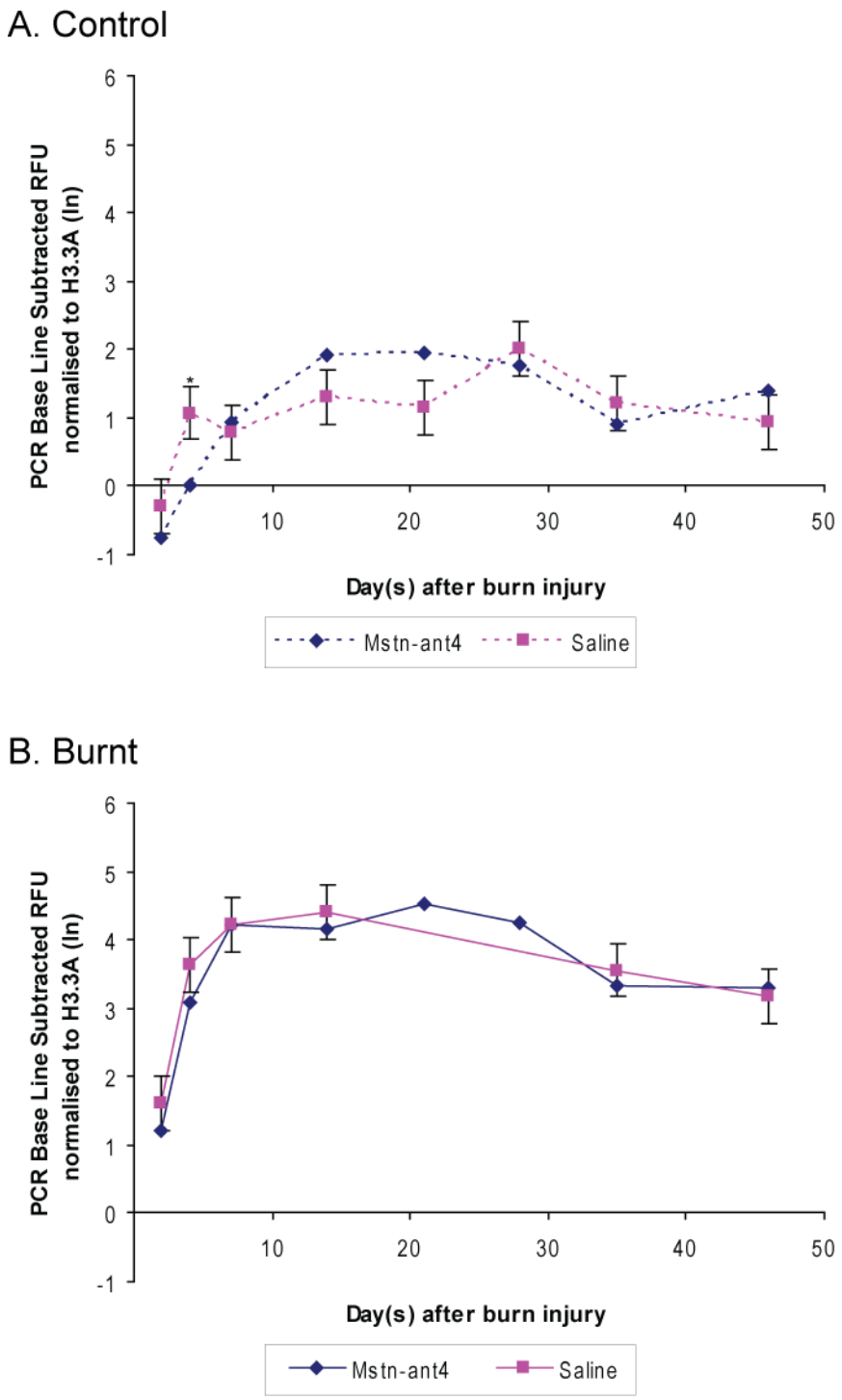

3.11: Collagen I gene expression in the control and burnt muscles of Mstn-ant4 and saline-treated mice

A) Collagen I gene expression was significantly higher ($p<0.05$) in the control muscles of saline-treated mice at day 4 post-injury compared to the Mstn-ant4-treated mice. **B)** There were no significant differences in collagen I expression between the burnt muscles of Mstn-ant4 and saline-treated mice. Values represent the mean of 3 animals ± SED. SED calculated as the pooled standard error of all animals. *$p<0.05$ by Student's t-test. RFU=Relative Fluorescent Units.

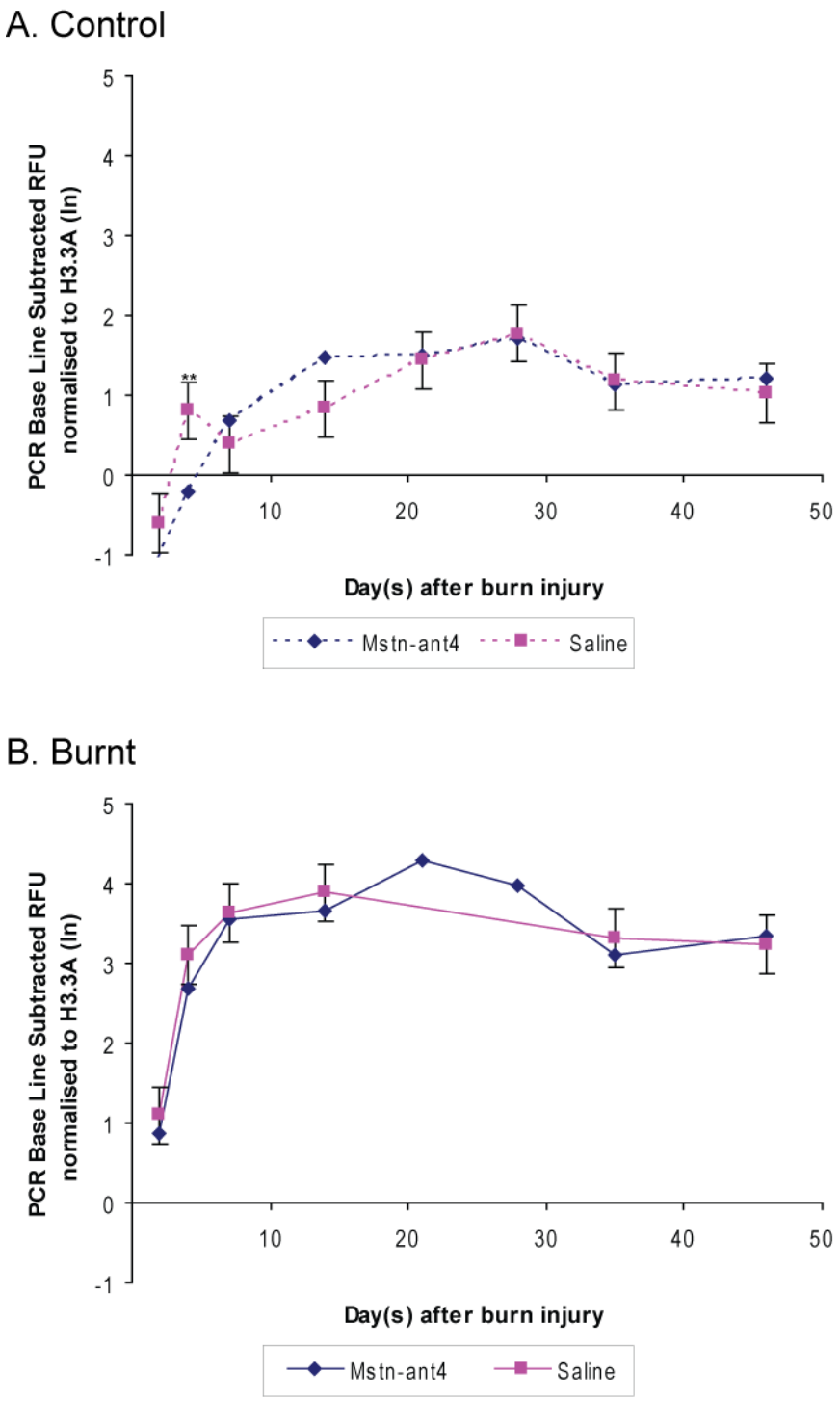

3.12: Collagen III gene expression in the control and burnt muscles of Mstn-ant4 and saline-treated mice

A) Collagen III gene expression was significantly higher ($p<0.01$) in the control muscles of saline-treated mice at day 4 post-injury compared to the Mstn-ant4-treated mice. **B)** There were no significant differences in collagen III expression between the burnt muscles of Mstn-ant4 and saline-treated mice. Values represent the mean of 3 animals ± SED. SED calculated as the pooled standard error of all animals. **$p<0.01$ by Student's t-test. RFU=Relative Fluorescent Units.

saline-treated mice compared to the Mstn-ant4-treated mice. Overall, no significant treatment differences in collagen I and III expression were detected by ANOVA analysis, therefore supporting the results generated by Van Gieson staining of the muscle sections. In addition, the fibrotic index, which is the ratio of collagen type III to collagen type I gene expression (see Section 1.7.2) was also calculated for these muscle samples, but no significant differences between the treatment groups were detected (data not shown).

3.3.3. Inflammatory Cell Response to Burn Injury

A key event of the inflammatory response is the infiltration of macrophages to the wound site, which can be detected using a Mac1 ICC (see Section 1.7.2). As expected, no macrophages were detected in the control muscles of saline and Mstn-ant4-treated mice, as macrophages are specifically associated with the inflammatory response and wound healing. Therefore, the number of macrophages present in the burnt muscles was significantly higher ($p<0.001$) than their respective control muscles (data not shown). Moreover, Figure 3.13 shows an overall decline in macrophage infiltration over time, which ANOVA analysis detected as highly significant ($p<0.001$). However, further analyses of the burnt muscles revealed no significant differences in the level of macrophage infiltration between the Mstn-ant4 and saline-treated burnt muscles.

3.3.4. Expression of Myogenic Genes in Control and Burnt Muscles

As mentioned in Section 3.3.2.2 of this thesis, a useful tool for evaluating expression patterns of genes is to amplify target sequences using PCR. Two different types of PCR reactions were used in this thesis, first Semi-Quantitative PCR and then Real-Time PCR.

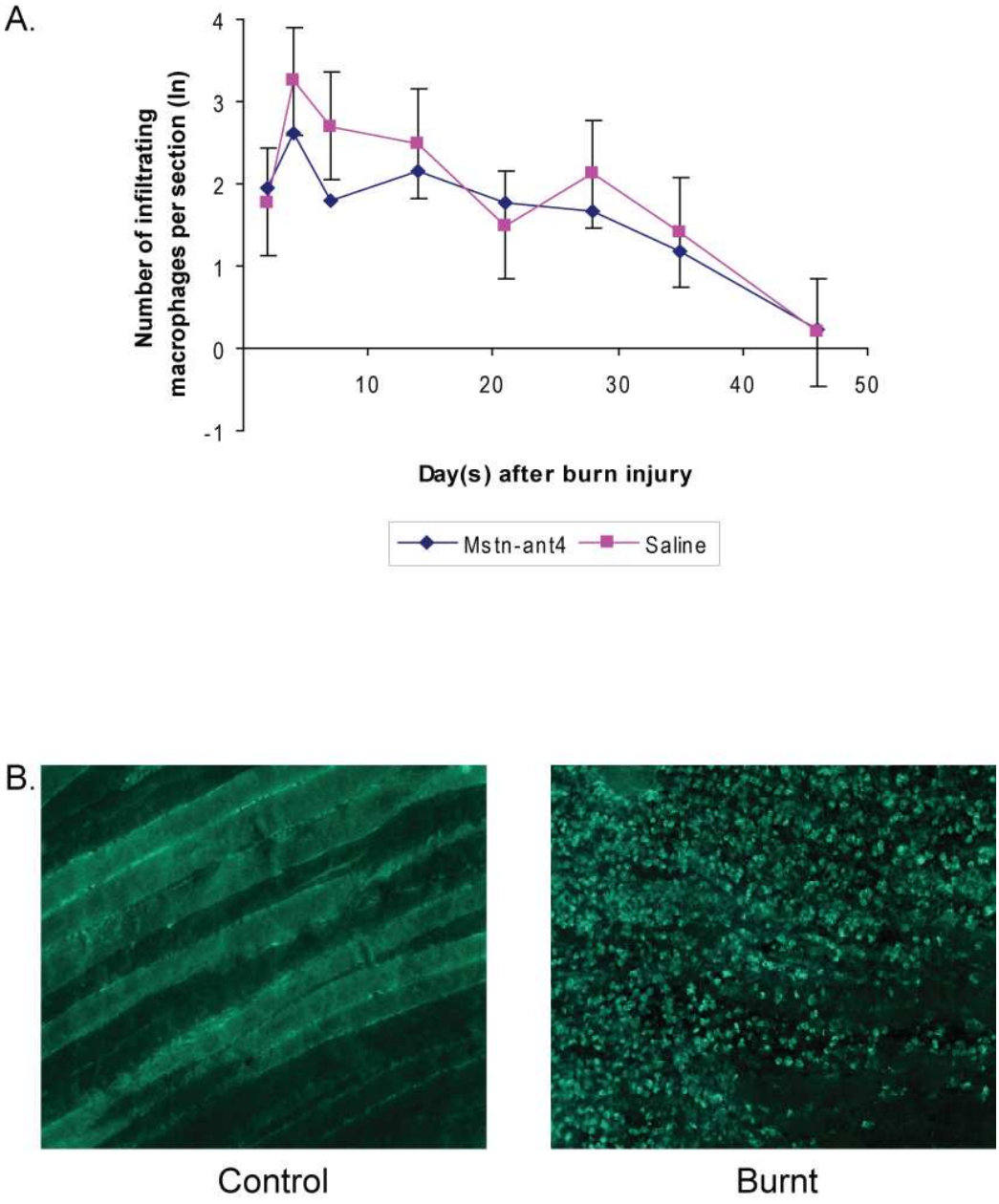

Figure 3.13: Macrophage infiltration in the control and burnt muscles of Mstn-ant4 and saline-treated mice.

A) There were no significant differences between the levels of infiltrating macrophages in the burnt muscles of Mstn-ant4 and saline-treated mice. Overall, levels of infiltrating macrohpages decreased over time, as expected. Values represent the mean of 3 animals ± SED. SED calculated as the pooled standard error of all animals. **B)** Macrophage infiltration was evaluated using a Mac1 ICC. Macrophages appear as green dots in the burnt muscles, but were not present in the control muscles. Magnification: 200x.

As previously shown in Section 3.3.2.2, it is common practise to normalise gene expression to a housekeeping gene when carrying out PCR amplifications, in order to control for variations in sample concentrations and loading. For this thesis, the four myogenic genes of interest were normalised to 18S rRNA for the Semi-Quantitative PCRs and H3.3A for the Real-Time PCRs. Both of these housekeeping genes are widely used in many biological science laboratories, including FMG at AgResearch Ltd. Unfortunately no data was obtained for the day 21 and day 28 burnt muscles of the saline-treated mice, as a result of human error during the RNA extraction.

3.3.4.1. Mighty

Mighty is a downstream target of myostatin (see Section 1.7.2). Figure 3.14, shows the level of mighty expression detected by Semi-Quantitative PCR in the control muscles of Mstn-ant4 and saline-treated mice was very similar throughout the *in vivo* trial, except at day 14 post-injury when mighty was significantly ($p<0.01$) upregulated in the Mstn-ant4-treated mice. In contrast, the saline-treated mice had significantly higher ($p<0.05$) levels of mighty expression at day 14 post-injury compared to the Mstn-ant4-treated mice. ANOVA analysis detected a significant interaction ($p<0.01$) between treatment and muscle condition, with an overall tendency for mighty expression to be higher in the burnt muscles of saline-treated mice compared to the Mstn-ant4-treated mice, for the majority of the trial duration. By day 46 however, the level of mighty expression was higher in the Mstn-ant4-treated mice compared to the saline-treated mice, although this difference was not statistically significant by Student's t-test. Interestingly, both the control and burnt muscles of Mstn-ant4 and saline-treated mice showed a large increase in mighty expression between

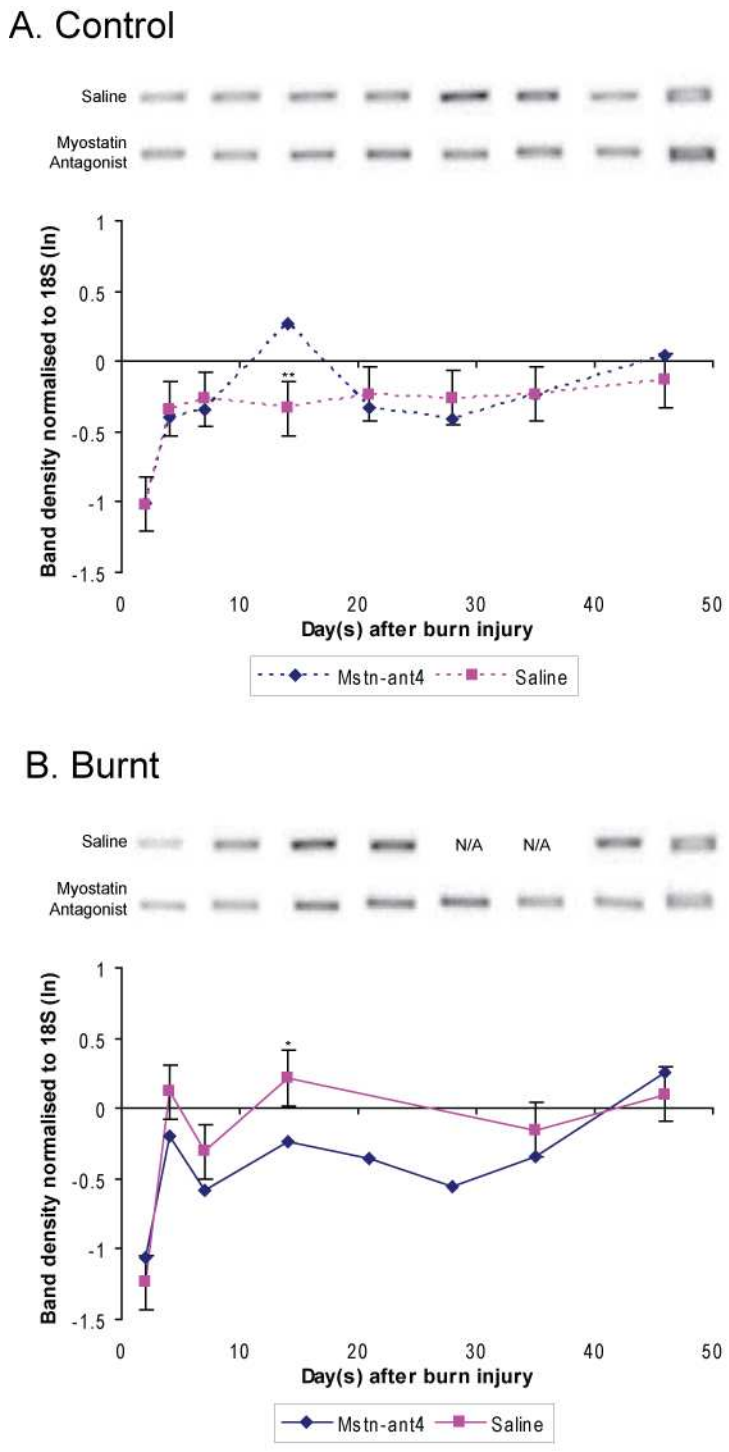

Figure 3.14: Mighty gene expression in the control and burnt muscles of Mstn-ant4 and saline-treated mice (Semi-Quantitative PCR).

A) Mighty expression in the control muscle of Mstn-ant4 and saline-treated mice was similar throughout the *in vivo* trial, except at day 14 post-injury when mighty was significantly ($p<0.01$) upregulated in the Mstn-ant4-treated mice. **B)** Saline-treated mice had significantly higher levels of mighty expression in the burnt muscles at day 14 ($p<0.05$) post-injury. An overall tendancy for mighy expression to be higher in the saline-treated mice was detected by ANOVA analysis ($p<0.01$). Values represent the mean of 3 animals ± SED. SED calculated as the pooled standard error of all animals. *$p<0.05$ and **$p<0.01$ by Student's t-test. Bands are indicative of overall results. N/A = samples lost due to human error.

days 2 and 4 post-injury, which is consistent with other injury models (Senna Salerno et al., submitted).

Conflicting results were generated from the Real-Time PCRs. Figure 3.15 shows more variation in the levels of mighty gene expression in the control muscles of Mstn-ant4 and saline-treated mice. Specifically, mighty expression was significantly higher in the Mstn-ant4-treated mice at days 2 ($p<0.05$), 4 and 28 ($p<0.01$), compared to the saline-treated mice. Mighty expression was also significantly higher in the burnt muscles of Mstn-ant4-treated mice at days 2 ($p<0.05$) and 4 ($p<0.01$) post-injury, compared to the saline-treated mice. A significant ($p<0.01$) treatment effect was detected by ANOVA analysis, with an overall tendency for mighty expression to be higher in the Mstn-ant4-treated mice than saline-treated mice. In agreement with the Semi-Quantitative PCR results, Real-Time PCR also indicated a large increase in mighty expression between days 2 and 4 for both the control muscles of Mstn-ant4 and saline-treated mice and also for the burnt muscles of Mstn-ant4 treated mice. However, the burnt muscles of saline-treated mice no longer showed this trend.

In addition to PCRs, ICC can also be a useful tool for evaluating gene expression. Mighty ICCs were carried out on the burnt and control muscle samples of Mstn-ant4 and saline-treated mice. Based on visual estimation, no significant differences were apparent between the two treatment groups. However, the extent of mighty expression in the burnt muscles did increase over the duration of the *in vivo* trial, as expected (Figure 3.16).

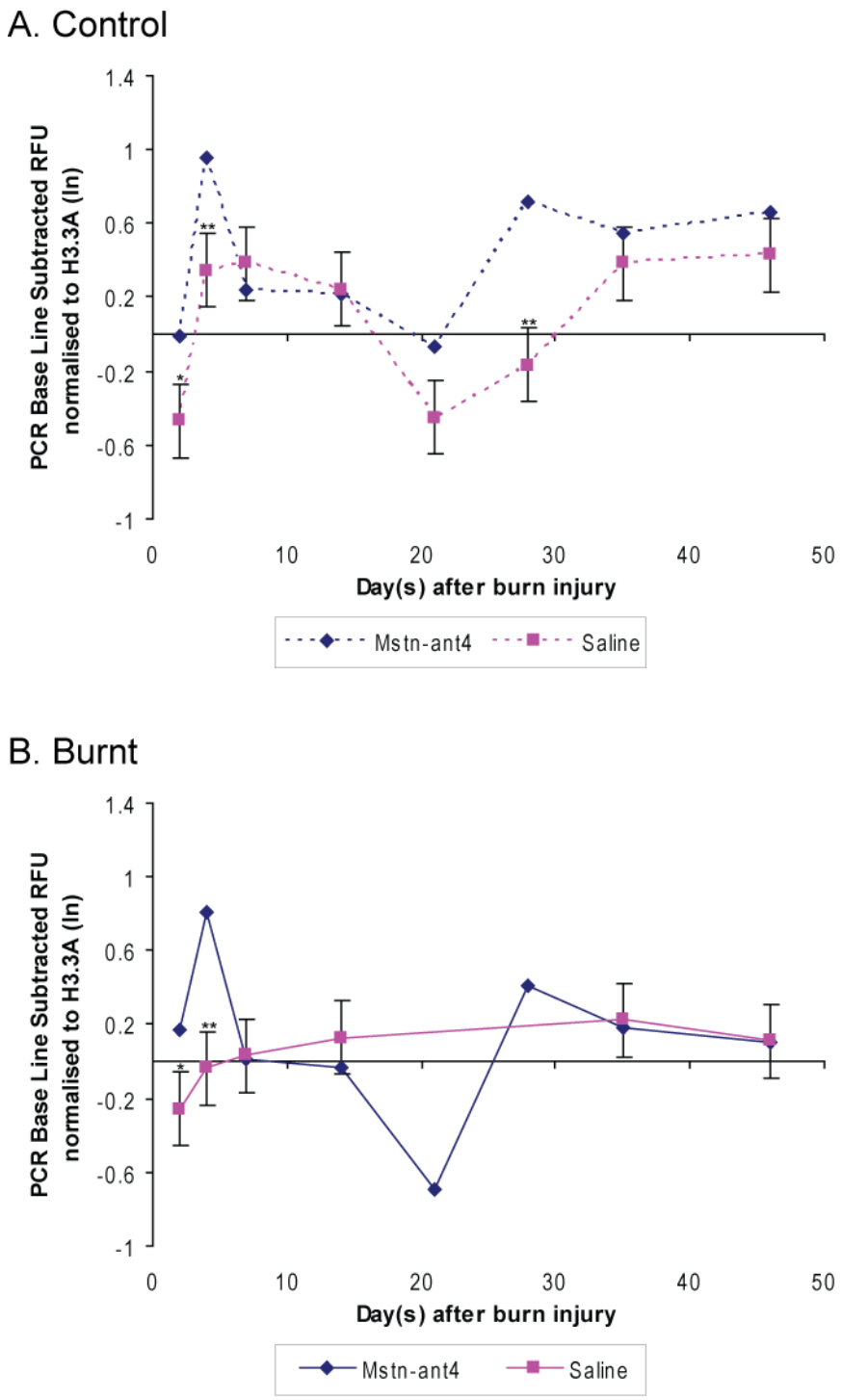

Figure 3.15: Mighty gene expression in the control and burnt muscles of Mstn-ant4 and saline-treated mice (Real-Time PCR).

A) Mighty gene expression was significantly higher ($p<0.01$) in the control muscles of Mstn-ant4 mice at day 4 and 28 post-injury compared to saline-treated mice. **B)** Mstn-ant4-treated mice had significantly higher levels of mighty gene expression at day 2 ($p<0.05$) and 4 ($p<0.01$) post-injury compared to saline-treated mice. An overall tendancy for mighty expression to be higher in the Mstn-ant4-treated mice was detected by ANOVA analysis ($p<0.01$). Values represent the mean of 3 animals ± SED. SED calculated as the pooled standard error of all animals. *$p<0.05$ and **$p<0.01$ by Student's t-test. RFU=Relative Fluorescent Units.

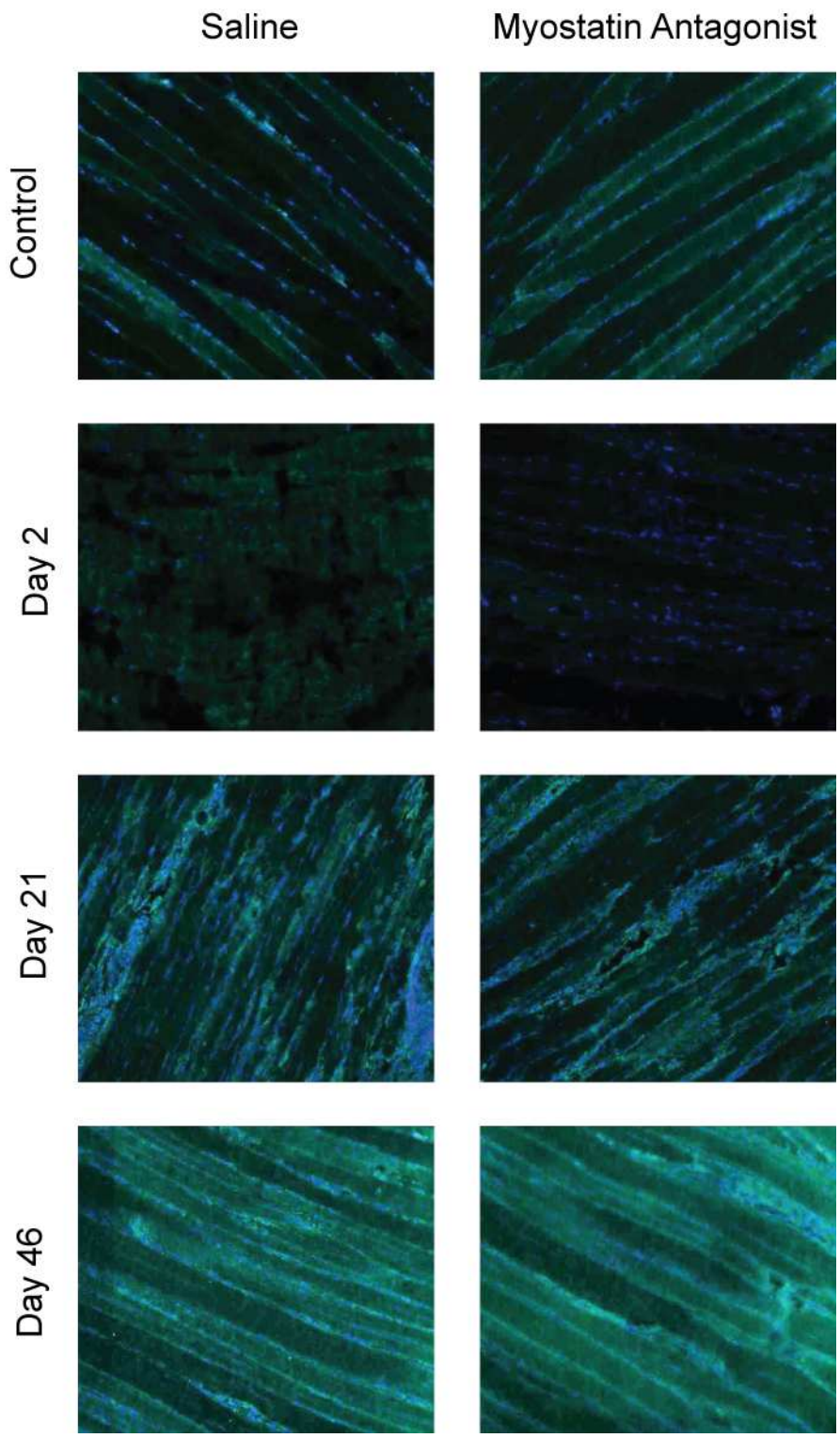

Figure 3.16: Mighty gene expression in the control and burnt muscles of Mstn-ant4 and saline-treated mice (ICC).

Mighty gene expression was detected using ICC. Mighty expression is stained green and nuclei are blue. No significant treatment differences in mighty expression were evident by visual estimation; however expression in burnt muscles did increase over time compared to control muscles. Magnification: 200x.

3.3.4.2. MyoD and Myogenin

As discussed in Section 1.7.2, MyoD and myogenin are MRFs that are essential for the growth of muscle during skeletal muscle development. The levels of MyoD expression detected by Semi-Quantitative PCR in the burnt and control muscles of Mstn-ant4 and saline-treated mice, are shown in Figure 3.17. There was some variation in MyoD expression in the control muscles, with significantly higher ($p<0.05$) levels in the Mstn-ant4-treated mice at day 14 post-injury compared to the saline-treated mice. In the burnt muscles, MyoD expression was significantly higher ($p<0.05$) in the saline treated mice at day 14 post-injury compared to the Mstn-ant4-treated mice. ANOVA analysis detected a significant interaction ($p<0.01$) between treatment and muscle condition, with an overall tendency for MyoD expression to be higher in the burnt muscles of saline-treated mice compared to Mstn-ant4-treated mice.

In contrast, the Real-Time PCR results in Figure 3.18 show MyoD expression to be higher ($p<0.01$) in the saline-treated mice at day 4 post-injury compared to the Mstn-ant4-treated mice. An erratic pattern of MyoD expression emerges in the burnt muscles. The Mstn-ant4-treated mice had significantly higher ($p<0.05$) levels of MyoD expression at days 2 and 35 post- injury, compared to the saline-treated mice. However, the saline-treated mice had significantly higher ($p<0.05$) levels of MyoD expression at days 14 and 46 post-injury, compared to the Mstn-ant4-treated mice. Interestingly, the standard curve used to generate these MyoD gene expression measurements had the largest error associated with it, compared to the standard curves for the other genes. Due to time constraints, this variability in the MyoD standard curve could not be improved upon and

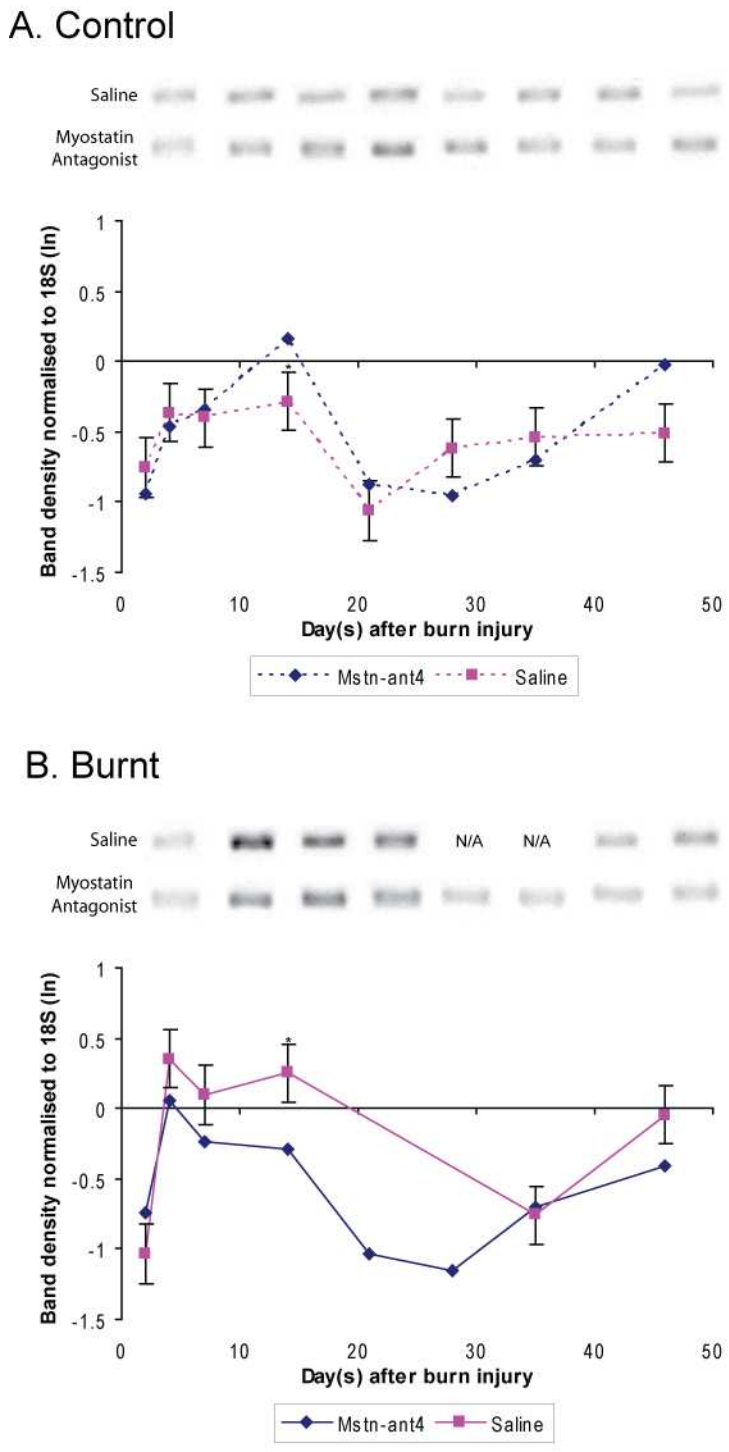

Figure 3.17: MyoD gene expression in the control and burnt muscles of Mstn-ant4 and saline-treated mice (Semi-Quantitative PCR).

A) At day 14 post-injury, MyoD expression was significantly higher ($p<0.05$) in the control muscles of Mstn-ant4-treated mice. **B)** An overall tendancy for MyoD expression to be higher in the burnt muscle of saline-treated mice was detected by ANOVA analysis, with a significant difference occurring at day 14 ($p<0.05$) post-injury. Values represent the mean of 3 animals ± SED. SED calculated as the pooled standard error of all animals. *$p<0.05$ by Student's t-test. Bands are indicative of overall results. N/A = samples lost due to human error.

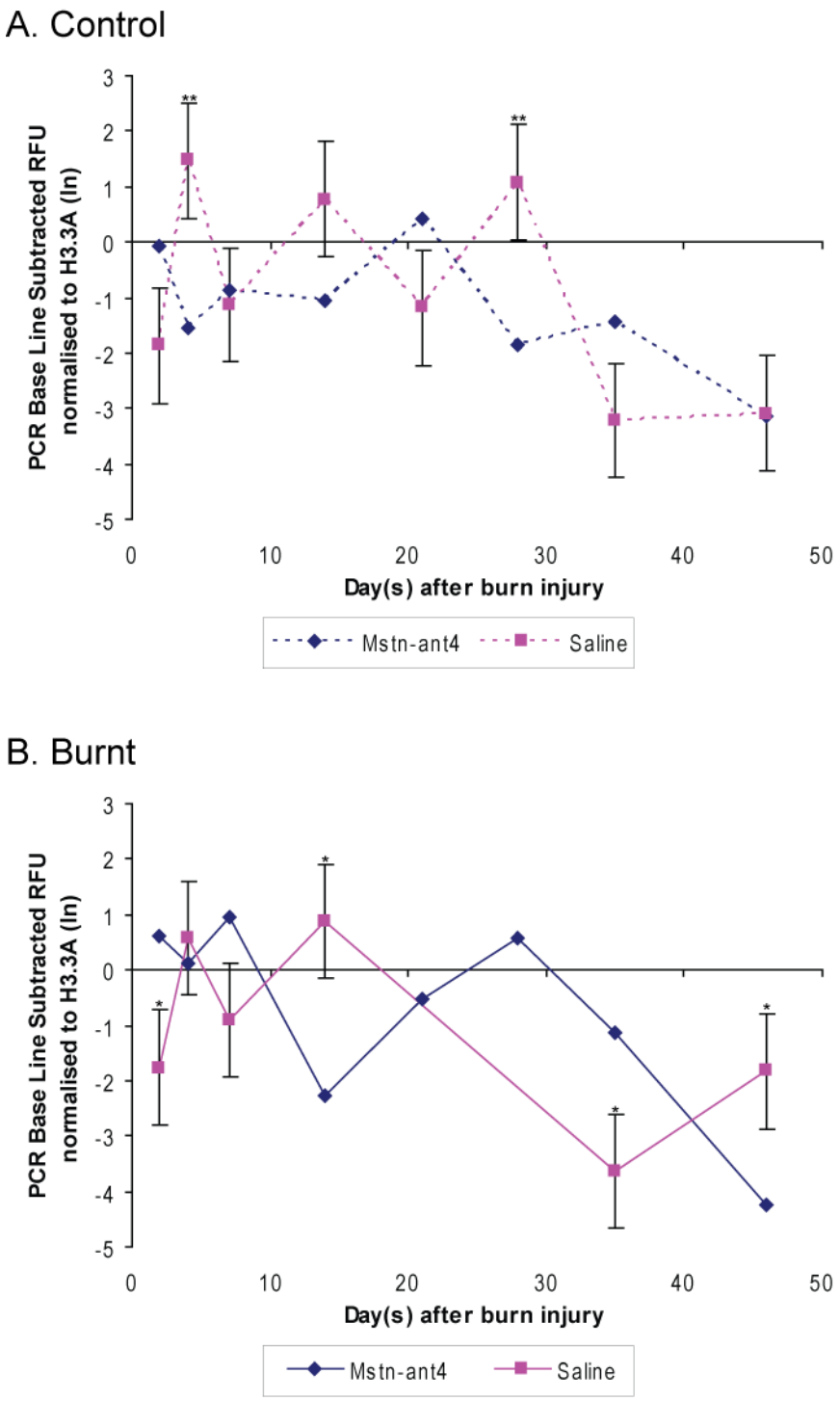

Figure 3.18: MyoD gene expression in the control and burnt muscles of Mstn-ant4 and saline-treated mice (Real-Time PCR).

A) At day 4 and 28 post-injury, MyoD expression was significantly higher ($p<0.01$) in the control muscles of saline-treated mice compared to Mstn-ant4-treated mice. **B)** MyoD expression was significantly higher in the burnt muscles of saline-treated mice at day 14 and 46 post-injury ($p<0.05$) but was significantly higher in the Mstn-ant4-treated mice at day 2 and 35 ($p<0.05$). No significant treatment differences were detected by ANOVA analysis. Values represent the mean of 3 animals ± SED. SED calculated as the pooled standard error of all animals. *$p<0.05$ and **$p<0.01$ by Student's t-test. RFU=Relative Fluorescent Units.

therefore may account for the erratic pattern of gene expression observed. No overall significant treatment differences in MyoD gene expression between the Mstn-ant4 and saline-treated mice were detected by ANOVA analysis.

Figure 3.19 illustrates the expression levels of myogenin detected by Semi-Quantitative PCR in the burnt and control muscles of Mstn-ant4 and saline-treated mice. Again, some variation in the control muscles was present. Myogenin expression was significantly higher ($p<0.05$) in the control muscles of Mstn-ant4-treated mice at days 4 and 28 post-injury, but this was reversed at day 21 post-injury with the saline-treated mice expressing significantly higher ($p<0.05$) levels of myogenin than Mstn-ant4-treated mice. No significant differences in the levels of myogenin expression between the Mstn-ant4 and saline treated mice were detected in the burnt muscles. Therefore, no overall treatment differences were detected by ANOVA analysis. Similarly, Figure 3.20 shows that no significant differences in myogenin expression in either the control or burnt muscles of Mstn-ant4 and saline-treated mice were detected by Real-Time PCR. Unlike the Semi-Quantitative PCR results however, the Real-Time results show a large increase in myogenin expression between days 2 and 4 post-injury in the burnt muscles of Mstn-ant4 and saline-treated mice before a gradual decrease over time to return to expression levels similar to those observed at day 2. This is similar to the trends observed for mighty gene expression.

3.3.4.3. Pax7

Pax7 has been identified as a key factor involved in satellite cell activity and self-renewal (see Section 1.7.2). The levels of Pax7 expression detected by

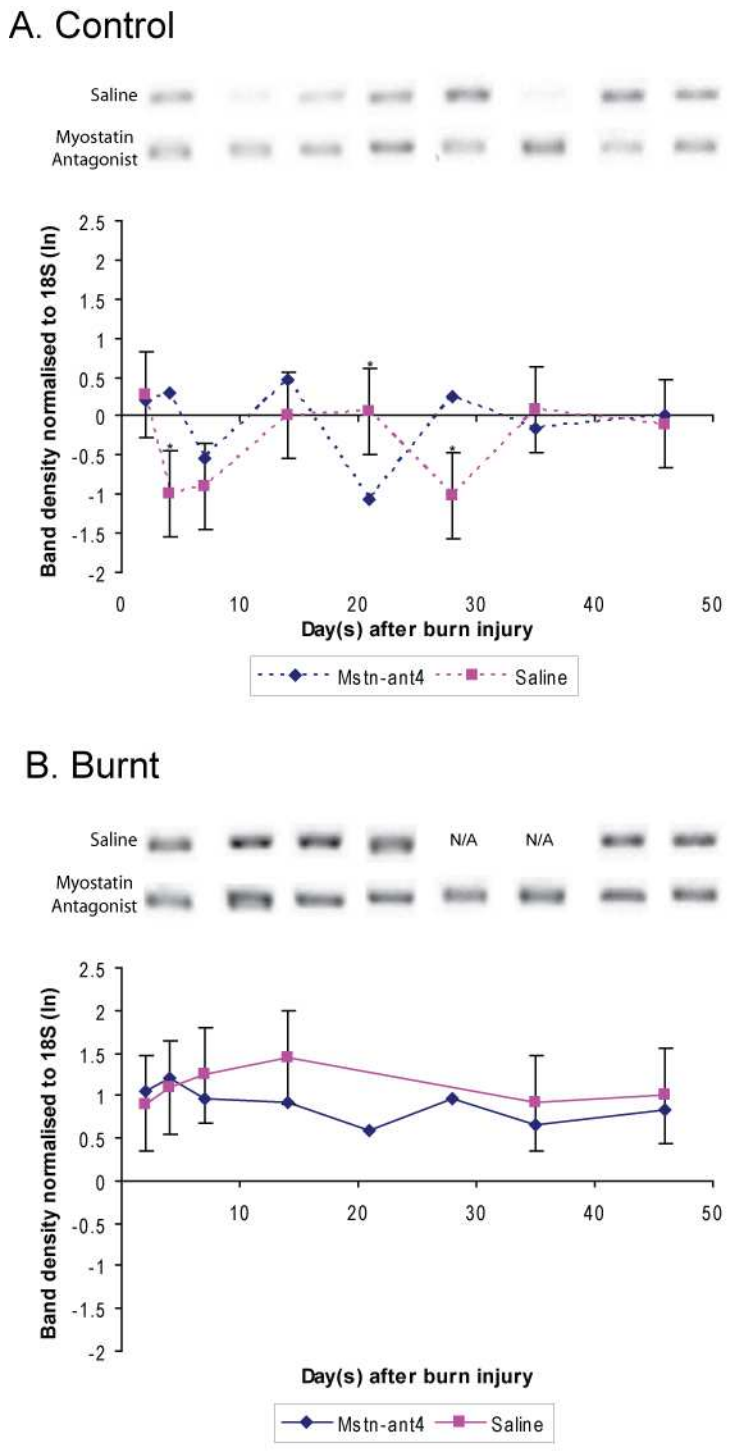

Figure 3.19: Myogenin gene expression in the control and burnt muscles of Mstn-ant4 and saline-treated mice (Semi-Quantitative PCR).

A) At day 4 and 28 post-injury, myogenin expression was significantly higher ($p<0.05$) in the control muscles of Mstn-ant4-treated mice. However, saline-treated mice showed significantly higher ($p<0.05$) levels of myogenin expression at day 21 post-injury. **B)** There were no significant differences between the levels of myogenin expression in the burnt muscles of Mstn-ant4 and saline- treated mice. Values represent the mean of 3 animals ± SED. SED calculated as the pooled standard error of all animals. *$p<0.05$ by Student's t-test. Bands are indicative of overall results. N/A = samples lost due to human error.

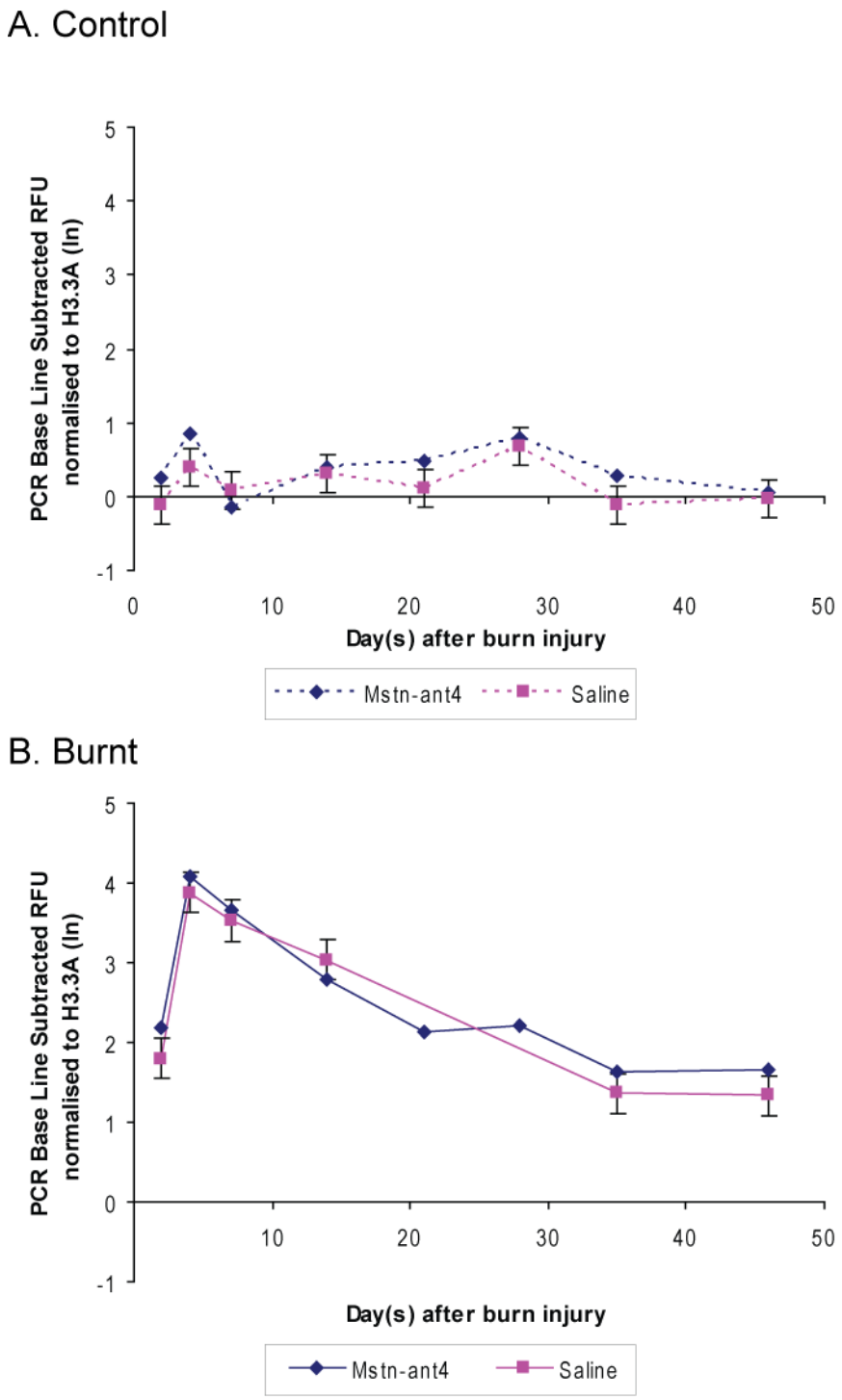

Figure 3.20: Myogenin gene expression in the control and burnt muscles of Mstn-ant4 and saline-treated mice (Real-Time PCR).

A) There were no significant differences in myogenin expression between the control muscles of Mstn-ant4 and saline-treated mice. **B)** There were no significant differences in myogenin expression between the burnt muscles of Mstn-ant4 and saline-treated mice. Values represent the mean of 3 animals ± SED. SED calculated as the pooled standard error of all animals. RFU=Relative Fluorescent Units. RFU=Relative Fluorescent Units.

Semi-Quantitative PCR in the burnt and control muscles of Mstn-ant4 and saline-treated mice are shown in Figure 3.21. No significant differences in Pax7 expression in either the control or burnt muscles of Mstn-ant4 and saline-treated mice were detected. However, a significant ($p<0.01$) treatment effect was detected by ANOVA analysis, with an overall tendency for Pax7 expression to be higher in the saline-treated mice than the Mstn-ant4-treated mice. Interestingly, like mighty expression, both the control and burnt muscles of Mstn-ant4 and saline-treated mice showed a large increase in Pax7 expression between days 2 and 4 post-injury.

No significant differences in Pax7 expression between the Mstn-ant4 and saline-treated mice were detected by Real-Time PCR (Figure 3.22). Although not detected by ANOVA analysis, it appears the overall trend for Pax7 expression to be higher in the saline-treated mice, as detected by Semi-Quantitative PCR, was reversed in the results generated by Real-Time PCR. Furthermore, the trend for Pax7 expression to increase between days 2 and 4 post-injury was no longer evident in the control muscles, and a decrease in Pax7 expression between days 2 and 4 was observed in the burnt muscles of Mstn-ant4 and saline-treated mice analysed by Real-Time PCR.

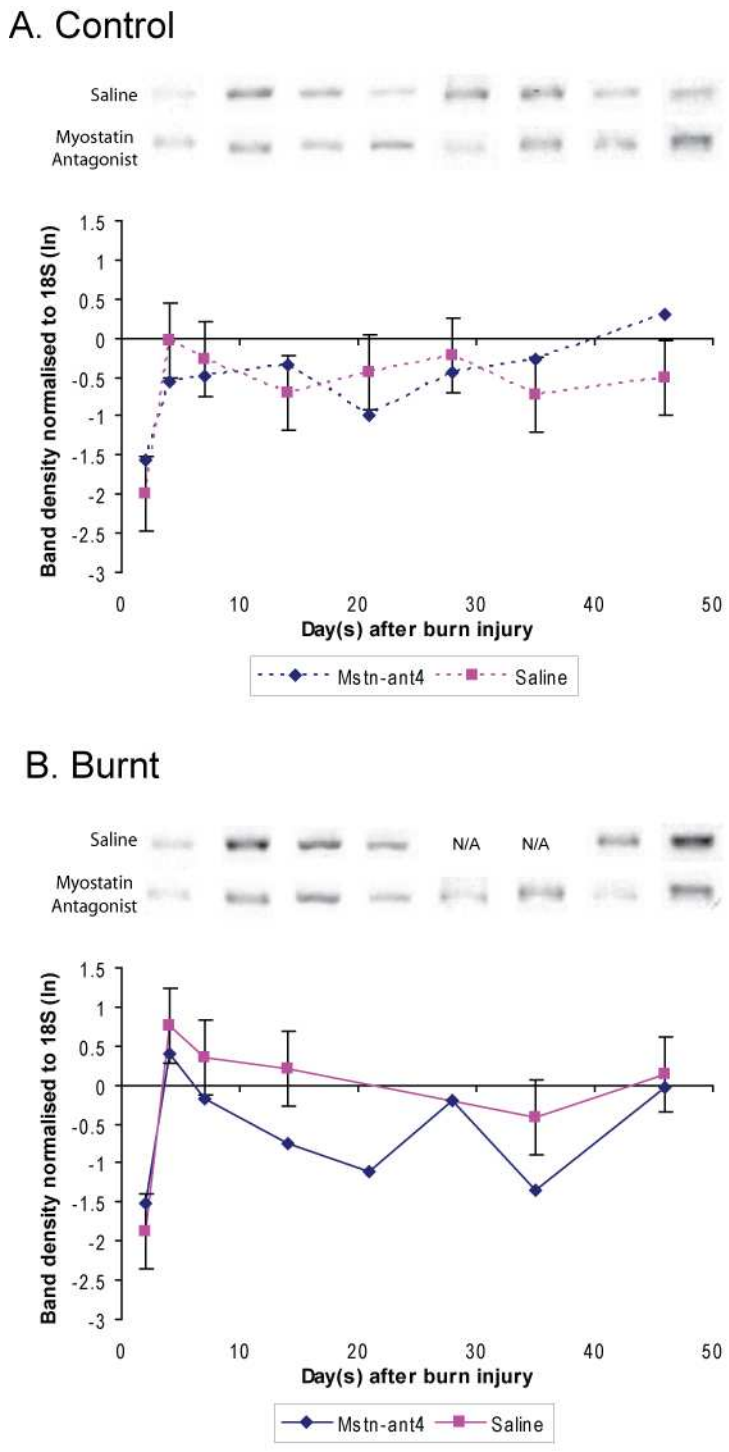

Figure 3.21: Pax7 gene expression in the control and burnt muscles of Mstn-ant4 and saline-treated mice (Semi-Quantitative).

A) No significant differences in Pax7 expression were detected in the control muscles of Mstn-ant4 and saline-treated mice. **B)** No significant differences in Pax7 expression were detected in the burnt muscles of Mstn-ant4 and saline-treated mice. However, an overall tendancy for Pax7 expression to be higher ($p<0.01$) in the burnt muscle of saline-treated mice was detected by ANOVA analysis. Values represent the mean of 3 animals ± SED. SED calculated as the pooled standard error of all animals. Bands are indicative of overall results. N/A = samples lost due to human error.

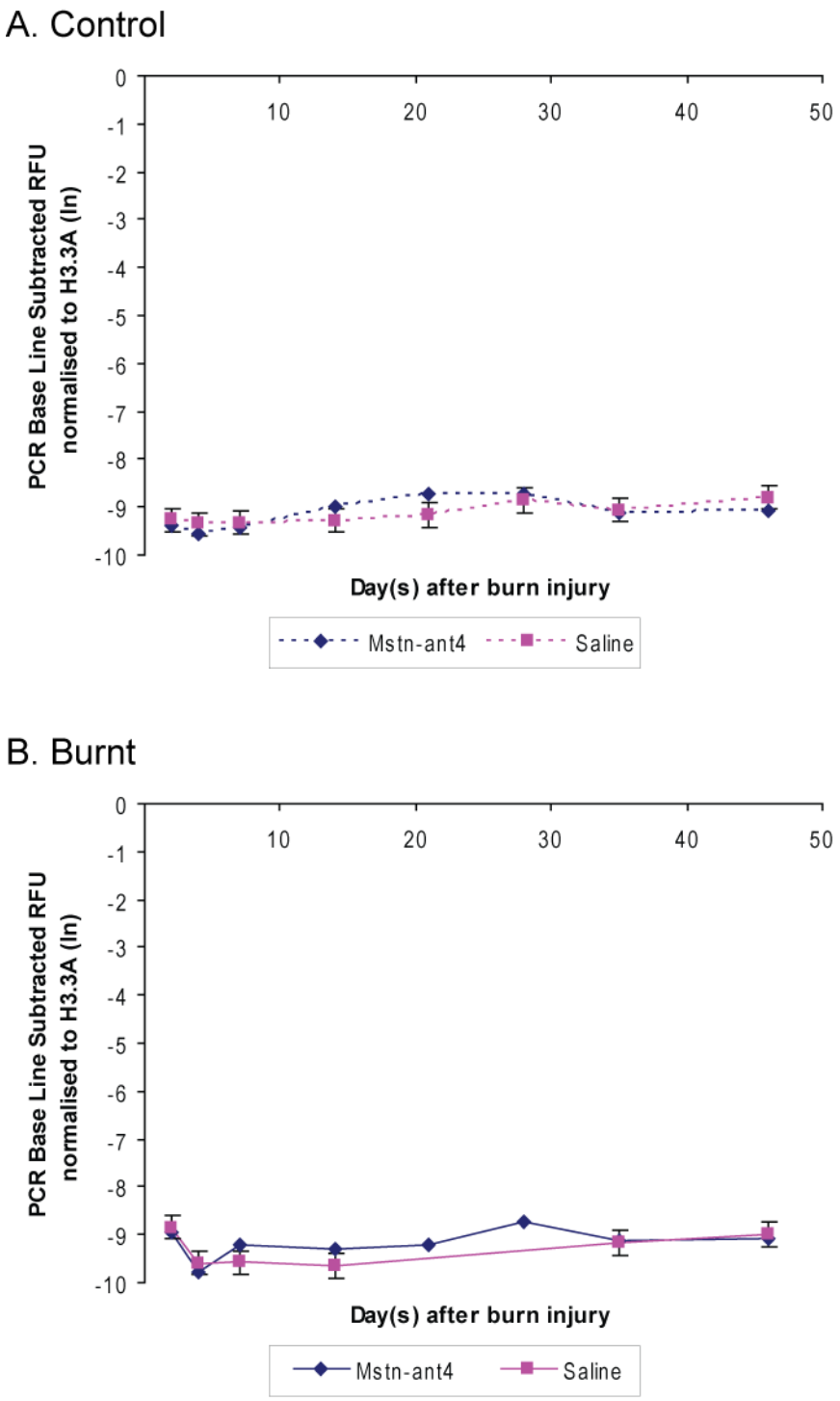

Figure 3.22: Pax7 gene expression in the control and burnt muscles of Mstn-ant4 and saline-treated mice (Real-Time PCR).

A) There were no significant differences in Pax7 expression between the control muscles of Mstn-ant4 and saline-treated mice. **B)** There were no significant differences in Pax7 expression between the burnt muscles of Mstn-ant4 and saline-treated mice. No overall significant treatment differences were detected by ANOVA analysis. Values represent the mean of 3 animals ± SED. SED calculated as the pooled standard error of all animals. RFU=Relative Fluorescent Units.

Chapter Four: Discussion and Future Direction

4.1. Discussion

4.1.1. Introduction

Myostatin is a growth and differentiation factor that belongs to the TGF-β superfamily of genes (McPherron et al., 1997; Thomas et al., 2000). Mutations or deletions in the myostatin gene lead to the heavy muscling phenotypes seen in various breeds of cattle, sheep and dogs, and also in myostatin knock-out mice (Kambadur et al., 1997; McPerron & Lee, 1997; Berry et al., 2002; Schuelke et al., 2004). More recently, a human child with the heavy muscling phenotype was also found to carry a mutation in the myostatin gene (Walsh & Celeste, 2005). Conversely, increased expression of myostatin has been linked to various muscle wasting conditions induced by ageing or disease. Myostatin is therefore regarded as a strong inhibitor of muscle growth. In addition, myostatin has also been shown to control satellite cell activation post-natally, and is considered a potent negative regulator of muscle regeneration and repair as well (McCroskery et al., 2003; Bishop et al., 2005). The ability to block myostatin function would therefore have enormous potential in the treatment of muscle injuries and various muscle wasting conditions.

The FMG group at AgResearch Ltd. have begun to investigate this concept. By truncating the biologically active mature myostatin sequence at different amino acids, they have produced several myostatin antagonists that have shown promising results in the *in vitro* studies carried out so far. Specifically, all the antagonists elicited a strong antagonistic effect on both endogenous and

exogenous myostatin. Furthermore, the ability of myostatin to influence the chemotactic capacity of myogenic cells was interupted by all antagonists when tested *in vitro* (Kambadur et al., 2006a; 2006b; 2006c; unpublished data). Therefore, subsequent *in vivo* studies commenced to test the efficacy of myostatin antagonists in different wound healing models.

4.1.2. Development of the Muscle Burn Injury Model

Wound healing is characterised by three broad stages, the inflammatory response, proliferation and remodelling. The inflammatory response was discussed in detail in Section 1.5 of this thesis. The proliferative phase involves the formation of granulation tissue to fill the wound area, particularly through fibroblast proliferation, collagen and extracellular matrix deposition and re-epithilialisation. Once the formation of new tissue in the wound area is complete, the functionality of the tissue is restored in the remodelling phase. The three phases of wound healing often overlap, and numerous growth factors and cytokines are involved in regulating each step, thereby making it a very complex process. Furthermore, any disruptions to this coordinated wound healing process may cause further damage to the tissue, and hence delay repair (Greenhalgh, 1996; Li et al., 2007). Therefore, determining the mechanisms behind any therapy developed to improve wound healing is a difficult and time-consuming process.

Nevertheless, both acute and chronic wound healing models are widely used throughout the literature and can provide valuable information during the development of wound healing therapies. As discussed in Section 1.6.4 of this thesis, Siriett et al. (2007) of the FMG group recently tested Mstn-ant1 using an

acute notexin injury model. The authors reported enhanced regeneration levels in Mstn-ant1-treated mice compared to placebo-treated mice. In addition, the Mstn-ant1-treated mice showed reduced levels of scarring after the injury, suggesting Mstn-ant1 was improving wound healing following the notexin injury. Similar results were also obtained when Mstn-ant1 was tested in sarcopenia, a chronic injury model, with the authors reporting improved wound healing and increased muscle strength of the aged mice (Siriett et al., 2007). An alternative myostatin antagonist, Mstn-ant3, has also been shown to attenuate muscle wasting in *mdx* mice, a murine model of the chronic Duchenne and Becker muscular dystrophies (Kambadur et al., 2006c).

However, to confirm and further characterise the effects of these myostatin antagonists, auxiliary testing in a range of injury models is required, which provided the basis for this thesis. There is not a standardised protocol for a muscle burn injury in any of the published wound healing models. However, upon examining the plethora of literature on skin burn injuries, the burn injury is often classified as the most devastating injury a person can endure (Greenhalgh, 1996), and therefore the ability to improve wound healing following a burn injury would be very valuable. For that reason, Orico Ltd. wanted to establish the potential of myostatin antagonists for the treatment of burn injuries by funding two different projects, which tested the effect of Mstn-ant4 on both skin and muscle burn injuries, with the muscle burn injury being the focus of this thesis.

As discussed in Section 3.1, the murine muscle burn injury developed for this thesis was found to produce a very severe injury, more severe in fact than any

other acute injury model previously used by the FMG group at AgResearch Ltd. This was particularly evident when the frozen TA muscles were sectioned for histology. The burn injury made the tissue very fragile and therefore very difficult to section, particularly at days 2 and 4 post-injury. The FMG group at AgResearch Ltd. have not encountered any such difficulties when sectioning TA muscle samples subjected to an acute notexin or incision injury in the past (personal communication).

In the case of skin burns, the degree of severity is classified as a first-, second-, third-, and in some instances, a fourth-degree burn. These levels relate to the depth of the burn injury through the layers of the skin, with sunburn being classified as a first-degree burn and a fourth-degree burn extending into underlying muscle or bone; and also to the extent of body surface area affected by the burn (Greenhalgh, 1996). This classification system can obviously not be applied to the burn injury developed for this thesis; however, one could estimate that the severity of the muscle burn injury would compare to at least a third-degree skin burn.

4.1.3. *In vivo* Trial

The *in vivo* trial undertaken as part of this thesis was based on the notexin trial described by Siriett et al. (2007), as this also used an acute injury model. However, instead of extending the results of Mstn-ant1 reported by Siriett et al. (2007) to the burn injury model, Orico Ltd. wanted to test the efficacy of Mstn-ant4, following its very promising results *in vitro*, for patent purposes.

As shown in Section 3.3 of this thesis, the *in vivo* trial did produce some promising results which supported the initial hypotheses and were consistent with the findings for Mstn-ant1 by Siriett et al. (2007), along with other studies using myostatin antagonists carried out by the FMG group at AgResearch Ltd. (Kambadur et al., 2006a; 2006b; 2006c). Firstly, the Mstn-ant4-treated mice recovered from the burn-induced loss of body weight earlier than the saline-treated mice (see Section 3.3.1). Real-Time PCR also revealed a tendency for mighty expression to be higher in the burnt muscles of Mstn-ant4-treated mice than those of saline-treated mice. This confirmed the orginial hypothesis that because mighy is a downstream target of myostatin (Marshall et al., 2008), an inhibiton of myostatin function by the antagonist would result in an increase in mighty gene expression levels, above those of saline-treated mice during muscle regeneration following the burn injury. In addition, mighty expression levels increased significantly between days 2 and 4 post-injury, which is consistent with previous results obtained using both notexin and incision injury models (Senna Salerno et al., submitted).

Although contradictory results for the expression of mighty were obtained from the Semi-Quantitative PCR results, Real-Time PCR is often considered to be a more sensitive and accurate technique. There are three phases to PCR amplifications, the exponential phase where doubling of the amplicon (product) occurs; the linear phase where the reaction components are being consumed, the reaction is slowing down and PCR products are beginning to degrade; and finally a plateau phase where the reaction has completely stopped and no more product is being made. Semi-Quantitative PCR detects the PCR amplification at the plateau phase, hence why it is often referred to as end-point PCR. In

contrast, Real-Time PCR allows PCR amplification to be detected during the early exponential growth phase of the reaction. Furthermore, the increase in SYBR Green fluorescent signal is directly proportional to the number of amplicons produced, explaining why Real-Time PCR is often considered a more accurate and sensitive technique. Therefore, by using a combination of both PCR techniques, a more comprehensive analysis of myogenic gene expression could be carried out (Kubista et al., 2006).

The other very interesting result generated from this *in vivo* trial was found during the histological analysis of CFN. As discussed in Sections 1.7.2 and 3.3.2.1, one of the key indicators of skeletal muscle regeneration is the presence of CFN in the muscle fibres (Brazelton et al., 2003). In theory, greater numbers of CFN and CFN number per muscle fibre correspond to increased levels of wound healing. Therefore, it was hypothesised that Mstn-ant4-treated mice would show higher levels of CFN and CFN per muscle fibre than saline-treated mice, when analysed by histological staining. Although no overall significant differences in CFN number or CFN to CFN fibre ratio were evident between the two treatment groups, there was a significant increase in the CFN to CFN fibre ratio in the burnt muscles of Mstn-ant4-treated mice at day 14 post-injury; however, this rapidly decreased after day 14 and closely followed the trend of the saline-treated mice for the remaining time points. This is a particularly important observation because the final subcutaneous injection of Mstn-ant4 was administered on day 15 post-injury, and therefore this sudden decline in the CFN to CFN fibre ratio after day 14 in the burnt muscles of Mstn-ant4-treated mice may indicate that administration of the myostatin antagonist was terminated too early during the course of the *in vivo* trial.

Unfortunately, no other results obtained from the histological, gene expression, or immunocytochemical analyses obtained from the *in vivo* trial, supported these findings. However, if this study was repeated using optimised conditions, more promising results, similar to those of other myostatin antagonists (Kambadur et al., 2006a; 2006b; 2006c; Siriett et al., 2007), would be expected. To clarify, this was the first attempt using both the murine burn injury model and Mstn-ant4 for an *in vivo* trial. Although the *in vivo* trial was based on the notexin injury trial by Siriett et al. (2007), also an acute injury like the burn, the burn injury proved to be more severe than the notexin injury and every other injury model that has been used by the FMG group at AgResearch Ltd. Therefore, perhaps the schedule for administering Mstn-ant4 should have been modelled on the recent sarcopenia trial (Siriett et al., 2007) or *mdx* trial (Kambadur et al., 2006c), involving three injections per week for three weeks, thus supplying the antagonist for longer. This is supported by the CFN to CFN fibre ratio results, where the ratio in the Mstn-ant4-treated mice showed a sudden decline after day 14 post-injury, suggesting that administration of Mstn-ant4 should be extended past day 15 post-injury, the final injection day for this *in vivo* trial.

In addition, the burn injury may have been variable among animals as it was inflicted manually, with no way of consistently controlling the pressure used to apply the hot metal rod to the TA muscle. Furthermore, because of the wide range of time points that needed to be examined to follow the different healing milestones after the burn injury (because of its severity), all measurements were only based on three animals per treatment per time point. This is because the *in vivo* trial already involved ninety-six mice and it was not logistically possible to obtain any more animals that were of the same age. The prospect of inflicting

burn injuries on both hind limbs of the mice was also investigated to double the amount of data that could be generated, but this was not approved by the Ruakura Animal Ethics Committee. Furthermore, samples were not able to be processed in duplicate. For example, first-strand cDNA synthesis would ideally have been performed in duplicate for each muscle sample which would have therefore allowed duplicate PCRs to be generated in order to minimise variability. Due to time restrictions this was not possible. Hence natural variation among animals and experimental samples may have obscured treatment differences.

As a result of the limitation in animal number, there were also insufficient muscle samples to extract both RNA and protein separately, which may have given a more comprehensive assessment of the efficacy of Mstn-ant4 on muscle wound healing. To counteract this problem, an attempt was made to extract protein using the Trizol method detailed in Section 2.2.5.1, but this was unsuccessful, and due to time constraints the technique could not be standardised. However, a kit has now become available that enables RNA, DNA and protein to be extracted from a single tissue sample (Innovative Sciences Ltd.), which will be a useful tool for future *in vivo* studies of this kind. For this thesis however, the results of the *in vivo* trial were limited to only histology, immunocytochemistry and gene expression analyses using Semi-Quantitative PCR and Real-Time PCR.

4.2. Future Direction

In summary, any further development of Mstn-ant4 as a pharmaceutical therapy for muscle wound healing and disease would need to have a very specific regimen designed according to the type of injury being treated. In the case of the burn injury used in this thesis, more frequent administration of Mstn-ant4 for an extended period of time would be suggested. The burn injury itself may also need to be further standardised to limit variability between animals. Perhaps the use of lasers to inflict the burn injury, as discussed in Section 3.1 of this thesis, could be investigated. Furthermore, a trial comparing the efficacy of Mstn-ant1 and Mstn-ant4 on wound healing following the burn injury may be very useful. In addition, as Real-Time PCR is considered to be a more sensitive and accurate technique, Semi-Quantitative PCR would probably not be necessary for future studies. Historically only Semi-Quantitative PCR has been used by the FMG group at AgResearch, hence its inclusion in this thesis. However, due to the variability generated in these results, Real-Time PCR was then carried out. This is a fairly new technique being adopted by the FMG group at AgResearch and it is proving to be very time-efficient and accurate.

Overall, Mstn-ant4 has shown potential to improve wound healing following a burn injury, and incorporating these suggestions into future studies would progress the development of Mstn-ant4 as a commercially viable pharmaceutical therapy.

Appendix

1% Agarose
0.5 g UltraPure agarose (Invitrogen)
50 ml 1 x TAE
Boiled until agarose is dissolved.
1 µl 10 mg/ml ethidium bromide per 50 ml Agarose.

10% Buffered Formalin
32.5 g Na_2HPO_4
20 g NaH_2PO_4.H2O
500 ml formalin
4.5 L H_2O

Coomassie Blue Stain
2.5 g Coomassie Brilliant Blue R-250
45% methanol
10% acetic acid

DEPC-treated water
2 ml DEPC
2 L MilliQ water
Mixed overnight then autoclaved.

DNA 1kb+ Ladder
90 µl 10 x DNA loading dye
810 µl MilliQ water
100 µl 1 µg/ml 1kb+ ladder

DNA Loading Dye (10 x)
10 ml 50% glycerol
2 ml 50 x TAE
Bromophenol blue

Eosin (1% solution)
10 g Eosin Y
1 L MilliQ water
2.0 ml acetic acid (5% aqueous)
1 crystal of thymol

Gill's Haematoxylin
4.0 g Haematoxylin
0.4 g sodium iodate
35.2 g aluminium sulphate
710 ml MilliQ water
250 ml ethylene glycol
40 ml glacial acetic acid

LB Broth
20 g LB Broth Base
1 L MilliQ water
autoclaved

PBS (Phosphate Buffered Saline)
1 PBS tablet (Oxoid)
100 ml MilliQ water

PBS-T
1 L PBS
2 µl tween-20

PBS-T + 0.2% BSA
100ml PBS-T
0.2 g BSA

Scott's tap-water
2.0 g sodium bicarbonate
20.0 g magnesium sulphate
1 L MilliQ water
1 crystal of thymol

TAE (Tris-acetate EDTA) (1 x)
400ml TAE (50 x)
19.6 L DEPC-treated water

TAE (50 x)
242 g Tris (base)
57.1 ml glacial acetic acid
100 ml 0.5 M EDTA (ph 8.0)
Made up to 1 L with MilliQ water

Van Gieson Solution
10 ml 1% aqueous acid fuchsin
90 ml saturated Picric acid
0.25 ml concentrated HCl

Weigert's Iron Haematoxylin Solution A
1% haematoxylin in absolute alcohol

Weigert's Iron Haemotoxylin Solution B
4 ml 30% Ag ferric chloride
1 ml concentrated HCl
100 ml distilled H_2O

References

Abmayr, S.M., Balagopalan, L., Galletta, B.J., & Hong, S.J. (2003). Cell and molecular biology of myoblast fusion. *International Review of Cytology 225*, 33-89.

Allen, R.E., & Boxhorn, L.K. (1989). Regulation of skeletal muscle satellite cell proliferation and differentiation by transforming growth factor-beta, insulin-like growth factor 1, and fibroblast growth factor. *Journal of Cellular Physiology 138*, 311-315.

Anderson, J.E. (2000). A role for nitric oxide in muscle repair: nitric oxide-mediated activation of muscle satellite cells. *Molecular Biology of the Cell 11*, 1859-1874.

Armand, O., Boutineau, A.M., Mauger, A., Pautou, M.P., & Kieny, M. (1983). Origin of satellite cells in avian skeletal muscles. *Archives d'Anatomie Microscopique et de Morphologie Experimentale 72*, 163-181.

Arnold, H.H., & Braun, T. (1996). Targeted inactivation of myogenic factor genes reveals their role during mouse myogenesis: a review. *International Journal of Developing Biology 40*, 345-363.

Arnold, H.H., & Winter, B. (1998). Muscle differentiation: more complexity to the network of myogenic regulators. *Current Opinion in Genetics and Development 8*, 539-544.

Asakura, A., Komaki, M., & Rudnicki, M (2001). Muscle satellite cells are multipotential stem cells that exhibit myogenic, osteogenic, and adipogenic differentiation. *Differentiation 68*, 245-53.

Asakura, A., Seale, P., Girgis-Gabardo, A., & Rudnicki, M.A. (2002). Myogenic specification of side population cells in skeletal muscle. *The Journal of Cell Biology 159*, 123-134.

Astrakas, L.G., Goljer, I., Yasuhara, S., Padfield, K.E., Zhang, Q., Gopalan, S., Mindrinos, M.N., Dai, G., Yu, Y., Martyn, J.A.J., Tompkins, R.G., Rahme, L.G., & Tzika, A.A. (2005). Proton NMR spectroscopy shows lipid accumulate in skeletal muscle in response to burn trauma-induced apoptosis. *The FASEB Journal 19*, 1431-1440.

Aulehla, A., Wehrle, C., Brand-Saberi, B., Kemler, R., Gossler, A., Kanzler, B., & Herrmann, B.G. (2003). Wnt3a plays a major role in the segmentation clock controlling somitogenesis. *Developmental Cell 4*, 395-406.

Ausubel, F., Brent, R., Kingston, R., Moore, D., Seidman, J., Smith, J., & Struhl, K. (1987). *Current protocols in Molecular Biology*. New York, Wiley Interscience.

Bairy, K.L., Somayaji, S.N., & Rao, C.M. (1997). An experimental model to produce partial thickness burn wound. *Indian Journal of Experimental Biology 35*, 70-72.

Ballard-Croft, C., Carlson, D., Maass, D.L., & Horton, J.W. (2004). Burn trauma alters calcium transporter protein expression in the heart. *Journal of Applied Physiology 97*, 1470-1476.

Beauchamp, J.R., Heslop, L., Yu, D.S.W., Tajbakhsh, S., Kelly, R.G., Wernig, A., Buckingham, M.E., Partridge, T.A., & Zammit, P.S. (2000). Expression of CD34 and Myf5 defines the majority of quiescent adult skeletal muscle satellite cells. *The Journal of Cell Biology 151*, 1221-1233.

Berry, C., Thomas, M., Langley, B., Sharma, M., & Kambadur, R. (2002). Single cysteine to tyrosine transition inactivates the growth inhibitory function of piedmontese myostatin. *American Journal of Physiology and Cellular Physiology 283*, 135-141.

Birchmeier, C., & Brohmann, H. (2000). Genes that control the development of migrating muscle precursor cells. *Current Opinion in Cell Biology 12*, 725-730.

Bischoff, R. (1986). A satellite cell mitogen from crushed adult muscle. *Developmental Biology 115*, 140-147.

Bishop, A., Kambadur, R., & Sharma, M. (2005). The therapeutic potential of agents that inactivate myostatin. *Expert Opinion on Investigational Drugs 14*, 1099-1106.

Black, B.L., & Olson, E.N. (1998). Transcriptional control of muscle development by myocyte enhancer factor-2 (MEF2) proteins. *Annual Review of Cell and Development Biology 14*, 167-96.

Black, B.L., Molkentin, J.D., & Olson, E.N. (1998). Multiple roles for the MyoD basic region in transmission of transcriptional activation signals and interaction with MEF2. *Molecular and Cellular Biology 18*, 69-77.

Bogdanovich, S., Krag, T.O.B., Barton, E.R., Morris, L.D., Whittemore, L.A., Ahima, R.S., & Khurana, T.S. (2002). Functional improvement of dystrophic muscle by myostatin blockade. *Nature 420*, 418-421.

Borycki, A., & Emerson, C.P. (1997). Muscle determination: another key player in myogenesis? *Current Biology 7*, 620-623.

Brand, N.J. (1997). Myocyte enhancer factor 2 (MEF2). *International Journal of Biochemistry and Cell Biology 29*, 1467-1470.

Brazelton, T.R., Nystron, M., & Blau, H.M. (2003). Significant differences among skeletal muscles in the incorporation of bone marrow-derived cells. *Developmental Biology 262*, 64-74.

Brent, A.E. (2005). Somite Formation: Where left meets right. *Current Biology 15*, 468-470.

Buckingham, M., Bajard, L., Chang, T., Daubas, P., Hadchouel, J., Meilhac, S., Butterfield, T.A., Best, T.M., & Merrick, M.A. (2006). The dual roles of neutrophils and macrophages in inflammation: a critical balance between tissue damage and repair. *Journal of Athletic Training 41*, 457-465.

Buckingham, M., Bajard, L., Chang, T., Daubas, P., Hadchouel, J., Meilhac, S., Montarras, D., Rocancourt, D., & Relaix, F. (2003). The formation of skeletal muscle: from somite to limb. *Journal of Anatomy 202*, 59-68.

Butterfield, T.A., Best, T.M., & Merrick, M.A. (2006). The dual roles of neutrophils and macrophages in inflammation: a critical balance between tissue damage and repair. *Journal of Athletic Training 41*, 457-465.

Carlson, C.J., Booth, F.W., & Gordon, S.E. (1999). Skeletal muscle myostatin mRNA expression is fiber-type specific and increased during hindlimb unloading. *American Journal of Physiology. Regulatory, Integrative and Comparative Physiology 277*, 601-606.

Cerletti, M., Molloy, M.J., Tomczak, K.K., Yoon, S., Ramoni, M.F., Kho, A.T, Beggs, A.H., & Gussoni, E. (2006). Melanoma cell adhesion molecule is a novel marker for human fetal myogenic cells and affects myoblast fusion. *Journal of Cell Science 119*, 3117-3127.

Chakravarthy, M. V., Davis, B.S., & Booth, F.W. (2000). IGF-I restores satellite cell proliferative potential in immobilized old skeletal muscle. *Journal of Applied Physiology 89*, 1365-79.

Chargé, S., & Rudnicki, M.A. (2003). Fusion with the fused: a new role for interleukin-4 in the building of muscle. *Cell 113*, 422-423.

Chargé, S.B.P., & Rudnicki, M.A. (2004). Cellular and molecular regulation of muscle regeneration. *Physiology Review 84*, 209-238.

Christ, B., & Brand-Saberi, B. (2002). Limb muscle development. *International Journal of Developmental Biology 46*, 905-914.

Cohen, M., Ravid, A., Scharf, V., Hauben, D., & Katzir, A. (2003). Temperature controlled burn generation system based on a CO_2 laser and a silver halide fiber optic radiometer. *Lasers in Surgery and Medicine 32*, 413-416.

Collins, C.A. (2006). Satellite cell self-renewal. *Current Opinion in Pharmacology 6*, 1-6.

Conboy, I.M., & Rando, T.A. (2002). The regulation of notch signalling controls satellite cell activation and cell fate determination in postnatal myogenesis. *Developmental Cell 3*, 397-409.

Coolican, S.A., Samuel, D.S., Ewton, D.Z., McWade, F.J., & Florini, J.R. (1997). The mitogenic and myogenic actions of insulin-like growth factors utilize distinct signalling pathways. *The Journal of Biological Chemistry 272*, 6653-6662.

Cooper, R.N., Tajbakhsh, S., Cossu, M.G., Buckingham, M., & Butler-Browne, G.S. (1999). In vivo satellite cell activation via Myf5 and MyoD in regenerating mouse skeletal muscle. *Journal of Cell Science 112*, 2895-2901.

Cornelison, D.D.W., & Wold, B.J. (1997). Single-cell analysis of regulatory gene expression in quiescent and activated mouse skeletal muscle satellite cells. *Developmental Biology 191*, 270-283.

Cornelison, D.D.W., Olwin, B.B., Rudnicki, M.A., & Wold, B.J. (2000). MyoD-/- satellite cells in single-fiber culture are differentiation defective and MRF4 deficient. *Developmental Biology 224*, 122-137.

Daopin, S., Piez, K., Ogawa, Y., & Davies, D.R. (1992). Crystal structure of transforming growth factor-β2: an unusual fold for the superfamily. *Science 257*, 369-373.

De Angelis, L., Berghella, L., Coletta, M., Lattanzi, L., Zanchi, M., Cusella-De Angelis, M.G., Ponzetto, C., & Cossu, G. (1999). Skeletal myogenic progenitors originating from embryonic dorsal aorta coexpress endothelial and myogenic markers and contribute to postnatal muscle growth and regeneration. *Journal of Cell Biology 147*, 869-878.

Dhawan, J., & Rando, T.A. (2005). Stem cells in postnatal myogenesis: molecular mechanisms of satellite cell quiescence, activation and replenishment. *Trends in Cell Biology 15*, 666-673.

Dietrich, S., Abou-Rebyeh, F., Brohman, H., Bladt, F., Sonnenberg-Riethmacher, E., Yamaai, T., Lumsden, A., Brand-Saberi, B., & Birchmeier, C. (1999). The role of SF/HGF and c-Met in the development of skeletal muscle. *Development 126*, 1621-1629.

DiPietro, L.A. (1995). Wound healing: the role of the macrophage and other immune cells. *Shock 4*, 233-240.

Doherty, K.R., Cave, A., Davis, D.B., Delmonte, A.J., Posey, A., Earley, J.U., Hadhazy, M., & McNally, E.M. (2005). Normal myoblast fusion requires myoferlin. *Development 132*, 5565-5575.

Doumit, M.E., Cook, D.R., & Merkel, R.A. (1993). Fibroblast growth factor, epidermal growth factor, insulin-like growth factors, and platelet-derived growth factor-BB stimulate proliferation of clonally derived porcine myogenic satellite cells. *Journal of Cellular Physiology 157*, 326-332.

Dovi, J.V., He, L.K., & DiPietro, L.A. (2003). Accelerated wound closure in neutrophil-depleted mice. *Journal of Leukocyte Biology 73*, 448-455.

Duance, V.C., Restall, D.J., Beard, H., Bourne, F.J., & Bailey, A.J. (1977). The location of three collagen types in skeletal muscle. *FEBS Letters 79*, 248-252.

Dubrulle, J., & Pourquié, O. (2004). Coupling segmentation to axis formation. *Development 131*, 5783-5793.

Forbes, D., Jackman, M., Bishop, A., Thomas, M., Kambadur, R., & Sharma, M. (2006). Myostatin auto-regulates its expression by feedback loop through smad7 dependent mechanism. *Journal of Cellular Physiology 206*, 264-272.

Garcia-Filipe, S., Barbier-Chassefiere, V., Alexakis, C., Huet, E., Ledoux, D., Kerros, M.E., Petit, E., Barritault, D., & Kern, C.P. (2006). RGTA OTR4120, a heparin sulphate mimetic, is a possible long-term active agent to heal burned skin. *Journal of Biomedical Materials Research Part A 80*, 75-84.

Gestrelius, S., & Borgström, P. (1986). A dynamic model of smooth muscle contraction. *Biophysical Journal 50*, 157-169.

Gibson, M.C., & Schultz, E. (1982). The distribution of satellite cells and their relationship to specific fiber types in soleus and extensor digitorum longus muscles. *The Anatomical Record 202*, 329-337.

Gilson, H., Schakman, O., Combaret, L., Lause, P., Grobet, L., Attaix, D., & Ketelslegers, J.M. (2007). Myostatin gene depletion prevents glucocorticoid-induced muscle atrophy. *Endocrinology 148*, 452-460.

Gordon, A.M., Regnier, M., & Homsher, E. (2001). Skeletal and cardiac muscle contractile activation: tropomyosin "rocks and rolls". *News in Physiological Sciences 16*, 49-55.

Gore, D.C., Rinehart, A., & Asimakis, G. (2005). Temporal changes in cellular energy following burn injury. *Burns 31*, 998-1002.

Gossett, L.A., Kelvin, D.J., Sternberg, E.A., & Olson, E.N. (1989). A new myocyte-specific enhancer-binding factor that recognizes a conserved element associated with multiple muscle-specific genes. *Molecular Cell Biology 9*, 5022-5033.

Greenhalgh, D.G. (1996). The healing of burn wounds. *Dermatology Nursing 8*, 13-25.

Gridley, T. (2006). The long and the short of it: somite formation in mice. *Developmental Dynamics 235*, 2330-2336.

Grobet, L., Martin, L.J.R., Poncelet, D., Pirottin, D., Brouwers, B., Riquet, J., Schoeberlein, A., Dunner, S., Ménissier, F., Massabanda, J., Fries, R, Hanset, R., & Georges, M. (1997). A deletion in the bovine myostatin gene causes the double-muscled phenotype in cattle. *Nature Genetics 17*, 71-74.

Gross, M.K., Moran-Rivard, L., Velasquez, T., Nakatsu, M.N., Jagla, K., & Goulding, M. (2000). Lbx1 is required for muscle precursor migration along a lateral pathway into the limb. *Development 127*, 413-424.

Hasty, P., Bradley, A., Morris, J.H., Edmondson, D.G., Venuti, J.M., Olson, E.N., & Klein, W.H. (1993). Muscle deficiency and neonatal death in mice with a targeted mutation in the myogenin gene. *Nature 364*, 501-506.

Hawke, T.J., & Garry, D.J. (2001). Myogenic satellite cells: physiology to molecular biology. *Journal of Applied Physiology, 91*, 535-551.

Higashimori, H., Whetzel, T.P., Mahmood, T., & Carlsen, R.C. (2005). Peripheral axon calibre and conduction velocity are decreased after burn injury in mice. *Muscle and Nerve 31*, 610-620.

Hirsinger, E., Duprez, D., Jouve, C., Malapert, P., Cooke, J., & Pourquié, O. (1997). Noggin acts downstream of Wnt and Sonic Hedgehog to antagonize BMP4 in avian somite patterning. *Develoment 124*, 4605-4614.

Hollway, G., & Currie, P. (2005). Vertebrate myotome development. *Birth Defects Research 75*, 172-179.

Hollway, G.E., & Currie, P.D. (2003). Myotome meanderings: cellular morphogenesis and the making of muscle. *EMBO Reports 4*, 855-860.

Holterman, C.E., & Rudnicki, M.A. (2005). Molecular regulation of satellite cell function. *Seminars in Cell and Developmental Biology 16*, 575-584.

Horsley, V., Jansen, K.M., Mills, S.T., & Pavlath, G.K. (2003). IL-4 acts as a myoblast recruitment factor during mammalian muscle growth. *Cell 113*, 483-494.

Houzelstein, D., Auda-Boucher, G., Chéraud, Y., Rouaud, T., Blanc, I., Tajbakhsh, S., Buckingham, M.E., Fontaine-Pérus, J., & Robert, B. (1999). The homeobox gene Msx1 is expressed in a subset of somites, and in muscle progenitor cells migrating into the forelimb. *Development 126*, 2689-2701.

Hu, X., Zhang, D., Pang, H., Caudle, W.M., Li, Y., Gao, H., Liu, Y., Qian, L., Wilson, B., Di Monte, D.A., Ali, S.F., Zhang, J., Block, M.L., & Hong, J.S. (2008). Macrophage antigen complex-1 mediates reactive microgliosis and progressive dopaminiergic neurodegeneration in the MPTP model of parkinsons disease. *The Journal of Immunology 181*, 7194-7204.

Ingalls, R.R., Arnaout, M.A., Delude, R.L., Flaherty, S., Savedra, R., & Golenbock, D.T. (1998). The CD11/CD18 integrins: characterization of three novel LPS signallilng receptors. *Progressive Clinical Biology Research 397*, 107-117.

Irintchev, A., Zeschnigk, M., Starzinski-Powitz, A., & Wernig, A. (1994). Expression pattern of m-cadherin in normal, denervated and regenerating mouse muscle. *Developmental Dynamics 199*, 326-337.

Jeanplong, F., Sharma, M., Somers, W.G., Bass, J.J., & Kambadur, R. (2001). Genomic organization and neonatal expression of the bovine myostatin gene. *Molecular and Cellular Biochemistry 220*, 31-37.

Ji, S., Losinski, R.L., Cornelius, S.G., Frank, G.R., Willis, G.M., Gerrard, D.E., Depreux, F.F., Spurlock, M.E. (1998). Myostatin expression in porcine tissues: tissue specificity and developmental and postnatal regulation. *American Journal of Physiology 275*, 1265-1273.

Johnson, S.E., & Allen, R.E. (1995). Activation of skeletal muscle satellite cells and the role of fibroblast growth factor receptors. *Experimental Cell Research 219*, 449-453.

Jones, N.C., Fedorov, Y.V., Rosenthal, R.S., & Olwin, B.G. (2001). ERK1/2 is required for myoblast proliferation but is dispensable for muscle gene expression and cell fusion. *Journal of Cellular Physiology 186*, 104-115.

Joulia, D., Bernardi, H., Garandel, V., Rabenoelina, F., Vernus, B., & Cabello, G. (2003). Mechanisms involved in the inhibition of myoblast proliferation and differentiation by myostatin. *Experimental Cell Research 286*, 263-275.

Kääriänen, M., Järvinen, T., Järvinen, M., Rantanen, J., & Kalimo, H. (2000). Relation between myofibers and connective tissue during muscle injury repair. *Scandinavian Journal of Medicine and Science in Sports 10*, 332-337.

Kambadur, R., Bishop, A., Senna Salerno, M., McCroskery, S., Sharma, M. (2004). Role of Myostatin in Muscle Growth. In te Pas, M.F.W., Everts, M.E., Haagsman, H.P. (Eds). *Muscle Development in Livestock* (pp. 297-316). CAB International.

Kambadur, R., Sharma, M., Senna Salerno, M., & Hennebry, A. (2006a). PCT patent application entitled “Muscle Regeneration” (PCT/NZ2006/000010).

Kambadur, R., Sharma, M., Senna Salerno, M., & Hennebry, A. (2006b). PCT patent application entitled “Methods and Composition for Improving Wound Healing” (PCT/NZ2006/000009).

Kambadur, R., Sharma, M., Senna Salerno, M., Siriett, V., & Berry, C. (2006c). Provisional patent application entitled “Myostatin Antagonist (awaiting number).

Kambadur, R., Sharma, M., Smith, T.P.L., & Bass, J.J. (1997). Mutations in myostatin (GDF8) in double-muscled Belgian blue and Piedmontese cattle. *Genome Research 7*, 910-915.

Kassar-Duchossoy, L., Gayraud-Morel, B., Gomés, D., Rocancourt, D., Buckinghma, M., Shinin, V., & Tajbakhsh, S. (2004). Mrf4 determines skeletal muscle identity in Myf5:MyoD double-mutant mice. *Nature 421*, 466-471.

Katz, F. (1961). The termination of the afferent nerve fiber in the muscle spindle of the frog. *Philosophical Transactions of the Royal Society of London 243*, 221-225.

Kocamis, H., & Killefer, J. (2002). Myostatin expression and possible functions in animal muscle growth. *Domestic Animal Endocrinology 23*, 447-454.

Krüger, M., Mennerich, D., Fees, S., Schäfer, R., Mundlos, S., & Braun, T. (2001). Sonic hedgehog is a survival factor for hypaxial muscles during mouse development. *Development 128*, 743-752.

Kuang, S., Charge, S.B., Seale, P., Huh, M., & Rudnicki, M.A. (2006). Distinct roles for Pax7 and Pax3 in adult regenerative myogenesis. *Journal of Cell Biology 172*, 103-113.

Kubista, M., Andrade, J.M., Bengtsson, M., Forootan, A., Jonák, J., Lind, K., Sindelka, R., Sjöback, R., Sjögreen, B., Strömbom, L., Ståhlberg, A., & Zoric, N. (2006). The real-time polymerase chain reaction. *Molecular Aspects of Medicine 27*, 95-125.

Kurek, J.B., Nouri, S., Kannourakis, G., Murphy, M., & Austin, L. (1996). Leukemia inhibitory factor and interleukin-6 are produced by muscle cells in diseases and regenerating skeletal muscle. *Muscle Nerve 19*, 1291-1301.

LaBarge, M.A., & Blau, H.M. (2002). Biological progression from adult bone marrow to mononucleate muscle stem cell to multinucleate muscle fiber in response to injury. *Cell 111*, 589-601.

Langley, B., Thomas, M., Bishop, A., Sharma, M., Gilmour, S., & Kambadur, R. (2002). Myostatin inhibits myoblast differentiation by down-regulating MyoD expression. *Journal of Biological Chemistry 277*, 49831-49840.

Langley, B., Thomas, M., McFarlane, C., Gilmour, S., Sharma, M., & Kambadur, R. (2004). Myostatin inhibits rhabdomyosarcoma cell proliferation through an Rb-independent pathway. *Oncogene 23*, 524-534.

Le Grand, F., & Rudnicki, M.A. (2007). Skeletal muscle satellite cells and adult myogenesis. *Current Opinion in Cell Biology 19*, 628-633.

Lee, S.J. (2004). Regulation of muscle mass by myostatin. *Annual Review of Cellular Developmental Biology 20*, 61-86.

Lee, S.J. & McPherron, A.C. (2001). Regulation of myostatin activity and muscle growth. *Proceedings of the National Academy of Sciences of the United States of America 98*, 9306-9311.

Leibovich S.J., & Ross, R. (1975). The role of the macrophage in wound repair: a study with hydrocortisone and antimacrophage serum. *American Journal of Pathology 78*, 71-100.

Lescaudron, L., Creuzet, S.E., Li, Z., Paulin, D., & Fontaine-Pérus, J. (1997). Desmin-lacZ transgene expression and regeneration within skeletal muscle transplants. *Journal of Muscle Research and Cell 18*, 631-641.

Lescaudron, L., Li, Z., Paulin, D., & Fontaine-Pérus, J. (1993). Desmin-lacZ transgene, a marker of regenerating skeletal muscle. *Neurmuscular Disorders 3*, 419-422.

Li, J., Chen, J., & Kirsner, R. (2007). Pathophysiology of acute wound healing. *Clinics in Dermatology 25*, 9-18.

Li, Z.B., Kollias, H.D., & Wagner, K.R. (2008). Myostatin directly regulates skeletal muscle fibrosis. *Journal of Biological Chemistry 283*, 19371-19378.

Lillie, R. (1965). *Histopathologic, technic and practical histochemistry*. New York, McGraw-Hill.

Linnane, L., Serrano, A.L., & Rivero, J.L.L. (1999). Distribution of fast myosin heavy chain-based muscle fibres in the gluteus medius of untrained horses: mismatch between antigenic and ATPase determinants. *Journal of Anatomy 194*, 363-372.

Listrat, A., Picard, B., & Geay, Y. (1999). Age-related changes and location of type I, III, IV, V and VI collagens during development of four foetal skeletal muscles of double-muscled and normal bovine animals. *Tissue and Cell 31*, 17-27.

Ludolph, D.C., & Konieczny, S.F. (1995). Transcription factor families: muscling in on the myogenic program. *The FASEB Journal 9*, 1595-1604.

Ma, K., Mallidis, C., Bhasin, S., Mahabadi, V., Artaza, J., Gonzalez-Cadavid, N., Arias, J., & Salehian, B. (2003). Glucocorticoid-induced skeletal muscle atrophy is associated with upregulation of myostatin gene expression. *American Journal of Physiology, Endocrinology and Metabolism 285*, 363-371.

Mallo, M. (2007). And the segmentation clock keeps ticking. *BioEssays 29*, 412-415.

Marcelle, C., Stark, M.R., & Bronner-Fraser, M. (1997). Coordinate actions of BMPs, Wnts, Shh and Noggin mediate patterning of the dorsal somite. *Development 124*, 3955-3963.

Marshall, A., Senna Salerno, M., Thomas, M., Davies, T., Berry, C., Dyer, K., Bracegirdle, J., Watson, T., Dziadek, M., Kambadur, R., Bower, R., & Sharma, M. (2008). Mighty is a novel promyogenic factor in skeletal myogenesis. *Experimental Cell Research 314*, 1013-1029.

Martin, P., & Leibovich, S.J. (2005). Inflammatory cells during wound repair: the good, the bad and the ugly. *Trends in Cell Biology 15*, 599-607.

Martini, F. H. (1998). *Fundamentals of Anatomy and Physiology (4th Edition)*. New Jersey, Prentice Hall / Pearson Education.

Martini, F. H. (2002). *Fundamentals of Anatomy and Physiology (6th Edition)*. New Jersey, Prentice Hall / Pearson Education.

Mauro, A. (1961). Satellite cell of skeletal muscle fibres. *Journal of Biochemistry and Biophysiology 9*, 493-495.

Mayadas, T.N., & Cullere, X. (2005). Neutrophil B2 integrins: moderators of life or death decisions. *Trends in Immunology 26*, 388-395.

McCroskery, S., Thomas, M., Maxwell, L., Sharma, M., & Kambadur, R. (2003). Myostatin negatively regulates satellite cell activation and self-renewal. *The Journal of Cell Biology 162*, 1135-1147.

McCroskery, S., Thomas, M., Platt, L., Hennebry, A., Nishimura, T., McLeay, L., Sharma, M., & Kambadur, R. (2005). Improved muscle healing through enhanced regeneration and reduced fibrosis in myostatin-null mice. *Journal of Cell Science 118*, 3531-3541.

McElhinny, A.S., Schwach, C., Valichnac, M., Mount-Patrick, S., & Gregorio, C.C. (2005). Nebulin regulates the assembly and lengths of the thin filaments in striated muscle. *Journal of Cell Biology 170*, 947-957.

McFarlane, C., Hennebry, A., Thomas, M., Plummer, E., Ling, N., Sharma, M., & Kambadur, R. (2008). Myostatin signals through Pax7 to regulate satellite cell self-renewal. *Experimental Cell Research 314*, 317-329.

McFarlane, C., Plummer, E., Thomas, M., Hennebry, A., Ashby. M., Ling, N., Smith, H., Sharma, M., & Kambadur, R. (2006). Myostatin induces cachexia by activating the ubiquitin proteolytic system through an NF-κB-independent, FoxO1-dependent mechanism. *Journal of Cellular Physiology 209*, 501-514.

McPherron, A.C., & Lee, S.J. (1997). Double muscling in cattle due to mutations in the myostatin gene. *Proceedings of the National academy of Sciences of the United States of America 94*, 12457-12461.

McPherron, A.C., Lawler, A.M., & Lee, S. (1997). Regulation of skeletal muscle mass in mice by a new TGF-β superfamily member. *Nature 387*, 83-90.

Medvedev, A.E., Flo, T., Ingalls, R.R., Golenbock, D.T., Teti, G., Vogel, S.N., & Espevik, T. (1998). Involvement of CD14 and complement receptors CR3 and CR4 in nuclear factor-kappaB activation and TNF production induced lipopolysaccharide and group B streptococcal cell walls. *Journal of Immunology 160*, 4535-4542.

Merly, F., Lescaudron, L., Rouaud, T., Crossin, F., & Gardahaut, M.F. (1999). Macrophages enhance muscle satellite cell proliferation and delay their differentiation. *Muscle and Nerve 22*, 724-732.

Meyer, T.N., & da Silva, A.L. (1999). A standard burn model using rats. *Acta Cirurgica Brasileira 14*, 199-202.

Molkentin, J.D., & Olson, E.N. (1996a). Combinatorial control of muscle development by basic helix-loop-helix and MADS-box transcription factors. *Proceedings of the National academy of Sciences of the United States of America 93*, 9366-9373.

Molkentin, J.D., & Olson, E.N. (1996b). Defining the regulatory networks for muscle development. *Current Opinion in Genetics and Development 6*, 445-453.

Molkentin, J.D., Black, B.L., Martin, J.F., & Olson, E.N. (1995). Cooperative activation of muscle gene expression by MEF2 and myogenic bHLH proteins. *Cell 83*, 1125-1136.

Møller-Kristensen, M., Hamblin, M.R., Thiel, S., Jensenius, J.C., & Takahashi, K. (2007). Burn injury reveals altered phenotype in mannan-binding lectin-deficient mice. *Journal of Investigative Dermatology 127*, 1524-1531.

Møller-Kristensen, M., Ip, W.K.E., Shi, L., Gowda, L.D., Hamblin, M.R., Thiel, S., Jensenius, J.C., Ezekowitz, R.A.B., & Takahashi, K. (2006). Deficiency of mannose-binding lectin greatly increases susceptibility to postburn infection with *Pseudomonas aeruginosa*. *The Journal of Immunology 176*, 1769-1775.

Morgan, J.E., & Partridge, T.A. (2003). Muscle satellite cells. *The International Journal of Biochemistry and Cell Biology 35*, 1151-1156.

Mutsaers, S.E., Bishop, J.E., McGrouther, G., & Laurent, G.J. (1997). Mechanisms of tissue repair: from wound healing to fibrosis. *International Journal of Biochemistry and Cell Biology 29*, 5-17.

Nabeshima, Y., Hanaoka, K., Hayasaka, M., Esumi, E., Li, S., Nonaka, I., & Nabeshima, Y.I. (1993). Myogenin gene disruption results in perinatal lethality because of severe muscle defect. *Nature 364*, 532-535.

Naidu, P.S., Ludolph, D.C., To, R.Q., Hinterberger, T.J., & Konieczny, S.F. (1995). Myogenin and MEF2 function synergistically to activate the MRF4 promoter during myogenesis. *Molecular and Cellular Biology 15*, 2707-2718.

Naya, F.J., & Olson, E. (1999). MEF2: a transcriptional target for signalling pathways controlling skeletal muscle growth and differentiation. *Current Opinion in Cell Biology 11*, 683-688.

Neely, A.N., Holder, I.A., & Warden, G.D. (1999). Then and now: studies using a burned mouse model reflect trends in burn research over the past 25 years. *Burns 25*, 603-609.

Olson, E.N., Perry, M., & Schulz, R.A. (1995). Regulation of muscle differentiation by the MEF2 family of MADS box transcription factors. *Developmental Biology 172*, 2-14.

Ornatsky, O.I., Andreucci, J.J., & McDermott, J.C. (1997). A dominant-negative form of transcription factor MEF2 inhibits myogenesis. *Journal of Biological Chemistry 272*, 33271-33278.

Padfield, K.E., Astrakas, L.G., Zhang, Q., Gopalan, S., Dai, G., Mindrinos, M.N., Tompkins, R.G., Rahme, L.G., & Tzika, A.A. (2005). Burn injury causes mitochondrial dysfunction in skeletal muscle. *PNAS 102 (15)*, 5368-5373.

Padgett, R.W., Das, P., & Krishna, S. (1998). TGF-β signalling, smads, and tumour suppressors. *BioEssays 20*, 382-391.

Palmeirim, I., Henrique, D., Ish-Horowicz, D., & Pourquié, O. (1997). Avian *hairy* gene expression identifies a molecular clock linked to vertebrate segmentation and somitogenesis. *Cell 91*, 639-648.

Papp, A., Romppanen, E., Lahtinen, T., Uusaro, A., Härma, M., & Alhava, E. (2005). Red blood cell and tissue water content in experimental thermal injury. *Burns 31*, 1003-1006.

Park, J.E., & Barbul, A. (2004). Understanding the role of immune regulation in wound healing. *The American Journal of Surgery 187*, 11-16.

Pawlik, T.M., Carter, E.A., Bode, B.P., Fishmann, A.J., & Tompkins, R.G. (2003). Central role of interleukin-6 in burn induced stimulation of hepatic amino acid transport. *International Journal of Molecular Medicine 12*, 541-548.

Perry, R.L.S., & Rudnicki, M.A. (2000). Molecular mechanisms regulating myogenic determination and differentiation. *Frontiers in Bioscience 5*, 750-767.

Pinney, D.F., & Emerson, C.P. (1989). 10T1/2 cells: an *in vitro* model for molecular genetic analysis of mesodermal determination and differentiation. *Environmental Health Perspectives 80*, 221-227.

Potts, J.K., Echternkamp, S.E., Smith, T.P.L., & Reecy, J.M. (2003). Characterization of gene expression in double-muscled and normal-muscled bovine embryos. *Animal Genetics 34*, 438-44.

Pourquié, O. (2001). Vertebrate somitogenesis. *Annual Review of Cellular Developmental Biology 17*, 311-50.

Pourquié, O., Fan, C.M., Coltey, M., Hirsinger, E., Watanabe, Y., Bréant C., Francis-West, P., Brickell, P., Tessier-Lavigne, M., & Le Douarin, N.M. (1996). Lateral and axial signals involved in avian somite patterning: a role for BMP4. *Cell 9*, 461-71.

Pullen, A.H. (1977a). The distribution and relative sizes of fibre types in the extensor digitorum longus and soleus muscles of the adult rat. *Journal of Anatomy 123*, 467-486.

Pullen, A.H. (1977b). The distribution and relative sizes of three histochemical fibre types in the rat tibialis anterior muscle. *Journal of Anatomy 123*, 1-19.

Randall, D., Burggren, W., & French, K. (1997). *Eckert Animal Physiology, Mechanisms and Adaptations*. New York, W.H. Freeman and Company.

Rawls, A., Valdez, R., Zhang, W., Richardson, J., Klein, W., & Olson, E.N. (1998). Overlapping functions of the myogenic bHLH genes MRF4 and MyoD revealed in double mutant mice. *Development 125*, 2349-2358.

Relaix, F., Montarras, D., Zaffran, S., Gayraud-Morel, B., Rocancourt, D., Tajbakhsh, S., Mansouri, A., Cumano, A., & Buckingham, M. (2006). Pax3 and Pax7 have distinct and overlapping functions in adult muscle progenitor cells. *Journal of Cellular Biology 172*, 91-102.

Reznikoff, C.A., Brankow, D.W., & Heidelberger, C. (1973). Establishment and characterization of a cloned line of C3H mouse embryo cells sensitive to postconfluence inhibition of division. *Cancer Research 33*, 3231-3238.

Rios, R., Carneiro, I., Arce, V.M., & Devesa, J. (2002). Myostatin is an inhibitor of myogenic differentiation. *The American Journal of Physiology. Cell Physiology 282*, 993-999.

Roberts, A.B. (1999). TGF- β signalling from receptors to the nucleus. *Microbes and Infection 1*, 1265-1273.

Robinson, M.J., & Cobb, M.H. (1997). Mitogen-activated protein kinase pathways. *Current Opinion in Cell Biology 9*, 180-186.

Rudnicki M.A., Schnegelsber, P.N.J., Stead, R.H., Braun, T., Arnold, H.H., & Jaenisch, R. (1993). MyoD or Myf-5 is required for the formation of skeletal muscle. *Cell 75*, 1351-1359.

Rudnicki, M. A., T. Braun, S. Hinuma and R. Jaenisch (1992). Inactivation of MyoD in mice leads to up-regulation of the myogenic HLH gene Myf-5 and results in apparently normal muscle development. *Cell 71,* 383-90.

Sabourin, L.A., Girgis-Gabardo, A., Seale, P., Asakura, A., & Rudnicki, M.A. (1999). Reduced differentiation potential of primary MyoD-/- myogenic cells derived from adult skeletal muscle. *The Journal of Cell Biology 144*, 631-643.

Sakurai, H., Nozaki, M., Traber, L.D., Hawkins, H.K., & Traber, D.L. (2002). Microvascular changes in large flame burn wound in sheep. *Burns 28*, 3-9.

Schafer, K.A. (1998). The cell cycle: a review. *Veterinary Pathology 35*, 461-478.

Schmalbruch, H., & Hellhammer, U. (1977). The number of nuclei in adult rat muscles with special reference to satellite cells. *Anatomical Record 189*, 169-176.

Schuelke, M., Wagner, K.R., Stolz, L.E., Hübner, C., Riebel, T., Kömen, W, Braun, T., Tobin, J., & Lee, S.J. (2004). Myostatin mutation associated with gross muscle hypertrophy in a child. *New England Journal of Medicine 350*, 2682-2628.

Schultz, E. (1976). Fine structure of satellite cells in growing skeletal muscle. *American Journal of Anatomy 147*, 49-70.

Schultz, E. (1996). Satellite cell proliferative compartments in growing skeletal muscles. *Developmental Biology 175*, 84-94.

Senna Salerno, M., Bracegirdle, J., Dyer, K., Platt, L., Marshall, A., Thomas, M., Bower, R., Kambadur, R., & Sharma, M. (submitted). *Mighty*, a novel myogenic factor regulates muscle regeneration and cell chemotaxis. *Experimental Cell Research*.

Senna Salerno, M., Thomas, M., Forbes, D., Watson, T, Kambadur, R., & Sharma, M. (2004). Molecular analysis of fiber type-specific expression of murine myostatin promoter. *The American Journal of Physiology. Cell Physiology 287*, 1031-1040.

Sharma, M., Kambadur, R., Matthews, K.G., Somers, W.G., Devlin, G.P., Conaglen, J.V., Fowke, P.J., Bass, J.J. (1999). Myostatin, a transforming growth factor-β superfamily member, is expressed in heart muscle and is upregulated in cardiomyocytes after infarct. *Journal of Cellular Physiology 180*, 1-9.

Sheehan, S.M., & Allen, R.E. (1999). Skeletal muscle satellite cell proliferation in response to members of the fibroblast growth factor family and hepatocyte growth factor. *Journal of Cellular Physiology 181*, 499-506.

Shefer, G., Van de Mark, D.P., Richardson, J.G., & Yablonka-Reuveni, Z. (2006). Satellite-cell pool size does matter: defining the myogenic potency of aging skeletal muscle. *Developmental Biology 294*, 50-66.

Shelton, G.D., & Engvall, E. (2007). Gross muscle hypertrophy in whippet dogs is caused by a mutation in the myostatin gene. *Neuromuscular Disorders 17*, 721-722.

Shore, P., & Sharrocks, A.D. (1995). The MADS-box family of transcription factors. *European Journal of Biochemistry 229*, 1-13.

Simpson, D.M., & Ross, R. (1972). The neutrophilic leukocyte in wound repair. A study with antineutrophil serum. *Journal of Clinical Investigation 51*, 2009-2023.

Siriett, V., Senna Salerno, M., Berry, C., Nicholas, G., Bower, R., Kambadur, R., and Sharma, M. (2007). Antagonism of myostatin enhances muscle regeneration during sarcopenia. *Molecular Therapy 15*, 1463-70.

Siriett, V., Platt, L., Salerno, M.S., Ling, N., Kambadur, R., & Sharma, M. (2006). Prolonged absence of myostatin reduces sarcopenia. *Journal of Cellular Physiology 209*, 866-873.

Smith, C.K., Janney, M.J., & Allen, R.E. (1994). Temporal expression of myogenic regulatory genes during activation, proliferation, and differentiation of rat skeletal muscle satellite cells. *Journal of Cellular Physiology 159*, 379-385.

Squire, J.M. (1975). Muscle filament structure and muscle contraction. *Annual Review of Biophysics and Bioengineering 4*, 137-163.

Squire, J.M., & Morris, E.P. (1998). A new look at thin filament regulation in vertebrate skeletal muscle. *FASEB Journal 12*, 761-771.

Stieritz D.D., & Holder, I.A. (1975). Experimental studies of the pathogenesis of infections due to Pseudomonas aeruginosa: descripotion of a burned mouse model. *Journal of Infectious Diseases 131*, 688-691.

Sun, P.D. (1995). The cystine-knot growth-factor superfamily. *Annual Review of Biophysics and Biomolecular Structure 24*, 269-291.

Swartz, D.R., Greaser, M.L., & Marsh, B.B. (1990). Regulation of binding of subfragment 1 in isolated rigor myofibrils. *Journal of Cell Biology 111*, 2989-3001.

Tajbakhsh, S., Rocancourt, D., Cossu, G., & Buckingham, M. (1997). Redefining the genetic hierarchies controlling skeletal myogenesis: Pax-3 and Myf-5 act upstream of MyoD. *Cell 89*, 127-38.

Tapscott, S.J., & Weintraub, H. (1991). MyoD and the regulation of myogenesis by helix-loop-helix proteins. *Journal of Clinical Investigation 87*, 1133-1138.

Tatsumi, R., Anderson, J.E., Nevoret, C.J., Halevy, O., & Allen, R.E. (1998). HGF/SF is present in normal adult skeletal muscle and is capable of activating satellite cells. *Developmental Biology 194*, 114-128.

Tessema, M., Lehmann, U., & Kreipe, H. (2004). Cell cycle and no end. *Virchows Archive 444*, 313-323.

Thomas, M., Langley, B., Berry, C., Sharma, M., Kirk, S., Bass, J., & Kambadur, R. (2000). Myostatin, a negative regulator of muscle growth, functions by inhibiting myoblast proliferation. *The Journal of Biological Chemistry 275*, 40235-40243.

Tidball, J.G. (1995). Inflammatory cell response to acute muscle injury. *Medicine and Science in Sports and Exercise 27*, 1022-1032.

Tidball, J.G. (2005). Inflammatory processes in muscle injury and repair. *American Journal of Physiology. Regulatory, Integrative and Comparative Physiology 288*, 345-353.

Tiidus, P.M. (1998). Radical species in inflammation and overtraining. *Canadian Journal of Physiology and Pharmacology 76*, 533-538.

Toader-Radu, M. (1978). Dynamics of regeneration in skeletal muscle following localized heat injury. *Morphologie et embryologie 24*, 69-73.

Todaro, G.J., Green, H., & Goldberg, B.D. (1964). Transformation of properties of an established cell line by SV40 and polyoma virus. *Pathology 51*, 66-73.

Tregear, R.T., & Marston, S.B. (1979). The crossbridge theory. *Annual Review of Physiology 41*, 723-736.

Tsirogianni, A.K., Moutsopoulos, N.M., & Moutsopoulos, H.M. (2006). Wound healing: immunological aspects. *Injury 37*, 5-12.

Wagner, K.R., McPherron, A.C., Winik, N., & Lee, S.J. (2002). Loss of myostatin attenuates severity of muscular dystrophy in mdx mice. *Annals of Neurology 52*, 832-836.

Walsh, F.S., & Celeste, A.J. (2005). Myostatin: a modulator of skeletal-muscle stem cells. *Biochemical Society Transactions 33*, 1513-1517.

Walsh, K., & Perlman, H. (1997). Cell cycle exit upon myogenic differentiation. *Current Opinion in Genetics and Development 7*, 597-602.

Wang, Y., & Jaenisch, R. (1997). Myogenin can substitute for Myf5 in promoting myogenesis but less efficiently. *Development 124*, 2507-2513.

Whitman, M. (1998). Smads and early developmental signalling by the TGFβ superfamily. *Genes and Development 12*, 2445-2462.

Wigmore, P.M., & Dunglison, G.F. (1998). The generation of fiber diversity during myogenesis. *International Journal of Developmental Biology 42*, 117-125.

Willis, M.S., Carlson, D.L., DiMaio, J.M., White, M.D., White, D.J., Adams, G.A., Horton, J.W., & Giroir, B.P. (2005). Macrophage migration inhibitory factor mediates late cardiac dysfunction after burn injury. *American Journal of Physiology. Heart and Circulatory Physiology 288*, 795-804.

Xiao, Y.T., Xiang, L.X., & Shao, J.Z. (2007). Bone morphogenetic protein. *Biochemical and Biophysical Research Communications 362*, 550-553.

Yablonka-Reuveni, Z., Rudnicki, M.A., Rivera, A.J., Primig, M., Anderson, J.E., & Natanson, P. (1999a). The transition from proliferation to differentiation is delayed in satellite cells from mice lacking MyoD. *Developmental Biology 210*, 440-455.

Yablonka-Reuveni, Z., Seger, R., & Rivera, A.J. (1999b). Fibroblast growth factor promotes recruitment of skeletal muscle satellite cells in young and old rats. *The Journal of Histochemistry and Cytochemistry 47*, 23-42.

Yu, Y.T., Breitbart, R.E., Smoot, L.B., Lee, Y., Mahdavi, V., & Nadal-Ginard, B. (1992). Human myocyte-specific enhancer factor 2 comprises a group of tissue-restricted MADS box transcription factors. *Genes and Development 6*, 1783-98.

Yun, K., & Wold, B. (1996). Skeletal muscle determination and differentiation: story of a core regulatory network and its context. *Current Opinion in Cell Biology 8*, 877-889.

Yusuf, F., & Brand-Saberi, B. (2006). The eventful somite: patterning, fate determination and cell division in the somite. *Anatomy and Embryology 211*, 21-30.

Yusuf, I., & Fruman, D.A. (2003). Regulation of quiescence in lymphocytes. *Trends in Immunology 24*, 380-386.

Vitt, U.A., Hsu, S.Y., & Hsueh, J.W. (2001). Evolution and classification of cystine knot-containing hormones and related extracellular signalling molecules. *Molecular Endocrinology 15*, 681-694.

Zentella, A., & Massagué, J. (1992). Transforming growth factor β induces myoblast differentiation in the presence of mitogens. *Proceedings of the National academy of Sciences of the United States of America 89*, 5176-5180.

Zhang, W., Behringer, R.R., & Olson, E.N. (1995). Inactivation of the myogenic bHLH gene MRF4 results in the up-regulation of myogenin and rib abnormalities. *Genes and Development 9*, 1388-1399.

Zhao, P., & Hoffman, E.P. (2004). Embryonic myogenesis pathways in muscle regeneration. *Developmental Dynamics 229*, 380-392.

Zhu, J., Li, Y., Shen, W., Qiao, C., Ambrosio, F., Lavasani, M., Nozaki, M., Branca, M., & Huard, J. (2007). Relationships between transforming growth factor-β1, myostatin, and decorin: implications for skeletal muscle fibrosis. *The Journal of Biological Chemistry 282*, 25852-25863.

Zhu, X., Topouzis, S., Liang, L., & Stotish, R.L. (2004). Myostatin signalling through Smad2, Smad3 and Smad4 is regulated by the inhibitory Smad7 by a negative feedback mechanism. *Cytokine 26*, 262-272.

Zierath, J.R., & Hawley, J.A. (2004). Skeletal muscle fiber type: influence on contractile and metabolic properties. *PLoS Biology 2*, 1523-1527.

Zimmers, T.A., Davies, M.V., Koniaris, L.G., Haynes, P., Esquela, A.F., Tomkinson, K., McPherron, A., Wolfman, N.M., & Lee, S.J. (2002). Induction of cachexia in mice by systemically administered myostatin. *Science 296*, 1486-1488.